

An Intelligent Cell-Level Battery/Ultracapacitor Hybrid

(The Smart Cell)

An Intelligent Cell-Level Battery/Ultracapacitor Hybrid

(The Smart cell)

By: Mohammad Zeiaee

A Thesis

Submitted to the School of Graduate Studies

in Partial Fulfilment of the Requirements for the Degree of Master of Applied Science

McMaster University

© Copyright Mohammad Zeiaee, August 2016. All rights reserved

Master of Applied Science (2016)
(Mechanical Engineering)

McMaster University
Hamilton, Ontario

TITLE: An Intelligent Cell-Level Battery/Ultracapacitor Hybrid (The Smart Cell)

AUTHOR: Mohammad Zeiaee

SUPERVISOR: Dr. Saeid R. Habibi

NUMBER OF PAGES: XV, 112

Permission to Use

In presenting this thesis in partial fulfillment of the requirements for a Postgraduate degree from McMaster University, I agree that the Libraries of this University may take it freely available for inspection. I further agree that the permission for copying this thesis in any manner, in whole or in part for scholarly purposes, may be granted by the professors who supervised my thesis work or, in their absence, by the head of the Department or the Faculty Dean in which my thesis work was conducted. It is understood that any copying or publication or use of this thesis or parts thereof for financial gain shall not be allowed without my writing permission. It is also understood that due recognition shall be given to me and McMaster University in any scholarly use which may be made of any material in my thesis. Requests for permission to copy or to make other use of material in this thesis, in whole or part, should be addressed to:

Head of Department of Mechanical Engineering

McMaster University

Faculty of Engineering

1280 Main Street West

Hamilton, Ontario L8S 4L6

Canada

Abstract

In the strive to use electric energy as the sole source of traction force in the automotive industry, the electric storage unit poses serious challenges. Although Li-Ion batteries have shown promising features, there is still room to improve the shortcomings of the electric storage unit. The chemical process of energy extraction and storage in the batteries results in inherently limited power density and lifetime. The notion of pairing a Li-Ion battery cell with an ultracapacitor will invigorate power capability of the hybrid cell. Furthermore, enabling local processing capability in each hybrid cell makes it possible to run sophisticated control and power management algorithms that result in increased battery longevity. Also, hybridization at cell level provides greater access to each cell's momentary states which results in more accurate analysis, improved safety, and a broad control possibility.

In this research, a Li-Ion battery cell is combined with an ultracapacitor. An appropriate configuration is selected for this particular application after reviewing several hybridization schemes and converter structures. A comprehensive power management unit is designed and implemented that is able to execute several strategies to mitigate battery stresses while improving power capabilities. A current regulator is also designed and implemented to realize the proposed strategies by providing the power converter with proper duty cycle. Rather than simulation under a wide range of test loads, a prototype hybrid cell is built and tested in an experimental setup.

Acknowledgements

I would first like to express my sincere gratitude to my supervisor, Prof. Saeid R. Habibi, for his endless support. Special gratitude must be conveyed to Dr. Lucia Gauchia and Dr. Mehdi Narimani, for their assistance, technical expertise, and support during this research. Also, financial support provided by the School of Graduate Studies and the Department of Mechanical Engineering is acknowledged and greatly appreciated. I also would like to thank my friend Ali Delbari for his sincere help with the experimental setup.

Furthermore, without the loving support and continuing encouragement of my wife, Mina, this work would not have been possible.

Table of Contents

1. Introduction.....	1
1.1. RESEARCH MOTIVATION.....	1
1.2. PROBLEM STATEMENT	3
1.3. RESEARCH OBJECTIVES	4
1.4. THESIS OUTLINE	5
2. Transportation Electrification.....	6
2.1. THE NECESSITY OF CHANGE	6
2.1.1. SUSTAINABILITY	6
2.1.2. ENVIRONMENTAL CONCERNS	7
2.1.3. HEALTH ISSUES.....	9
2.1.4. POLITICAL CONCERNS	9
2.2. MODERN ENERGY SOURCES FOR VEHICULAR APPLICATIONS.....	10
2.2.1. BATTERIES.....	11
2.2.2. ULTRACAPACITORS.....	17
2.2.3. FUEL CELL.....	20
2.2.4. ENERGY VS. POWER.....	22
2.3. ELECTRIC VEHICLES	23
2.3.1. HYBRID ELECTRIC VEHICLES.....	23
2.3.2. PLUG-IN HYBRID ELECTRIC VEHICLES	28
2.3.3. FUEL CELL VEHICLES	30

2.4. BATTERY ELECTRIC VEHICLES	34
3. Smart Cell Design and Control Strategies.....	36
3.1. THE SMART CELL CONCEPT.....	36
3.2. SELECTION OF THE HYBRIDIZATION STRUCTURE	37
3.2.1. PASSIVE COMBINATION	38
3.2.2. ACTIVE COMBINATION	39
3.3. THE DC/DC CONVERTER	40
3.3.1. CONVERTER TOPOLOGY SELECTION	40
3.3.2. PRINCIPALS OF OPERATION.....	42
3.4. CONTROL STRATEGIES.....	48
3.4.1. THE FILTERING STRATEGY	48
3.4.2. ULTRACAPACITOR STATE OF CHARGE CONTROL	52
3.4.3. THE EQUALIZATION STRATEGY	53
3.4.4. EXTRA MITIGATION STRATEGY	53
3.4.5. SUPERVISORY AND PROTECTION STRATEGY	54
3.4.6. SUMMARY OF CONTROL AND SUPERVISORY UNIT.....	55
3.5. THE CURRENT REGULATOR	55
3.5.1. PROPORTIONAL INTEGRAL CONTROLLER.....	55
3.5.2. DISTURBANCE REJECTION.....	57
3.5.3. ANTI-WINDUP.....	58
3.5.4. DIGITAL IMPLEMENTATION IN THE MICROCONTROLLER.....	58
4. The Prototype and Results	61
4.1. TEST LOAD PROFILE.....	61

4.2. THE SMART CELL PROTOTYPE: DESIGN AND SIMULATIONS	65
4.3. EXPERIMENTAL SET UP AND TEST RESULTS	74
5. Conclusion	88

List of Figures

Figure 1.1. Energy generation in Canada.....	2
Figure 1.2. Energy production in Ontario.....	3
Figure 2.1. Non-renewable energy availability forecast.....	7
Figure 2.2. CO ₂ added to the atmosphere.....	8
Figure 2.3. CO ₂ emissions per person for different countries.....	8
Figure 2.4. BP statistical review of world energy: world reserves for 2002 and 2020.....	10
Figure 2.5. Illustration of the battery state of charge.....	12
Figure 2.6. The discharge mechanism for a sample Li-Ion battery cell.....	15
Figure 2.7. Block diagram of a generic BMS.....	16
Figure 2.8. An ultracapacitor's physical structure.....	18
Figure 2.9. Normalized OCV for various batteries and a typical ultracapacitor.....	19
Figure 2.10. An individual fuel cell's structure and operation.....	21
Figure 2.11. Ragone plot.....	22
Figure 2.12. Series hybrid structure.....	24
Figure 2.13. Energy flow in the parallel hybrid configuration.....	25
Figure 2.14. Energy flow in the parallel-through-the-road configuration.....	26
Figure 2.15. Energy flow in the series/parallel configuration.....	27
Figure 2.16. Planetary gears in series-parallel configuration.....	27
Figure 2.17. Transition from charge depleting mode to charge sustaining mode.....	29
Figure 2.18. Standards for vehicle charging systems.....	30

Figure 2.19. Honda FCX Clarity fuel cell car.....	31
Figure 2.20. A fuel cell/battery hybrid configuration.....	32
Figure 2.21. A fuel cell/ultracapacitor hybrid configuration.....	33
Figure 3.1. Smart cell configuration.....	36
Figure 3.2. Different possibilities to connect the battery and ultracapacitor cells.....	37
Figure 3.3. (a) Cascade buck-boost, (b) Half-bridge, (c) Cúk, (d) SEPIC converters.....	40
Figure 3.4. Half-bridge converter topology.....	42
Figure 3.5. Boost operation in the half-bridge converter during T_{on}	43
Figure 3.6. Boost operation in the half-bridge converter during T_{off}	43
Figure 3.7. Buck operation in the half-bridge converter during T_{on}	46
Figure 3.8. Buck operation in the half-bridge converter during T_{off}	46
Figure 3.9. Power sharing inside the smart cell.....	49
Figure 3.10. High pass filtering of an arbitrary signal.....	51
Figure 3.11. The effect of the adaptation algorithm on the filtering strategy.....	51
Figure 3.12. Filter adaptation algorithm.....	52
Figure 3.13. Fast equalization for a fully charged and discharged ultracapacitor cells....	53
Figure 3.14. Extra compensation gain as a function of state of charge.....	54
Figure 3.15. Smart Cell Control and Supervisory Unit.....	55
Figure 3.16. A simplified model of the converter.....	56
Figure 3.17. Control loop of the current regulator.....	56
Figure 3.18. Implementation of active damping for disturbance rejection.....	57
Figure 3.19. Complete control loop of the smart cell.....	58
Figure 4.1. Pack current demanded under normal highway drive cycle, WHEFT.....	62

Figure 4.2. Pack current demanded under harsh highway drive cycles, US06.....	62
Figure 4.3. Pack current demanded under normal urban drive cycle, UDDS	62
Figure 4.4. Pack current demanded under harsh urban drive cycles, LA92	63
Figure 4.5. Cell level current demanded under normal highway drive cycle, Load 1	63
Figure 4.6. Cell level current demanded under harsh highway drive cycles, Load 2.....	64
Figure 4.7. Cell level current demanded under normal urban drive cycle, Load 3	64
Figure 4.8. Cell level current demanded under harsh urban drive cycles, Load 4.....	64
Figure 4.9. Simulation of the converter in PLECS in the boost mode.....	67
Figure 4.10. Simulation of the converter in PLECS in the buck mode	67
Figure 4.11. The power converter's operation in boost mode (Simulated in PLECS)	68
Figure 4.12. The power converter's operation in buck mode (Simulated in PLECS)	69
Figure 4.13. Simulation of the smart cell in SIMULINK.....	70
Figure 4.14. The battery's current compared to the test load	71
Figure 4.15. RMS of the battery current is decreasing as a result of hybridization	72
Figure 4.16. Percentage of the battery RMS current decrease for the smart cell	72
Figure 4.17. The SOC stress factor is decreasing as a result of hybridization	74
Figure 4.18. Percentage of the SOC stress factor decrease in the smart cell	74
Figure 4.19. Experimental set up to evaluate smart cell's performance.....	75
Figure 4.20. The control panel including generation, acquisition, and monitoring.....	76
Figure 4.21. The data acquisition module that captures and logs the signals.....	76
Figure 4.22. The prototype circuit inside the test chamber.....	77
Figure 4.23. Load sharing in a snapshot of the oscilloscope compared to the simulation	78
Figure 4.24. Load sharing in a snapshot of the oscilloscope compared to the simulation	78

Figure 4.25. Results under Load 1 / Demand, battery and ultracapacitor currents.....	79
Figure 4.26. Results under Load 2 / Demand, battery and ultracapacitor currents.....	80
Figure 4.27. Results under Load 3 / Demand, battery and ultracapacitor currents.....	81
Figure 4.28. Results under Load 4 / Demand, battery and ultracapacitor currents.....	82
Figure 4.29. Ultracapacitor's SOC throughout the experimental tests	83
Figure 4.30. Experimental battery cell voltage and SOC / Load 1	84
Figure 4.31. Experimental battery cell voltage and SOC / Load 2	84
Figure 4.32. Experimental battery cell voltage and SOC / Load 3	85
Figure 4.33. Experimental battery cell voltage and SOC / Load 4	85
Figure 4.34. RMS of the battery's current is decreasing as a result of hybridization	86
Figure 4.35. Percentage of the battery's RMS current decrease for the smart cell.....	86
Figure 4.36. The SOC stress factor is decreasing as a result of hybridization	87
Figure 4.37. Percentage of the SOC stress factor decrease in the smart cell	87
Figure A.1. The simulation set up in Autonomie.....	102
Figure A.2. Power transmission scheme in Autonomie, the simulation software.	103
Figure A.3. Simulation of the smart cell / Electric Power System	104
Figure A.4. Simulation of the smart cell / Current Regulator.....	105
Figure A.5. Simulation of the smart cell / Power Management Unit	105
Figure A.6. Simulation of the smart cell / Extra mitigation (left), Equilizaer (right)	106
Figure A.7. Simulation of the smart cell / Ultracapacitor's SOC controller.....	106
Figure A.8. Simulation of the smart cell in SIMULINK / The Adaptation Algorithm ..	107
Figure A.9. Calculation of SOC stress factor in MATLAB	107
Figure A.10. The data acquisition chassis NI cDAQ-9188.	108

Figure A.11. NI 9264 analogue output module.	109
Figure A.12. Analogue input modeules used to capture signals for further analysis	109
Figure A.13. Half bridge drive circuit	110
Figure A.14. Pinout for PIC18F45K20.....	111
Figure A.15. Oscillator connection of the microcontroller.....	111

List of Tables

Table 1. Some standards related to electric vehicle charging.....	29
Table 2. Characteristics of battery electric, hybrid electric, fuel cell electric vehicles ...	35
Table 3. Selected drive cycles for the test pupose in this study.....	61
Table 4. Li-Ion battery cell characteristic	65
Table 5. Maxwell ultarcapacitors.....	66
Table 6. DC/DC converter characteristics	66

1. Introduction

1.1. Research Motivation

Fossil fuels still play a necessary role in the global energy market. Crude oil, gas, and coal are the primary energy resources for current demands. However, finite fossil fuel resources, environmental concerns, health problems, price fluctuations, and growing political tensions have led to the need for finding a sustainable alternative.

The transportation sector accounts for a considerable portion of total fossil fuel consumption. Despite the tank to wheel efficiency of around 12 to 18%, internal combustion engines have been the source of choice for vehicle propulsion with exceptional range and performance [1]. The traditional process of the energy extraction inside the combustion engine is highly afflicted with significant losses. Replacing it with a more efficient electric motor not only improves total fuel economy but also provides the possibility of recapturing kinetic energy and storing it for future usage. The whole idea leads to an overall increase in fuel efficiency.

The issue of fuel efficiency is also promoted by governments and legislatures officially. The direct result of stringent emission regulations has been that automakers have exceedingly begun to look into vehicles with alternative power sources. In hybrid electric

vehicles, the smaller internal combustion engine that is operating in an efficient region, as well as recapturing the energy while braking contribute to considerably higher overall efficiency. Electric vehicles with zero emissions have ignited the interest of automakers with growing consumer expectations. As projected in a report from international energy agency, 20 million passenger electric vehicles will be on the road by 2020 [2].

In Canada, the transportation sector accounted for 29.7 percent of energy use in 2008 while 78.9% is consumed on the roads [3]. The greenhouse gas emissions in transportation sector equaled 179.2 megatons in 2012 that accounted for 47% of the direct end-use emissions. In fact, transportation by itself emits more greenhouse gas than any other end-use sector in Canada [4]. But, Canada has a clean power mix especially in Ontario where 83% of the electricity is generated from non-fossil fuel as shown in Figure 1.1 and Figure 1.2 [5].

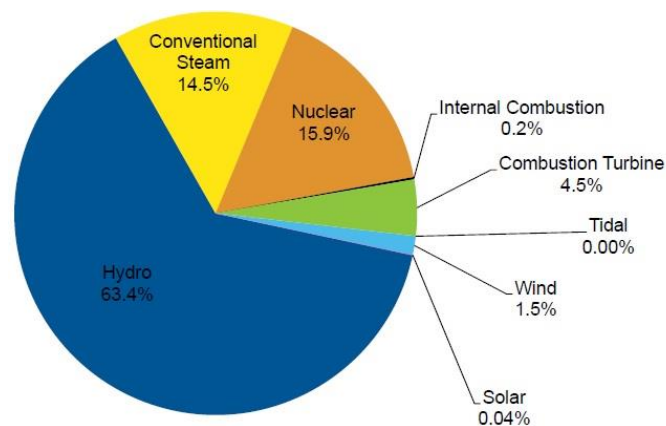


Figure 1.1. Energy generation in Canada [5]

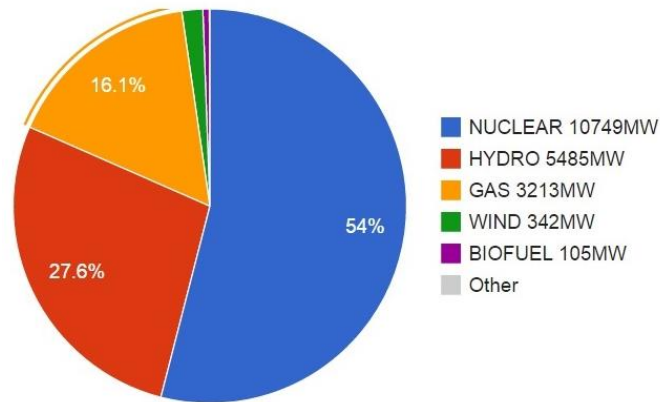


Figure 1.2. Energy production in Ontario [5]

1.2. Problem Statement

As the most common electrical energy storage, batteries would be the technology of choice. But, despite all the advances in the battery technology the currently available batteries seem to be too premature to be implemented in commercial systems. In other words, the technical expectations exceed the capabilities of standard batteries.

On the other hand, the current battery technology suffers seriously from lifetime issues. The battery cells are very sensitive to voltage and current ratings, temperature, and mechanical stresses which necessitates careful battery monitoring. Currently, their operating lifespan compromises their broad adoption in electrified vehicles in the automotive sector.

1.3. Research Objectives

Ultracapacitors have emerged as an attractive option with higher power capabilities, and much longer cycle and shelf life than batteries. Consequently, durable energy storage with an acceptable energy density of batteries and power density of ultracapacitors could be achieved by the combination of these two technologies. This research proposes a hybrid cell called the smart cell which is composed of one Li-Ion battery and one ultracapacitor forming a singular cell. This hybrid cell is intended to improve the battery life and power capabilities while providing modularity and low-level access to individual cells. In this research, the following issues are addressed:

- Investigation and selection of an appropriate hybridization scheme for the smart cell.
- Design and implementation of a switched mode power converter for hybridization.
- Design and implementation of the power management unit that is able to execute sophisticated control algorithms and has the capacity to initiate bidirectional links with the battery management unit and other cells.
- Design and implementation of a digital current regulator to realize control schemes of the power management unit by providing the proper duty cycle for the power converter designed.
- Design and development of a monitoring system to guarantee safety by keeping cells within safe operational limits while being able to respond to emergency cases.
- Design and implementation of a prototype smart cell and a testbed capable of capturing and logging real-time data to test the smart cell experimentally.

1.4. Thesis Outline

This thesis is divided into five chapters. Chapter one covers the introduction, the motivation for this research, and the objectives of this study. Chapter two offers an overview of the transportation electrification. The necessity of the change is discussed in details followed by considering alternative advanced energy sources. Chapter three provides the technical definition of the smart cell as well as a detailed illustration of the design specifications. The proposed power management strategies and the current regulator are also discussed in details. Chapter four demonstrates the prototype development with technical details. The testing procedure and the test setup is illustrated and the measurement/logging system is explained. Finally, chapter five provides a conclusion to this dissertation. Future recommendations are also included.

2. Transportation Electrification

2.1. The necessity of change

Our life is impacted by energy and energy has been extremely crucial for the continued development of humanity. The global demand for energy continues to increase with population growth, urbanization, and modernization. This increase in the global demand for energy is projected to rise sharply over the years to come. As such, the continuation of our current form of consumption will result in multiple challenges. In the following section, some of these challenges are discussed.

2.1.1. Sustainability

Access to a bountiful supply of safe, flexible in use, reliable, and affordable energy is indispensable to modern life. The dilemma of predicting the time that current non-renewable energy will be depleted is a fundamental and critical question investigated thoroughly in [6]. Figure 2.1 shows limited availability of non-renewable energy resources. Sustainability dictates a transition to renewable sources of energy such as solar, wind, and geothermal as a remedy to the sustainability challenge. The worldwide projection of growth for this sector is expected to be in the range of 15% to 25% by 2020 [7].

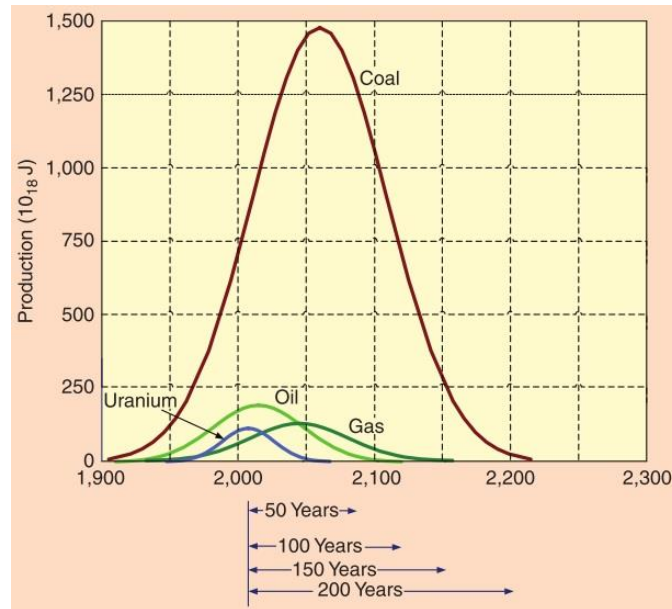


Figure 2.1. Non-renewable energy availability forecast [6]

2.1.2. Environmental Concerns

Present production and use of energy and consequent climate changes, particularly emissions of greenhouse gasses, poses severe threats to the global environment. Figure 2.2 demonstrates the effect of modernization on the dramatic increase in CO_2 emissions during the last 50 years. Half of the world oil is being consumed in the transportation sector. For example in the UK, road traffic in 1999 accounted for 77% of the petroleum consumed by that country [8]. Accordingly, a whole range of new policies are being examined to protect the environment while maintaining economic growth. Figure 2.3 shows CO_2 emitted to the atmosphere per person for different nations [9].

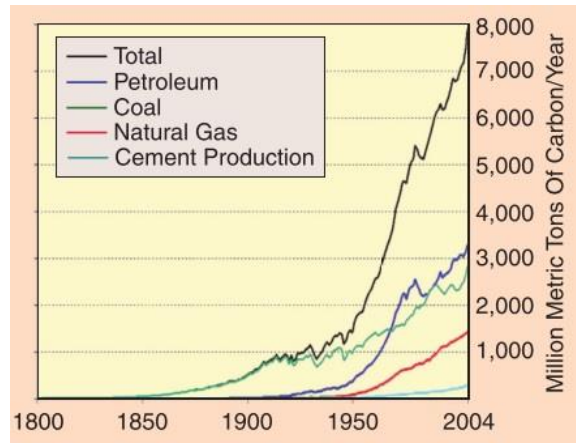


Figure 2.2. CO₂ added to the atmosphere [6]

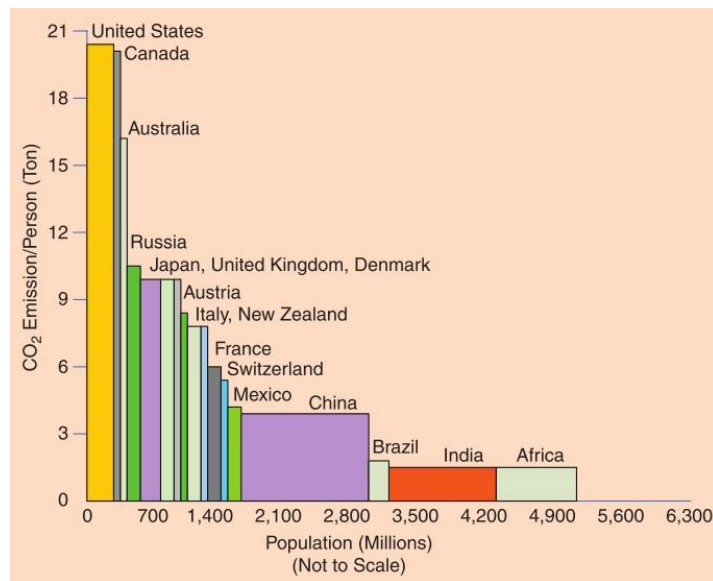


Figure 2.3. CO₂ emissions per person for different countries [6]

2.1.3. Health Issues

There is a direct and close link between fossil fuel extraction, refinement, and consumption versus environmental degradation. The level of pollution produced in the processes involved in refineries and power generation cause death and cancer and threatens human health and quality of life. The side effects of climate change account for the death of as many as 160,000 people as reported by the World Health Organization. Side effects range from malaria to malnutrition and diarrhea that follow in the wake of floods, droughts, and warmer temperature. The number, surprisingly, has the potential to double by 2020 [10].

2.1.4. Political Concerns

Energy supply security impacts all countries, and particularly the developed countries. Security means sufficient amount that is available consistently in various forms and affordable prices. There are serious considerations regarding the security of oil. As shown in Figure 2.4. BP statistical review of world energy: world reserves for 2002 and 2020 [10], 66% of current oil reserves in the world are distributed in Middle East [10]. Recent conflicts in that region show that the Middle East has a volatile geopolitical situation and therefore, production and supply channels are targets of radical elements. Millions of barrels of oil transported every day in tankers, pipelines and trucks are vulnerable. Current consensus indicates that the present situation is not sustainable and fails to guarantee secure supplies of energy.

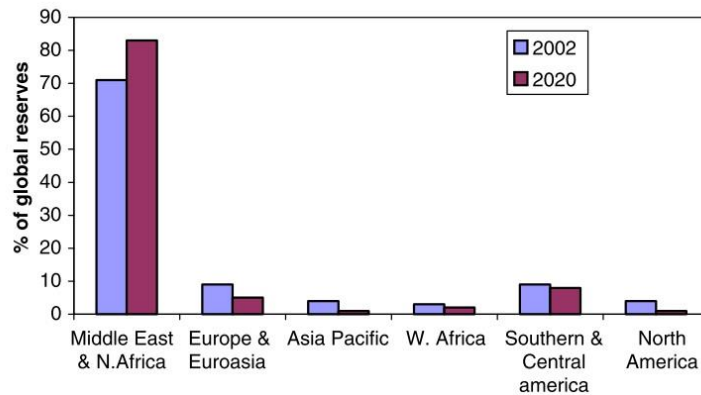


Figure 2.4. BP statistical review of world energy: world reserves for 2002 and 2020 [10]

2.2. Modern Energy Sources for Vehicular Applications

The recent revolution in power electronics has brought electric drivetrains with extremely high performance to the realm of possibility. Higher reliability and better performance are now available thanks to improved motors. Unfortunately, the only weak link remaining in this chain is energy storage.

Petroleum has high energy and power densities and comes at a reasonable price. But, an adequate replacement source that is capable of satisfying demands of modern vehicles is still unavailable. The most important characteristics of interest for electric energy storage in automotive applications are lifetime, specific energy, specific power, cost, and safety of the technology [11]–[14].

The onboard energy storage system is a challenge in the design of electrified vehicles. The electric energy may be stored electrochemically in a battery, chemically in hydrogen gas to be used by fuel cells, or electrostatically in a capacitor bank. In the following, different available alternatives for vehicular applications are discussed briefly.

2.2.1. Batteries

Batteries are the prevalent electric storage systems in the market presently. In an electric vehicle, batteries provide the traction force and store the energy recaptured while braking. Here are some basic definitions.

Battery Capacity: Battery capacity refers to the total accessible amount of energy. In vehicular terminology, the greater the capacity, the further the vehicle can travel. The capacity is expressed in “Ampere Hours” (Ah) or “Watt Hours” (Wh).

C-rate: It describes the current at which the battery is charged or discharged compared to its capacity. For instance, 1C is the current that can discharge a fully charged battery in 1 hour. For a battery with the capacity of 10 Amp-hour, 1C equals 10 Amps of charge or discharge current.

Energy Density: Refers to the energy a battery can store per unit volume or mass and is typically expressed in kWh/kg . In plug-in hybrid electric vehicles and battery electric vehicles, space is very limited. Therefore, a high energy density by volume will enable the vehicle to store more energy and have a greater “all electric” range.

Power Density: Refers to the power that a battery can deliver per unit volume or mass, and is typically expressed in kW/kg . Higher power density enables a vehicle to achieve greater acceleration and dynamic performance.

State of Charge or SOC: State of charge or SOC in short provides a measure of the amount of electric energy stored in a battery. It shows the remaining battery capacity like a fuel gauge on a conventional vehicle. The SOC is a dimensionless number between 0 and 1 representing a percentage. It is noteworthy that a zero SOC does not mean that the battery is fully empty, only that the battery cannot be discharged anymore without causing some permanent damage to it. Figure 2.5 shows this concept.

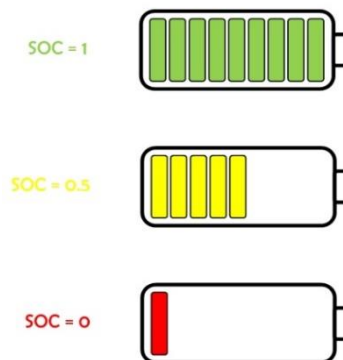


Figure 2.5. Illustration of the battery state of charge [15]

The Battery SOC provides the driver with an insight about how much energy is left in the battery. It is so critical for the driver especially if the battery is the only source of energy. The main challenge with SOC is that it cannot be measured hence requiring state and parameter estimation strategies [15]–[19].

Cycle Life: Refers to the number of charge and discharge times before the battery degrades past the point of usefulness. Assuming that a vehicle battery is drained and recharged once each day, the battery must have a cycle life of over 3600 cycles to meet a 10-year service life.

Calendar Life: Refers to the elapsed time before a battery degrades past the point of usefulness. A vehicle battery is idle most of the time, so degradation due to age must also be taken into account.

Li-Ion batteries are relatively new and are currently undergoing growth and development. They have already become the dominant choice for applications requiring high energy densities and light weight, such as the vehicular applications of today. In 2009, rechargeable Li-Ion batteries accounted for 11% of the \$16.4 billion total battery demand in the United States. Also, Li-Ion batteries are expected to be the fastest growing battery type in the coming years. The 2008 European lithium rechargeable market was similarly sized at \$1.62 billion [20].

Li-Ion batteries offer advantages over other battery types in several areas. They have higher operating voltage than other kinds, depending on their particular chemistry. This feature allows for an equivalent power operation at a lower current draw, and the battery will last longer on a single charge. They have a high energy density, are lightweight and compact. Unlike NiCad and older NiMH batteries, Li-ion batteries do not exhibit any memory effect. Also, Li-Ion batteries have long shelf lives. Additionally, they are capable of high discharge rates with high reversibility and good charge retention [21]. [22] provides a performance comparison between the NiMH battery by Primearth EV Energy Co. and the Li-ion battery by Hitachi Vehicle Energy Ltd. Also, [23] offers a concise review of batteries used in ground vehicles.

Common to all Li-ion battery types are the electrodes that are made of lithium intercalation compounds. Lithium ions travel between the two as the battery cycles. As with any galvanic cell, the two electrodes are separated from each other by an ionically conductive but electrically insulating medium. In a fully charged Li-Ion battery, the lithium ions are all intercalated into the anode and move through the electrolyte to the cathode during discharge. The discharge mechanism is shown in Figure 2.6.

The Li-ion battery has a complex aging process. It is not trivial to find an exact and universal relationship between the health of the battery and the precise factors that influence the health of the battery. There are, however, some different factors that in general affect the lifetime.

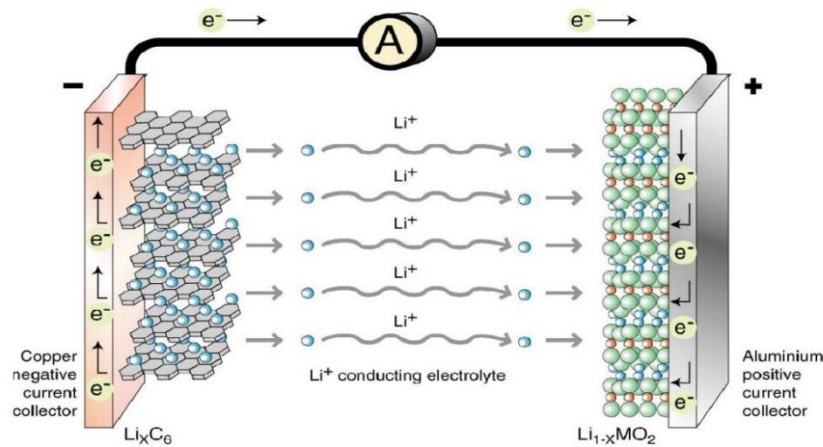


Figure 2.6. The discharge mechanism for a sample Li-Ion battery cell [20]

Either too high or too low SOC causes severe damages to the battery cell and the expected lifetime is shortened. Rather than over-charge, depth of discharge is an important parameter as well. For each charge-discharge cycle, depth of discharge should be kept as low as possible to optimize the life. For instance, it is better to have a depth of discharge of 20% rather than of 80%. This issue is a factor to consider mostly in hybrid vehicle applications. In electric vehicles, deep discharge is inevitable requiring a consideration of safety and preventing the over-discharge hazard [24].

Another important parameter in the aging process is temperature. One reason for increasing operating temperature is high current in combination with the battery's internal impedance. Power dissipates as heat and raises the temperature of the battery cell. A cooling system can manage this. High currents by itself also accelerates the battery's decay [21]. The Li-Ion battery is also damaged by excessively low temperatures, especially during charging, and should not be frozen [25].

As discussed earlier, accurate management, monitoring and control strategies are required to improve the performance, efficiency, safety, reliability and longevity of battery packs. Especially, in the case of vehicular applications, battery management systems play a significant role as the battery operating conditions are subjected to fast transients and frequent charging and discharging cycles due to sudden acceleration or regenerative braking. The battery management systems must also be able to provide an accurate real-time estimate of the state of charge, state of health, and remaining useful life [12], [26], [27].

The most basic battery management system implements under-voltage protection, over-voltage protection, maximum current limit, and thermal protection. Figure 2.7 demonstrates a basic battery management system in a simple form.

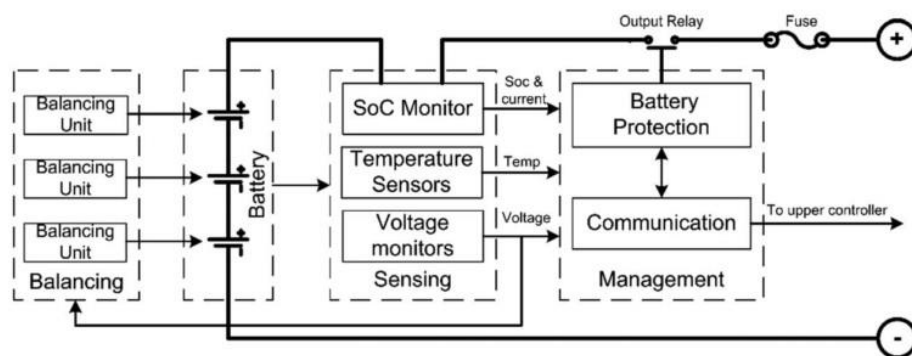


Figure 2.7. Block diagram of a generic BMS [1]

2.2.2. Ultracapacitors

Conventional capacitors store energy by physically separating unlike charges on two separate electrodes with a dielectric in between. This charge separation causes a potential between two electrodes. However, ultracapacitors do not use the electrolyte in the same way. The technology called electric double layer provides them a massive charge separation that results in very large capacitance. They are formed by two metal electrode foils coated with activated carbon, immersed in an electrolyte and separated by a paper separator as seen in Figure 2.8 [28].

Electrons accumulate in the electrode connected to the negative terminal and attract positive ions of the electrolyte. On the other electrode, positive charges accumulate attracting the negative electrolyte ions while current flows through the external load. The separator avoids current from flowing directly between both electrodes and causes the effect of having two charge layers, which is why ultracapacitors are also called electric double layer capacitors.

Since the electrodes are made of a porous material, the charge can be stored in the micropores at the interface between the electrode and the electrolyte. Moreover, the electrode surface significantly larger than a normal capacitor reaching $2000 \text{ m}^2/\text{gr}$ [29]. This combination of large surface and small separation between electrodes enables capacitances to reach thousands of farads. This structure has major implications on the properties such as cycle life, efficiency, energy and power density, and voltage as a function of SOC.

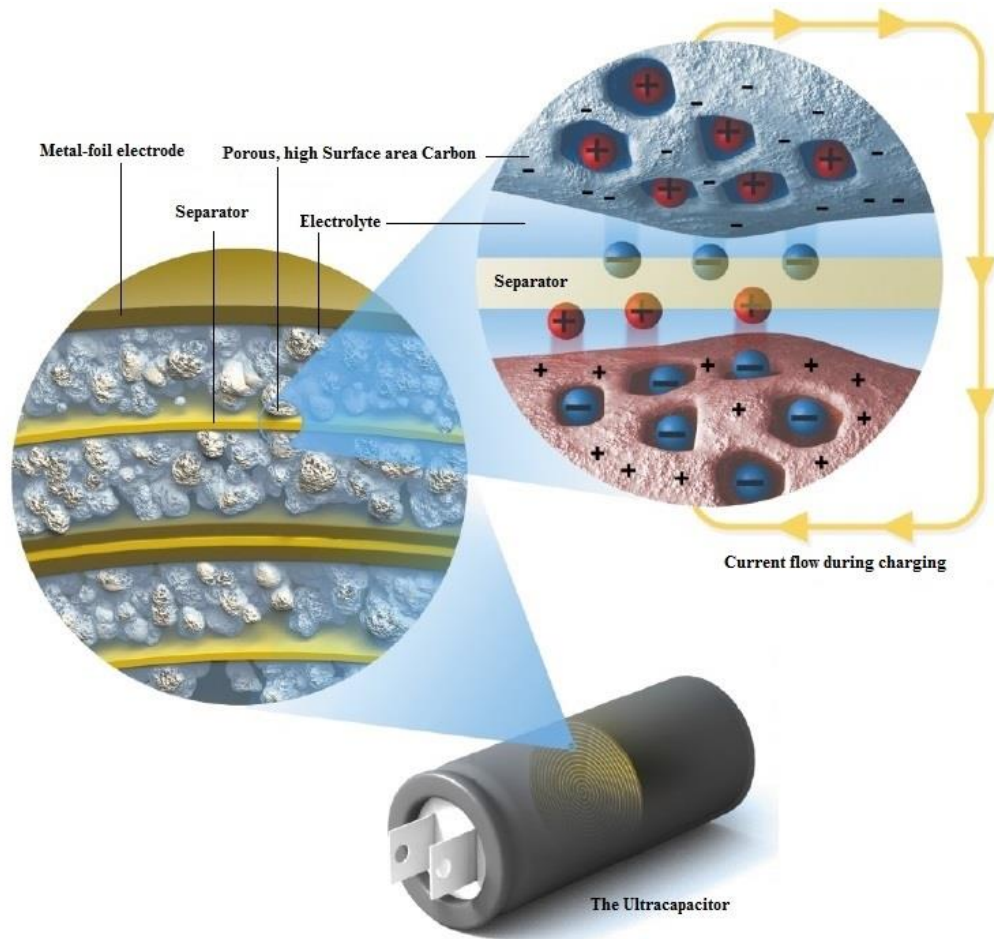


Figure 2.8. An ultracapacitor's physical structure [30]

Being able to release a significant amount of physically stored electric charge makes them extremely high power sources. Although power density is exceptional, energy density is low since the electrons are not bound by chemical reactions. This lack of chemical bonding also implies that the ultracapacitor can be completely discharged. Consequently, ultracapacitors will experience larger voltage swings as a function of the state of charge. Figure 2.9 depicts the linear dependency of ultracapacitor voltage to its state of charge.

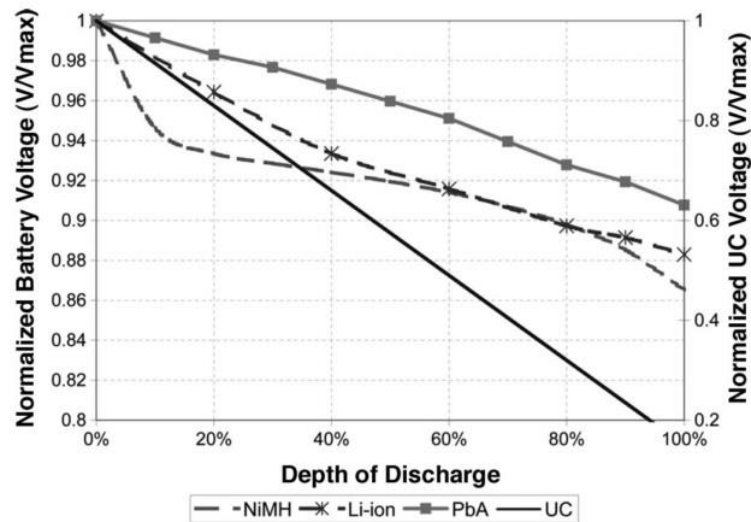


Figure 2.9. Normalized open circuit voltage for various battery chemistries and a typical ultracapacitor [1]

In addition to high power density, ultracapacitors present a long cycle life due to the fact that ideally there are no chemical changes on the electrodes in normal operation. They endure deep cycles at high rates often in numbers of more than hundreds of thousands without severely affecting their characteristics [31]. Moreover, ultracapacitors can be stored for long periods of time and remain near to their original conditions. Since the electric series resistance is very low in ultracapacitors, their efficiency is superior as a function of the ohmic resistance.

The aging process in an ultracapacitor is due to the increased reactivity of the electrolyte, which increases with impurities from reduction or oxidation. The aging leads to increasing internal resistance and self-discharge along with lower capacitance. The reduction process is accelerated by higher voltages. If the capacitor is subjected to high voltages or temperatures, its longevity is drastically shortened [32]. The lifetime is halved for each 100 mV or 10°C above the rated voltage or temperature [33]. Therefore, it is important to keep both the voltage and the current at reasonable levels, as high currents lead to RI^2 losses that generate higher temperatures.

2.2.3. Fuel Cell

Although recent literature portrays fuel cells as a newly emerging energy source, the technology was invented in the 19th century in 1839. In 1960, fuel cells were selected for the space program. They provided power for Gemini and Apollo missions, and at present, provide water and electricity for the International Space Station [34].

Fuel cells can generate power with high efficiency, low operating noise, and no emissions [28]. The input is hydrogen and air while by-products are exhausted gasses, water, and waste heat. Some types of fuel cells such as polymer electrolyte membrane or proton exchange membrane utilize a solid polymer electrolyte membrane. These fuel cells operate at lower temperatures and are considered to be suitable for vehicular applications [35]. Figure 2.10 illustrates the structure of an individual fuel cell.

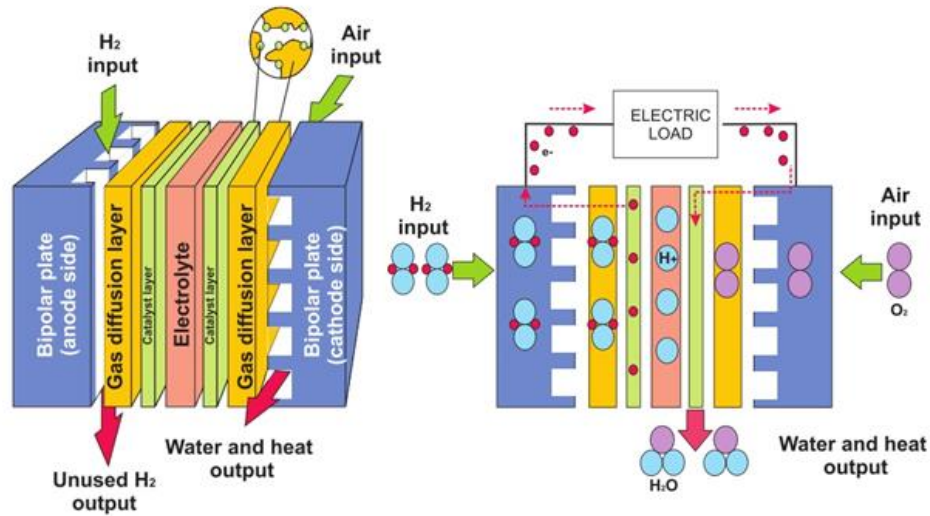


Figure 2.10. An individual fuel cell's structure and operation [28]

The constraints to operate a fuel cell can be summarized as follows [36], [37].

- The fuel cell power and current must be kept unidirectional and within an interval.
- The fuel cell current slope must be limited to the maximum absolute value to prevent the fuel cell stack from the fuel starvation phenomenon.
- The fuel cell's current ripple must meet specific conditions to ensure minor impact on the fuel cell conditions.

Marketable development of fuel cells is still facing problems. High manufacturing costs, fuel generation and distribution, and system complexity are some of the issues that have adversely affected its wider adoption [35]. The high manufacturing cost comes from costly raw materials used as catalyst or membrane such as platinum content of the electro catalyst, and the bipolar plates, and expensive fabrication process for collector plates [1].

2.2.4. Energy vs. Power

Conceptually, energy density describes how much energy is available while the power density shows how quickly that energy can be delivered. In the Ragone plot, energy density is plotted versus power density. The logarithmic axis allows comparing the performance of extremely high and extremely low densities.

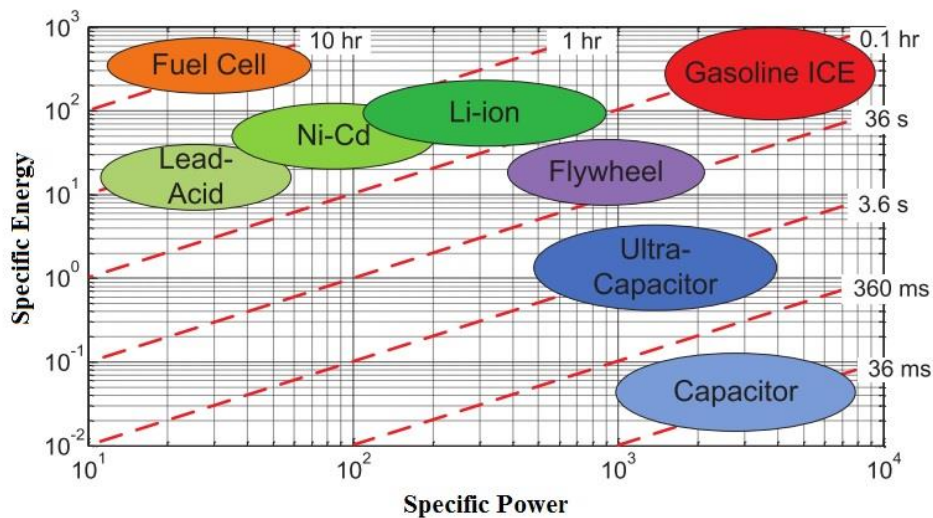


Figure 2.11. Ragone plot [38]

Figure 2.11 shows the superiority of Li-Ion batteries over other electric energy resources thanks to their high specific energy. Ultracapacitors have the highest power density among electric resources but with a poor energy density. Fuel cells possess the highest energy density, but they suffer from unacceptable power capability that limits their applications in the automotive industry. Unfortunately, none of the electric alternatives can beat energy and power of the fossil fuels yet as shown in the plot above.

2.3. Electric Vehicles

In a broad definition, electric vehicles are the ones augmented with the electric propulsion capability. Electric vehicles include hybrid and plug-in hybrid electric vehicles, fuel cell vehicles, and battery electric vehicles [11], [14], [39]. Except for hybrid and plug-in hybrid vehicles, fuel cell and battery electric vehicles do not have an engine on board and electricity is the sole energy form that is propelling the vehicle.

2.3.1. Hybrid Electric Vehicles

In a conventional vehicle, around 15% of the energy in gasoline is converted to traction at most [40]. Surprisingly, the efficiency is even lower at idle states. In hybrid electric vehicles, the power from the engine is combined with the power of an electric motor. A broad range of resources such as batteries, fuel cells, or ultracapacitors can supply the electric motor. Also, the efficiency can be doubled by using hybridization strategies [41].

Having an electric storage unit on board enables several energy-conserving features. First, a process called regenerative braking can recover the kinetic energy of the vehicle that was supposed to be wasted being converted to heat while braking. Also, the internal combustion engine can operate more frequently within its high-efficiency region which will reduce its fuel consumption significantly. Finally, the internal combustion engine can be downsized by augmenting the powertrain with an electric motor. The smaller engine will reduce the weight as well.

Different hybrid electric architectures are possible depending on the configuration of the internal combustion engine, the generator, the electric motors, and the battery pack.

I. Series Hybrid Configuration

In the series hybrid electric vehicles, the internal combustion engine provides mechanical energy to the generator, which produces electricity to charge the battery. The battery in turn drives an electric motor to propel the vehicle [42]. The two energy sources are thus in series. This configuration is illustrated in Figure 2.12.

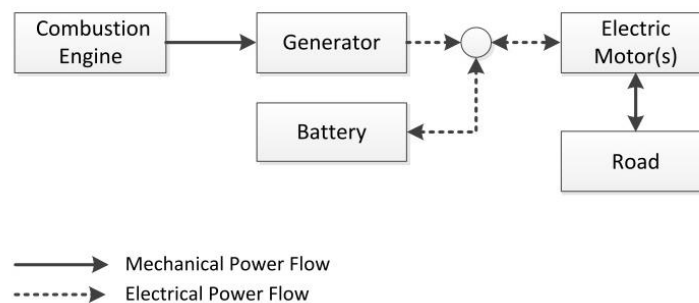


Figure 2.12. Series hybrid structure [20]

The main advantage of the series architecture is that the engine is mechanically decoupled from the road load. Therefore, it can be controlled always to operate in its narrow, efficient operating region. Although the internal combustion engine is maximally efficient in a series hybrid electric configuration, a penalty incurs in the rest of the powertrain due to the high number of energy conversions required and consequent losses [43].

II. Parallel Hybrid Configuration

In the parallel configuration shown in Figure 2.13, the mechanical power coming from both the motor and engine are transmitted directly to the drivetrain using a torque coupler. The connection between the engine and the torque coupler is typically clutched.

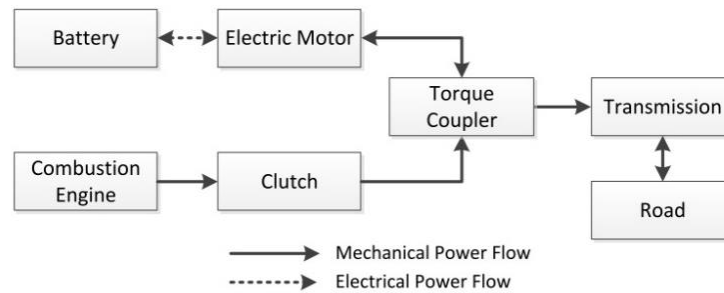


Figure 2.13. Energy flow in the parallel hybrid configuration [44]

Compared to the series hybrid electric vehicles, the parallel configuration requires a smaller engine. Parallel hybrid electric vehicles also have fewer powertrain losses than series since there are fewer energy conversion steps. The main disadvantage of the parallel architecture is that the engine cannot always operate within its efficient region. The engine speed depends on the vehicle speed since the engine is coupled to the road mechanically.

Although in this configuration the all-electric operation is feasible, the parallel hybridization architecture is not well suited as it would require upsizing the motor and the electric storage unit [20]. Three other operating modes are also achievable. First, the internal combustion engine can propel the vehicle only by itself. Second, the two energy sources can simultaneously provide power to the transmission. In the third mode, the engine produces power in excess of the road load to charge the storage unit.

III. Parallel-Through-The-Road Hybrid Configuration

In a variant of the parallel architecture, the torque coupling unit between the engine and the motor is removed, and the engine and the motor drive different axles of the vehicle. This configuration is called parallel-through-the-road. Figure 2.14 shows the energy flow in this structure. This hybridization scheme reduces weight, cost, and the complexity of the parallel architecture. The power is transferred from one axle to the other through the road to charge the battery if needed. Though this architecture is simple and inexpensive, the efficiency is too low due to the significant losses of transferring energy through the road.

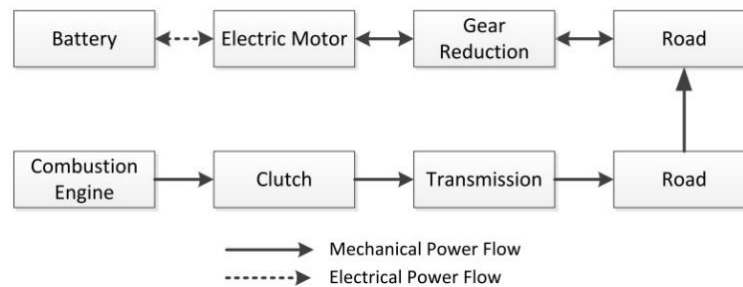


Figure 2.14. Energy flow in the parallel-through-the-road configuration [20]

IV. Series/Parallel Configuration

Series/Parallel architecture illustrated in Figure 2.15 is a combination of the series and parallel architectures. Similar to the series, the engine may operate in its highly efficient region while the providing torque to the wheels via mechanical linkages. This structure does not convert the energy to electricity such as in a parallel structure. The series/parallel architecture's ability to have both maximally efficient engine operation along with a mechanical energy pathway from the engine to the road is due to a torque splitting device.

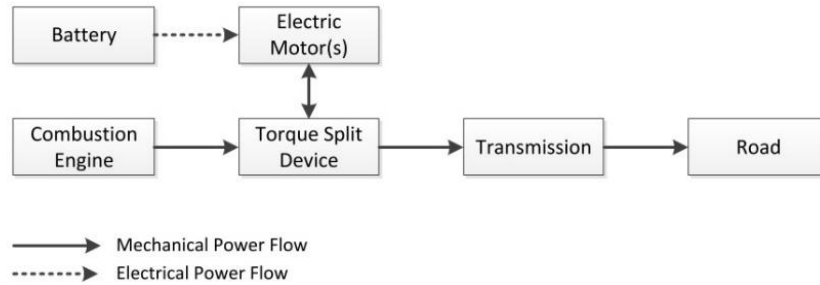


Figure 2.15. Energy flow in the series/parallel configuration [44]

There are several approaches to split the torque for series-parallel applications. One method utilizes a planetary gear set, as shown in Figure 2.16. The direct mechanical coupling of the ring gear to the first electric motor and the transmission shaft makes the vehicle speed a function of the ring gear speed. Also, the second electric motor is connected to the sun gear. The carrier holds the planet gears altogether connected to the internal combustion engine. Therefore, the carrier speed is a weighted average of the speeds of both motors.

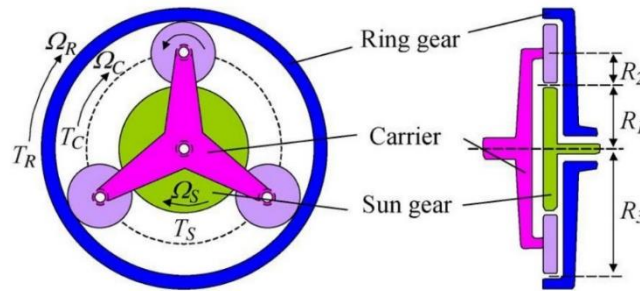


Figure 2.16. Planetary gears in series-parallel configuration [42]

Here is how the overall system works: the vehicle speed fixes the speed of the electric motor. By varying the second motor's speed, the speed of the carrier and the engine are controlled. Thus, the internal combustion engine can operate efficiently always.

All electric operation is also possible by controlling both electric motors such that the carrier speed is zero. Either regenerative braking or transferring power from the internal combustion engine through the sun gear to the second motor can charge the electric storage system [45]. Parallel and series/parallel hybrid electric vehicles can further be categorized by their level of hybridization [13]. Equation (2.1) defines the hybridization factor as follows. P_{EM} is the peak power of the electric motor and P_{ICE} is the peak power of the internal combustion engine.

$$HF = \frac{P_{EM}}{P_{EM} + P_{ICE}} \quad (2.1)$$

2.3.2. Plug-In Hybrid Electric Vehicles

In plug-in hybrid electric vehicles, the electric storage unit can be charged from the power grid. Two operating modes of charge depleting and charge sustaining are possible for this type of hybrid vehicles [46]. The charge depleting mode is for the cases that the electric storage unit is almost full. If the electric storage unit and motors have sufficient sizing, the vehicle can operate in all-electric mode [47].

Once the state of charge of the electric storage unit drops below a certain level, the internal combustion engine engages while working within its efficient operating range and the vehicle enters its charge sustaining mode. In this mode, the net energy in or out of the electric storage unit is zero and the vehicle operates like a hybrid electric vehicle [20]. The transition between charge depleting and charge sustaining regimes is shown in Figure 2.17.

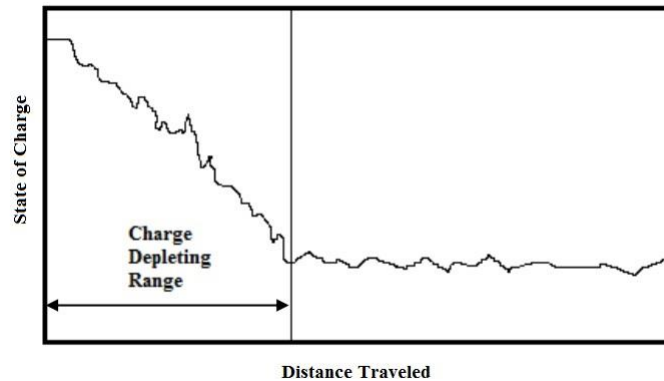


Figure 2.17. Transition from charge depleting mode to charge sustaining mode [46]

Homes and workplaces along with public areas are potential locations considered for charging stations. Regarding the energy transfer, connection interface and communication for vehicle charging, various standards have been developed [25], [48]. Table 1 and Figure 2.18 summarize some of the standards. These standards may be either updated with new revisions or replaced by new standards in the future.

Table 1. Some standards related to electric vehicle charging

Standard Name	Standard Title or Description
IEEE 1547.3	Interconnecting distributed resources with electric power systems
SAE J1772	Electric vehicle conductive charge coupler
SAE J1773	Electric vehicle inductively coupled charging
SAE J2293	Energy transfer system for electric vehicles
SAE J2836	Communication between plug-in vehicles and utility grid
IEC 62196	Plugs, socket outlets, vehicle couplers and vehicle inlets.
NEC (Article 625)	Electric Vehicle Charging System

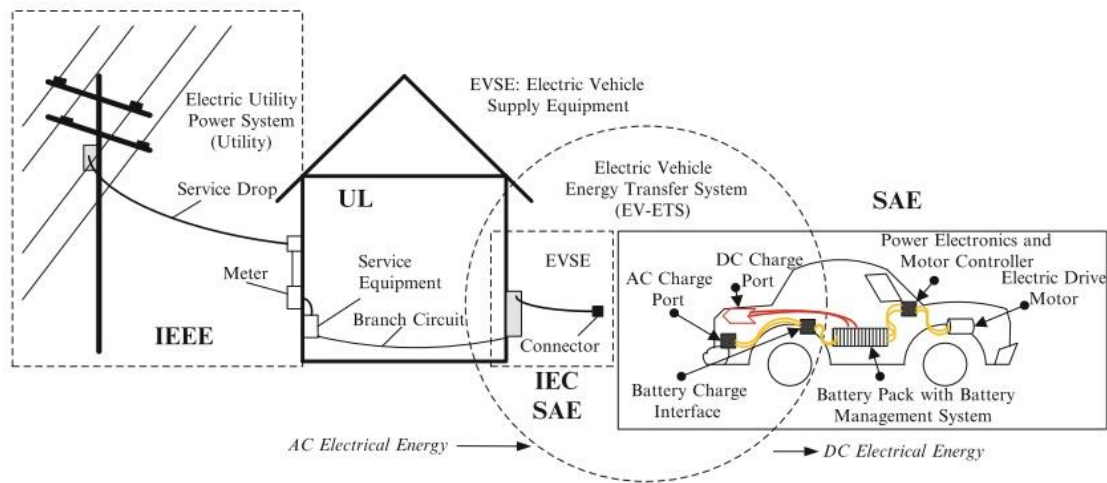


Figure 2.18. Standards for vehicle charging systems [22]

2.3.3. Fuel Cell Vehicles

Fuel cell vehicles use onboard fuel cells to generate electricity from hydrogen and air. The electricity is either used to drive the vehicle or stored in an energy-storage device, such as a battery pack or ultracapacitors. They emit only water vapor and have the potential to be highly efficient. Fuel cell vehicles can be considered as a type of series hybrid vehicle, in which the fuel cell acts as an electrical generator that uses hydrogen [49].

Fuel cell vehicles could be a long-term solution. There has been continuous progress in the fuel cell vehicle development. Although prototypes have already been proposed by manufacturers, the potential of fuel cell vehicles has yet to be proven. Price, hydrogen energy density, and refueling issues are major hurdles preventing commercial introduction of a mature design [50].

Despite high specific energy, one crucial weak point of the fuel cells is their slow dynamics. As a result, fast load demands in the case of the high power loads will result in severe voltage drops. This is recognized as starvation phenomenon [36]. This condition is evidently hazardous for the fuel cell stack [37]. Therefore, fuel cell applications in the vehicular context must include an auxiliary electric source which is able to improve system performance during high energy request during short time intervals. Figure 2.19 illustrates a sample commercial fuel cell vehicle. The electric storage unit is composed of high power density ultracapacitors that can provide demand surge while the high energy fuel cells provide a steady level of energy during driving course.

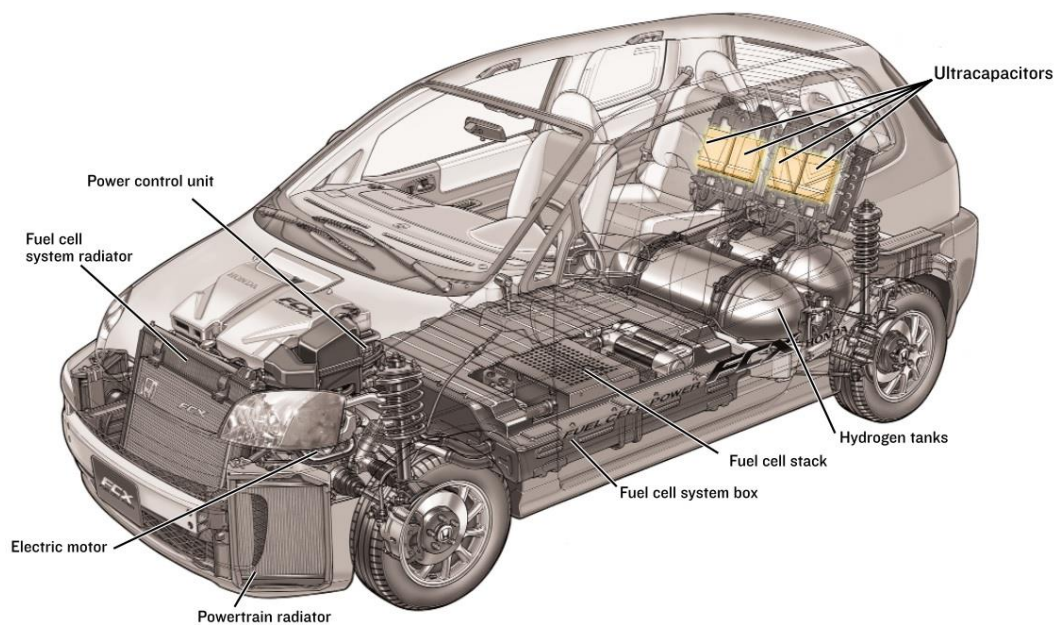


Figure 2.19. Honda FCX Clarity fuel cell car [30]

I. Fuel Cell/Battery Hybrid

In a fuel cell/battery hybrid, the battery stores regenerative braking energy, boosts power during accelerations, and propels the vehicle at low speeds to avoid low power operation of the fuel cell where its efficiency is low [51]. Connecting the battery to the DC bus improves the efficiency and decreases the cost by elimination of one power converter. As a result, the system will have unregulated bus voltage. Also, mechanical braking will be used if the battery is full [52]–[54]. A boost converter in the current control mode draws a certain amount of current from the fuel cell based on load condition. [35] provides a detailed overview of control strategies. Figure 2.20 shows fuel cell/battery hybrid.

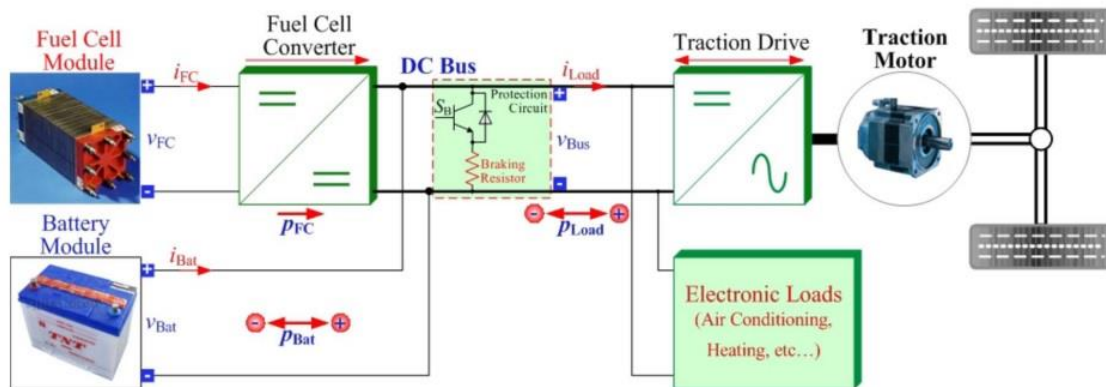


Figure 2.20. A fuel cell/battery hybrid configuration [35]

II. Fuel Cell/Ultracapacitor Hybrid

Fuel cell/ultracapacitor hybrid shown in Figure 2.21 consists of high energy fuel cells and high power ultracapacitors that absorbs sudden incoming power of regenerative braking and provides extra power during high demand acceleration [51]. Honda's FCX-V3 and V4 are commercialized vehicles of this type [30].

There is generally insufficient energy in the ultracapacitor pack to propel the vehicle at low speeds and the control strategy must ensure that the available energy capacity is utilized in the best way. Reference [55] compares three strategies and shows that keeping the sum of the kinetic energy of the vehicle and the energy stored in the ultracapacitor constant gives the best fuel economy. It is also noteworthy that the fuel cell can only provide electric energy and therefore, the possible interface converter should be unidirectional.

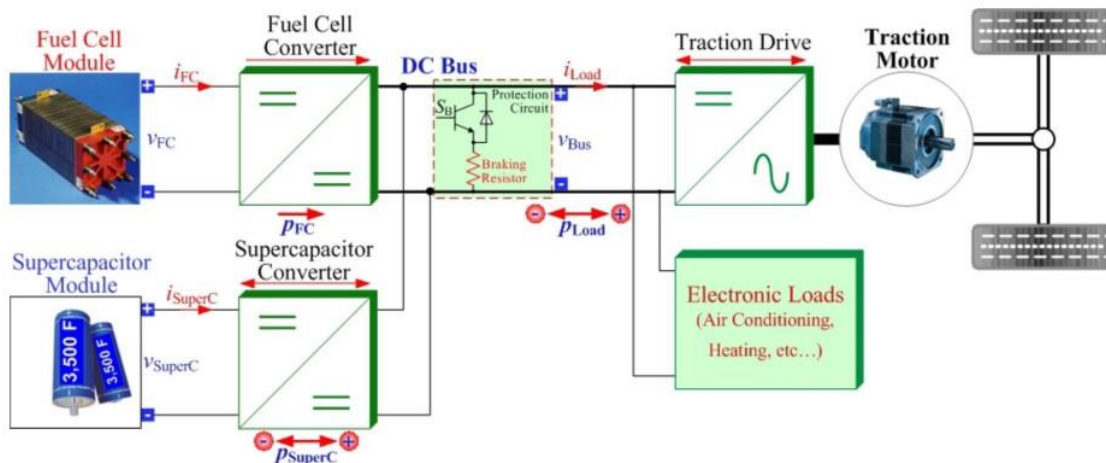


Figure 2.21. A fuel cell/ultracapacitor hybrid configuration [35]

III. Fuel Cell/Battery/Ultracapacitor Hybrid

The fuel cell vehicle can also be equipped with both batteries and ultracapacitors [59]–[63]. The onboard fuel cell produces electricity either for propulsion or to charge the battery or supercapacitor bank. The control strategy is to use the ultracapacitors to handle the bulk of the transient power demands. This strategy ensures that the battery lifetime is extended as a result of not being subjected to stresses while providing enough room to regeneration.

2.4. Battery Electric Vehicles

In a battery electric vehicle, the primary energy source is a battery pack that is being charged from the grid. Since battery electric vehicles do not have the traditional internal combustion engine, fossil fuel consumption is zero. To propel the vehicle, the energy from the battery is converted to the mechanical form using an electric motor. Also, the regenerative braking is a critical feature that impacts overall efficiency [38].

Compared to fossil fuels as the propulsion energy source, batteries have limited energy density and cycle life regardless of their technology. Excessive battery cycling in high power applications such as the transportation can accelerate the battery aging and reduce its lifetime as the primary energy source of this application. The combination of batteries with high power auxiliary electric storage can reduce the battery aging by eliminating harsh stresses in vehicular application. One favorable choice for hybridization of the battery technology is hybridization with ultracapacitors. Unlike batteries, ultracapacitors have high power density and cycle life. But they suffer from low energy density. Combining batteries with ultracapacitors in the form of a hybrid energy storage system can potentially overcome their individual drawbacks. Incorporation of ultracapacitors, also mitigates stresses over the battery in the vehicular applications resulting in longer battery life.

Most of the research in this area are focused on combining battery and ultracapacitor packs directly or through power electronics [24], [31], [60]–[84]. Each pack is formed from the combination of individual cells. Each battery cell ages differently due to the slight differences in the cell manufacturing and their different operating conditions. Also, in order

to be able to have a more accurate estimate of the total remaining energy of the electric storage unit, we have to gain access to individual cells and communicate directly with each one. Hybridization at the cell level not only provides a more accurate insight of the condition of individual cells, but also solves the balancing, monitoring, safety, state of health, and state of charge estimation problems. Table 2 summarizes important features of modern electric vehicles.

Table 2. Characteristics of battery electric, hybrid electric, and fuel cell electric vehicles [42]

	Battery Electric Vehicle	Hybrid Electric Vehicle	Fuel Cell Vehicle
Propulsion	<ul style="list-style-type: none"> • Electric motor drives 	<ul style="list-style-type: none"> • Electric motor drives • Internal Combustion engine 	<ul style="list-style-type: none"> • Electric motor drives
Energy Storage System	<ul style="list-style-type: none"> • Battery • Ultracapacitor 	<ul style="list-style-type: none"> • Battery • Ultracapacitor • Fossil or alternative fuels 	<ul style="list-style-type: none"> • Hydrogen tank • Battery/Ultracapacitor needed to enhance power density
Energy Infrastructure	<ul style="list-style-type: none"> • Grid charging facilities 	<ul style="list-style-type: none"> • Gasoline stations • Grid charging facilities for plug-in 	<ul style="list-style-type: none"> • Hydrogen • Hydrogen provision infrastructure
Characteristics	<ul style="list-style-type: none"> • Zero local emissions • High energy efficiency • Independent of fossil fuels • Relatively short range • High initial cost • Commercially available 	<ul style="list-style-type: none"> • Low local emissions • High fuel economy • Long driving range • Dependence on fossil fuel • Higher cost than traditional vehicle • Commercially available 	<ul style="list-style-type: none"> • Zero local emission • High energy efficiency • Independent of fossil fuel (if not using gas to produce hydrogen) • High cost • Under development
Major Issues	<ul style="list-style-type: none"> • Battery sizing and management • Charging facilities • Cost • Battery lifetime 	<ul style="list-style-type: none"> • Battery sizing and management • Control, optimization, and management of multiple energy sources 	<ul style="list-style-type: none"> • Fuel cell cost, life cycle, and reliability • Hydrogen production and distribution infrastructure • Cost

3. Smart Cell Design and Control Strategies

3.1. The Smart Cell Concept

The smart cell is a cell-level hybridization of the battery cell with an ultracapacitor. It is composed of a Li-Ion battery cell, associated electronic circuitry, and an ultracapacitor. The objective is to have a hybrid cell with excellent energy and power capabilities and improved battery life. Figure 3.1 illustrates a simplified smart cell with the most relevant components.

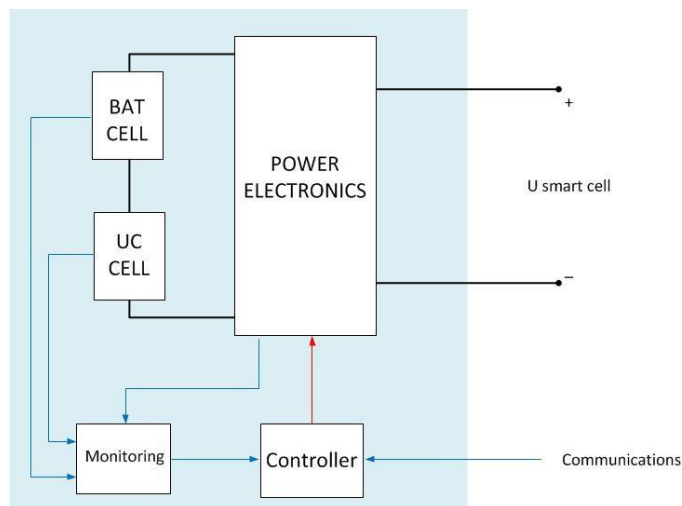


Figure 3.1. Smart cell configuration

Having the ultracapacitor included in the hybrid cell increases power density of the smart cell significantly compared to a battery cell alone. The improvement in the battery's life is achieved by using the ultracapacitor as a power source to handle highly dynamic loads including peak power demands and regenerative surges. Incorporation of sophisticated algorithms guarantees demand satisfaction while mitigating stresses over the battery.

The smart cell has local process and control capabilities. Each cell can communicate with other cells in the module, local supervisory unit, or the pack management system. As a result, the management system has a meticulous insight of all individual cells inside the pack such as temperature, terminal voltage, and load current.

3.2. Selection of the Hybridization Structure

There are four possible hybridization structures shown in Figure 3.2.

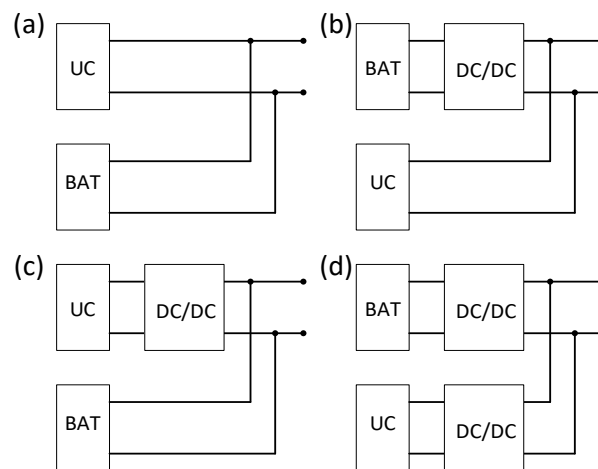


Figure 3.2. Different possibilities to connect the battery and ultracapacitor cells

3.2.1. Passive Combination

As shown in Figure 3.2-A, the battery and the supercapacitor are linked to the DC bus directly to deliver power. The advantage of the passive topology is its ease of implementation. Also, no complicated control is necessary. The first problem with this structure is the different voltage ratings for the battery cell and the ultracapacitor. For instance in this research, the Li-Ion battery's operation range is 2.8V to 4.2V while the ultracapacitor cell can tolerate up to 2.7V.

The other limitation of the passive structure lies in managing the power flow. As discussed in section 2.2.2, the ultracapacitor needs a wide voltage range variation to discharge or charge significant amounts of power. This large voltage range is in complete opposition to the smaller voltage change of batteries. Thus, the battery will prevent the ultracapacitor from being discharged, and the ultracapacitor will fail to maintain power efficiently [64], [86].

The bottom line is that the advantages of the battery and the supercapacitor are not effectively utilized in the passive combination. Therefore, the passive structure is not applicable when flexible and efficient power management is needed. To conclude for the smart cell application, option A in Figure 3.2 does not fit the design requirements. It is, more usual to find the battery and ultracapacitor interfaced with DC/DC converters to provide voltage flexibility while keeping the power flow under control. The converter can be single, on only one storage system, or on both.

3.2.2. Active Combination

Compared to the passive combination, active structures require a more sophisticated power electronics and control. To fully utilize the capabilities of the supercapacitor and the battery cell, we can employ two DC/DC converters as Figure 3.2-D suggests [64], [71], [86]. This structure exhibits the advantage in being able to impose a comprehensive control scheme. Besides, it increases the flexibility enabling the system functioning in various modes [87]. However, the cost, electric losses, and the volume and mass of realizing such a topology are significantly higher compared to the other alternative topologies. For our application where hundreds of smart cells must be used in a pack, the mass and the volume are serious concerns. Therefore, this combination is disregarded for the smart cell design.

In Figure 3.2-B and Figure 3.2-C where only one DC/DC converter is used, the power flow to the battery could be maintained while the supercapacitor is acting as a buffer [69]. Considering the fact that each battery cell ages differently due to slight differences in cell manufacturing and its position in the pack, configuration B in Figure 3.2 provides an active balance in pack design [88]–[90]. On the other hand, it is important for us to benefit from the buffering capability of the ultracapacitor in an efficient way. If the ultracapacitor is tied to the DC bus, its voltage will be fixed to the bus voltage. Therefore, the Li-Ion cell will be connected to the bus, and the ultracapacitor cell will be interfaced with the DC/DC converter as structure C in Figure 3.2. This structure enables the supercapacitor to function in a broad range of voltage independent of the battery [91]. Therefore, the structure C is selected to connect the ultracapacitor to the battery cell in a smart cell.

3.3. The DC/DC Converter

As discussed earlier, a DC/DC converter will interface the ultracapacitor. The modern converters have the ability to transform the voltage quickly. The plan here is to install a converter to control the power flow to and from the ultracapacitor depending on outer circumstances. These control strategies are designed to give a better system performance while mitigating the battery stresses. These strategies will be discussed in details.

3.3.1. Converter Topology Selection

There are a number of different power converter topologies that adjust the voltage level and control the power flow consequently. For this application, a non-isolated bi-directional operation seems necessary as the volume and mass are critical. In Figure 3.3, Cascade buck-boost, Half-bridge, Cúk, and SEPIC/Luo converters are shown respectively. This category of converters have a bi-directional power flow and the ability to raise the voltage level in one direction and lower it in the other [62], [80], [87], [92]–[102].

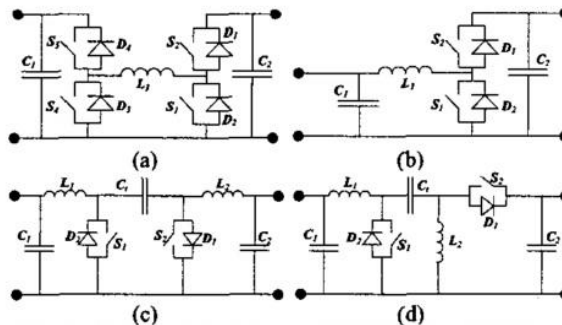


Figure 3.3. (a) Cascade buck-boost, (b) Half-bridge, (c) Cúk, (d) SEPIC/Luo converters [80]

For the proposed smart cell scheme, Cúk and SEPIC/Luo converters are not appropriate as they have two inductors that contribute to a higher price, volume, and weight. The buck-boost converter also has four switches in the structure making the circuit more expensive and less efficient because of the switching losses. Therefore, half-bridge DC/DC converter is selected for the smart cell application.

The half-bridge converter has the advantage that the number of components that is subjected to high currents is reduced. Also, one side always has to have a lower voltage than the other, which yields that the voltage over the supercapacitor can never exceed the battery voltage. This limitation is also consistent with the nominal voltage values of the battery and ultracapacitor in this research.

Since smart cell is a low voltage application, it is important to avoid diode forward voltage drop. Therefore, the switches will be triggered pairwise meaning that the lower switch is turned off when the upper switch is in on and vice versa. As a result of this pairwise gating strategy, freewheeling switch diodes can be eliminated resulting in less electronic parts per smart cell. One problem happens here as a result of physical characteristics of the electronic switches. It takes a while for an electronic switch to be fully turned off after receiving low trigger signal in the gate. Consequently, both switches may be conducting for a short time. This dangerous situation results in high amounts of shoot through current and can destroy components. The solution is to introduce a dead-time that gives a delay in the turn-on of each channel to give enough time for the other switch to be completely off. The dead-time will be implemented in the microcontroller which will provide the gating.

3.3.2. Principals of Operation

The functionality of the converter can be described as a buck, or boost converter depending on the direction of the average current through the inductor. The point of operation for the half-bridge converter depends on the voltages on both sides of the converter and the switching duty cycle. If the average inductor current is positive in the nomenclature of Figure 3.4. Half-bridge converter topology, the half-bridge functions as a step-down converter or buck. If the average inductor current is instead negative, the half-bridge is operating as a boost converter.

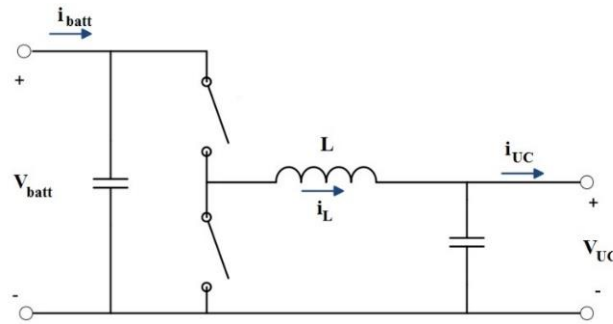


Figure 3.4. Half-bridge converter topology

It is worthwhile to mention that the half bridge converter selected for this application never reaches discontinuous mode [103]. The fact is that the power converter is bi-directional and has load and source on both sides. Instead, there is boundary when the inductor current reaches zero when the operation mode switches from boost to buck and vice versa.

I. The Boost Mode

For the boost mode operation, the gating signal of Q1 is a PWM signal with duty cycle D_{boost} and switching frequency f_{sw} where $f_{sw} = \frac{1}{T_{sw}}$. During T_{on} where the gating signal is high, Q1 closes and creates a short circuit in the first mesh as shown in Figure 3.5. The battery charges the inductance and the output capacitor supplies the load. During T_{off} as Figure 3.6 illustrates, the gating signal of both switches change their state. Thus, the energy stored in the inductor during the short circuit is being released on the other side and both the capacitor and load are supplied.

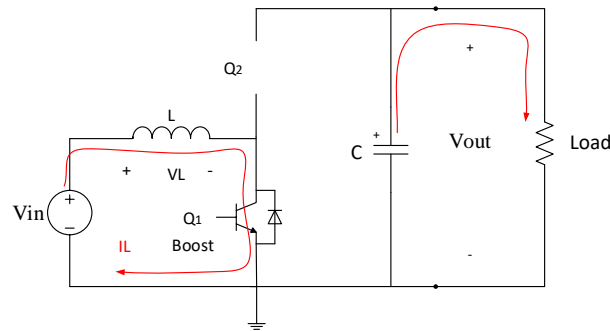


Figure 3.5. Boost operation in the half-bridge converter during T_{on}

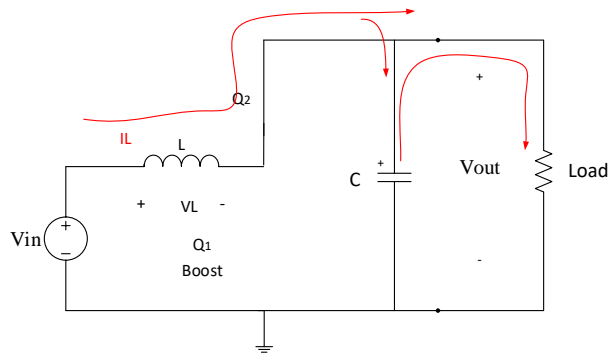


Figure 3.6. Boost operation in the half-bridge converter during T_{off}

For the boost mode, the following equation holds:

$$V_{out} = \frac{1}{1 - D_{boost}} \cdot V_{in} \quad (3.1)$$

D_{boost} is the duty cycle ranging between 0 and 1. Then, $\frac{1}{1 - D_{boost}}$ is a value larger than 1 and the output voltage will be boosted.

It is also important to calculate the inductance for the power converter. The inductance limits the current ripple. Therefore, the acceptable ripple value for the application will determine the inductance value. The inductor's voltage is related to its current as follows.

$$v_L(t) = L \frac{di_L(t)}{dt} \rightarrow di_L(t) = \frac{v_L(t) \cdot dt}{L} \quad (3.2)$$

During T_{on} we have $v_L = V_{in}$ as a result of the short circuit. The following equations hold.

$$\begin{aligned} \Delta i_L &= \frac{v_L \cdot \Delta t}{L} = \frac{v_L \cdot T_{on}}{L} = \frac{V_{in} \cdot (D_{boost} T_{sw})}{L} = \frac{V_{in}/V_{out} D_{boost} T_{sw}}{L} V_{out} \\ &= \frac{(1 - D_{boost}) D_{boost} T_{sw}}{L} V_{out} = \frac{(1 - D_{boost}) D_{boost}}{L \cdot f_{sw}} V_{out} \end{aligned} \quad (3.3)$$

The next step is to relate the ripple to the inductance. The ripple is defined as follows.

$$Ripple = \frac{\Delta i_L}{i_{Lavg}} \quad (3.4)$$

We need to calculate the average current flowing through the inductance. To obtain the average current, power balance is calculated knowing that the power stored in the battery should be then delivered.

$$P_{in} = P_{out} \Rightarrow V_{in} i_{Lavg} = V_{out} I_{out} \quad (3.5)$$

$$i_{Lavg} = \frac{V_{out}}{V_{in}} I_{out} = \frac{1}{1 - D_{boost}} I_{out} \quad (3.6)$$

Substituting in the ripple equation:

$$Ripple = \frac{\Delta i_L}{i_{Lavg}} = \frac{\frac{(1 - D_{boost})D_{boost}V_{out}}{L \cdot f_{sw}}}{\frac{1}{1 - D_{boost}} I_{out}} = \frac{D_{boost}(1 - D_{boost})^2}{L \cdot f_{sw} \cdot I_{out}} V_{out} \quad (3.7)$$

The inductance as a function of the acceptable current ripple will then be:

$$L_{boost} = \frac{D_{boost}(1 - D_{boost})^2}{Ripple \cdot f_{sw} \cdot I_{out}} V_{out} \quad (3.8)$$

II. The Buck Mode

Similar to the boost mode, two states can be defined for this mode. In the high state T_{on} , Q2 closes as a result of corresponding gating signal. Consequently, the load charges the output capacitor, the inductance and the input voltage source as Figure 3.7 shows.

During T_{off} or the low state, Q2 is open while Q1 is closed to provide a path for inductor's current. This scenario allows the inductance to charge the input source while the load supplies only the output capacitor as Figure 3.8 shows.

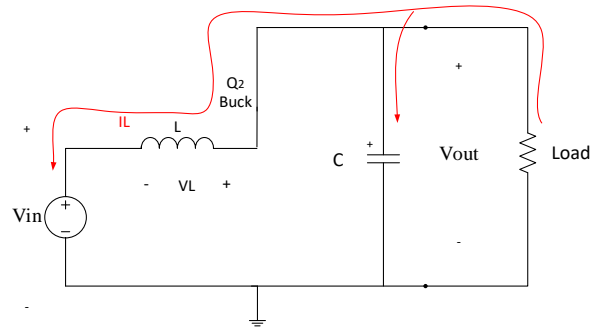


Figure 3.7. Buck operation in the half-bridge converter during T_{on}

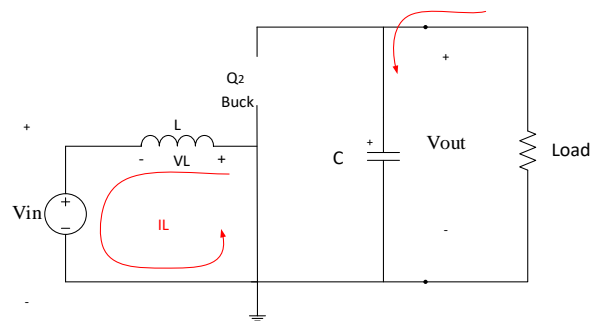


Figure 3.8. Buck operation in the half-bridge converter during T_{off}

For the buck mode, equation (3.9) holds. As the duty cycle is a value always less than 1, the buck mode operation is guaranteed.

$$V_{in} = D_{buck} \cdot V_{out} \rightarrow D_{buck} = \frac{V_{in}}{V_{out}} \quad (3.9)$$

The inductor voltage in this mode will be:

$$v_L(t) = L \frac{di(t)}{dt} \quad (3.10)$$

During T_{on} we have $v_L = V_{out} - V_{in}$ as shown in Figure 3.7. The following equations hold.

$$\begin{aligned}\Delta i_L &= \frac{v_L \cdot \Delta t}{L} = \frac{(V_{out} - V_{in}) \cdot T_{on}}{L} = \frac{(V_{out} - V_{in})(D_{buck} T_{sw})}{L} \\ &= \frac{(V_{out} - D_{buck} V_{out})(D_{buck})}{L f_{sw}} = \frac{(1 - D_{buck}) D_{buck}}{L f_{sw}} V_{out}\end{aligned}\quad (3.11)$$

$$Ripple = \frac{\Delta i_L}{i_{Lavg}} \quad (3.12)$$

We then need to calculate the average current flowing through the inductance. Similar approach is taken for the buck mode as well.

$$P_{in} = P_{out} \Rightarrow V_{in} i_{Lavg} = V_{out} I_{out} \quad (3.13)$$

$$i_{Lavg} = \frac{V_{out}}{V_{in}} I_{out} = \frac{I_{out}}{D_{buck}} \quad (3.14)$$

Substituting in the ripple equation:

$$Ripple = \frac{\Delta i_L}{i_{Lavg}} = \frac{\frac{(1 - D_{buck}) D_{buck}}{L f_{sw}} V_{out}}{\frac{I_{out}}{D_{buck}}} = \frac{D_{buck}^2 (1 - D_{buck})}{L \cdot f_{sw} \cdot I_{out}} V_{out} \quad (3.15)$$

The inductance will then be:

$$L_{buck} = \frac{D_{buck}^2 (1 - D_{buck})}{Ripple \cdot f_{sw} \cdot I_{out}} V_{out} \quad (3.16)$$

It is noteworthy that the inductor selected for the smart cell application will be the greatest of the values obtained from equations (3.8) for the boost mode and (3.16) for the buck mode. The equations will be used in the prototype design later in this thesis.

3.4. Control Strategies

With the devolvement of semiconductor-based power electronics, advanced power control has been available recently using switching circuits. Using the DC/DC power converter, it is possible to control current flow, voltage level, or power in other words. In this research, the power converter will be used to realize control algorithms with the target of improving battery's working conditions.

It is worth noting that the load on the terminals of a smart cell can be both positive and negative. Throughout the thesis, the negative load is defined as the power flowing into the smart cell's terminal as a result of the regenerative braking which corresponds to current flow into the circuit. The positive load is a demand over the smart cell's terminal while the current is flowing out.

3.4.1. The Filtering Strategy

As stated in section 2.2.1, the battery gets a longer life if exposed to less frequent charges and discharges, and with a reasonable load. The desirable condition is that the battery is isolated from peak current situations. Also, the high-frequency part of the load should be forwarded to the supercapacitor so that the battery cell is exposed to the low-frequency cycles. This strategy is implemented initially to catch up all transients that are detrimental to battery health. Figure 3.9 shows the power-sharing inside each smart cell which will be controlled and realized incorporating the DC/DC converter.

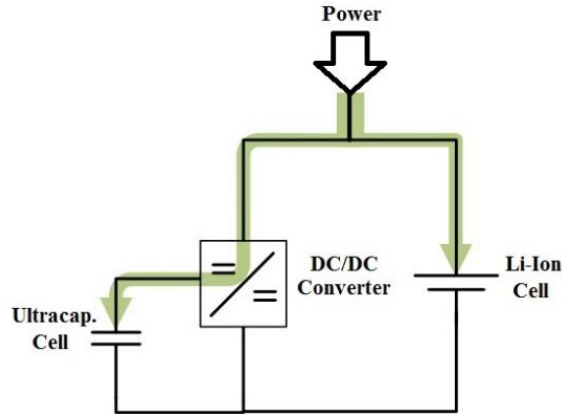


Figure 3.9. Power sharing inside the smart cell

A first-order high-pass filter described as (3.17) is designed to be implemented inside the microcontroller.

$$H_{HP}(s) = \frac{s}{\omega_c + s} \quad (3.17)$$

$\omega_c = 2\pi f_c$ where f_c is the cut-off frequency of the filter. The bilinear transformation is used with the sample time of T_s to discretize the filter.

$$s = \frac{2}{T_s} \frac{z - 1}{z + 1} \quad (3.18)$$

The discrete high-pass filter is formulated as follows:

$$H_{HP}(z) = \frac{Y(z)}{U(z)} = \frac{1 - z^{-1}}{a + bz^{-1}} \quad (3.19)$$

The filter coefficients are $a = \frac{\omega_c T_s}{2} + 1$, and $b = \frac{\omega_c T_s}{2} - 1$. To determine filter parameters, the step response of the filter and the corresponding time constant is considered. The realization of the filter then will be in the form of the equation below:

$$y_n = \frac{1}{a}u_n - \frac{1}{a}u_{n-1} - \frac{b}{a}y_{n-1} \quad (3.20)$$

This filter has a number of characteristics that are not acceptable for this application. The focus here is to charge the ultracapacitor only by regeneration as long as we can. Thus, the filtering should not force the battery to charge the ultracapacitor. This happens for instance when the load signal is positive and the filtered signal is negative. In such a condition, the battery should provide both the ultracapacitor and the load. The similar analysis is valid for negative terminal power as well.

In a completely different case where the filtered signal's amplitude exceeds the load as a result of the filtering, the ultracapacitor will actually be charging the battery. As discussed earlier, this is not favorable either because the effectiveness of the idea depends on the ability of the ultracapacitor to provide for sudden peak demands and absorb momentary regenerations. In other words, the filtering strategy should not force the ultracapacitor to discharge on the battery.

To make this clear, an arbitrary signal is filtered with the time constant of 5s, and the results are demonstrated in Figure 3.10. Then, the adaptation algorithm shown in Figure 3.12 is applied in addition to the filtering. The improved behaviour for the same arbitrary signal is shown in Figure 3.11.

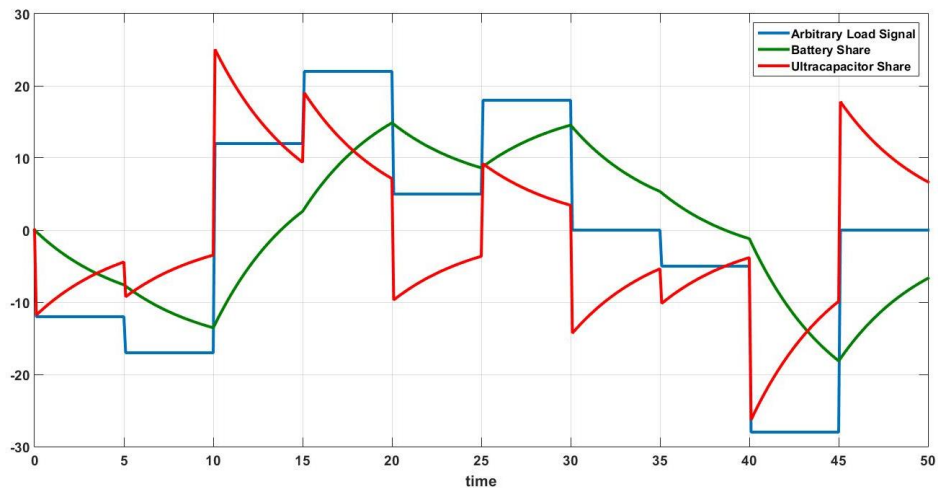


Figure 3.10. High pass filtering of an arbitrary signal

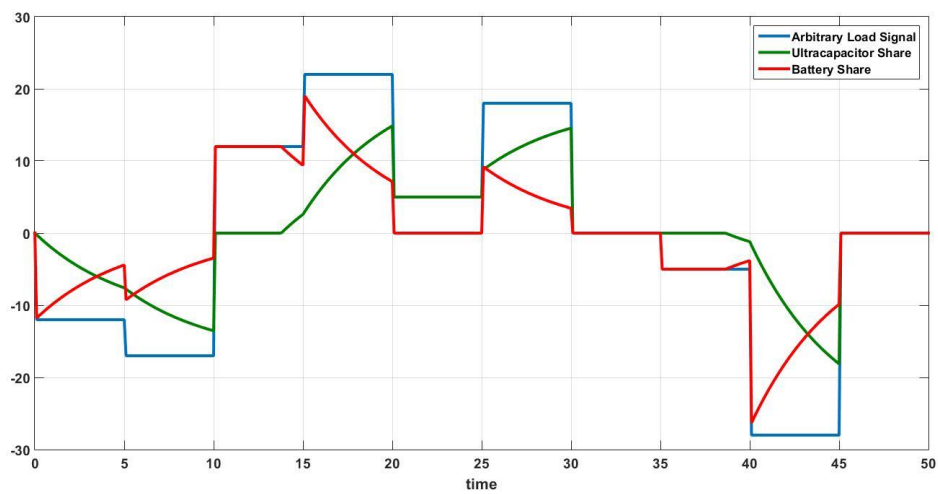


Figure 3.11. The effect of the adaptation algorithm on the filtering strategy of the smart cell

```
if sign(filtered) == sign(unfiltered)
    if abs(filtered) >= abs(unfiltered)
        out = unfiltered
    else
        out = filtered
    end
else
    out = 0
end
```

Figure 3.12. Filter adaptation algorithm

3.4.2. Ultracapacitor state of charge control

The ultracapacitor in the smart cell must always maintain a certain level of charge to be able to provide for sudden demands or power peaks to protect the battery. It should also keep enough empty room for sudden regenerations coming as a result of momentary braking. A dedicated controller is designed to try to maintain these conditions through the driving cycles to keep the smart cell effective. This SOC controller will be slower than the current regulator and therefore will not interfere with regulator's fast dynamics.

Due to practical considerations, the voltage of the ultracapacitor should not go below half of its maximum value. Since energy relates to voltage according to (3.21), the energy will swing between 25% and 100% of the maximum available amount.

$$SOC = \frac{E}{E_{max}} = \frac{(V)^2}{(V_{max})^2} \quad (3.21)$$

A PI voltage controller will be designed to keep ultracapacitor's SOC at $\frac{25+100}{2} = 62.5\%$ considering equation (3.21) that relates SOC to its voltage.

3.4.3. The Equalization Strategy

If the ultracapacitor is full, it should be engaged more in providing the demand. Likewise if it is empty, more power should be absorbed by the ultracapacitor. Both cases mitigate battery stresses further while helping the ultracapacitor SOC controller to maintain the predefined charge explained in 3.4.2. This strategy will add an extra portion to the ultracapacitor's share as a function of its state of charge illustrated in Figure 3.13.

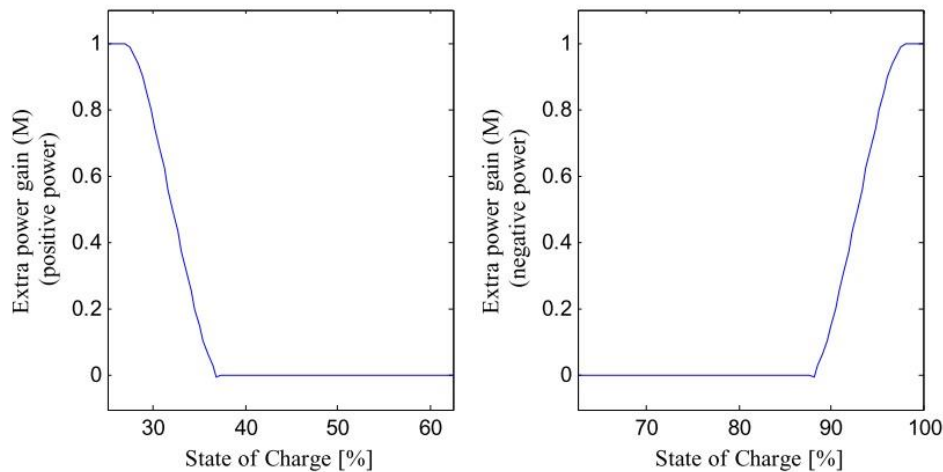


Figure 3.13. Fast equalization for a fully charged and discharged ultracapacitor cells

3.4.4. Extra Mitigation Strategy

If the ultracapacitor has the target charge level defined in 3.4.2, it is helpful to force the ultracapacitor to add an extra portion to its power share. As shown in Figure 3.14, the added share will be a function of ultracapacitor's state of charge. It will be maximum when the state of charge of the ultracapacitor is at the predefined value of 62.5% and will diminish as the ultracapacitor moves away from the set point charge.

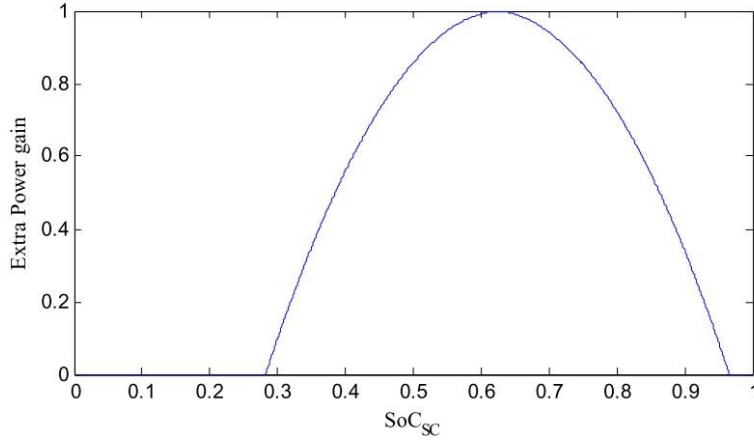


Figure 3.14. Extra compensation gain as a function of state of charge

3.4.5. Supervisory and Protection Strategy

To have a smooth protection of the ultracapacitor, soft and hard current limits are introduced. In the buck mode, the charging process is stopped if the ultracapacitor is full. But the charging is possible with a limited rate if the cell is near full. In the boost mode, discharge is possible with a limited rate if the cell gets near empty. But a hard lower limit is imposed if the cell is below a certain threshold. Equations (3.22) and (3.23) show the implementation of this protection. I_{ref} is the reference ultracapacitor current that is limited by a factor of M . The regulator will try to track this reference signal.

$$M = \begin{cases} 0 & I_{terminal} < 0 \text{ and } SOC_{UltraCap} \geq 100\% \\ -20 \cdot SOC_{UltraCap} + 20 & I_{terminal} < 0 \text{ and } SOC_{UltraCap} > 95\% \\ 1 & 30\% < SOC_{UltraCap} < 95\% \\ 20 \cdot SOC_{UltraCap} - 5 & I_{terminal} > 0 \text{ and } SOC_{UltraCap} < 30\% \\ 0 & I_{terminal} > 0 \text{ and } SOC_{UltraCap} \leq 25\% \end{cases} \quad (3.22)$$

$$I_{ref} = M \cdot I_c \quad (3.23)$$

3.4.6. Summary of control and supervisory unit

Figure 3.15 summarises proposed control strategies. I_c is the reference ultracapacitor current to mitigate stresses and relieve the battery while maintaining ultracapacitor's state of charge. I_c will be limited as a function of the state of charge of the ultracapacitor later.

Finally, $I_{reference}$ will be fed to the current regulator.

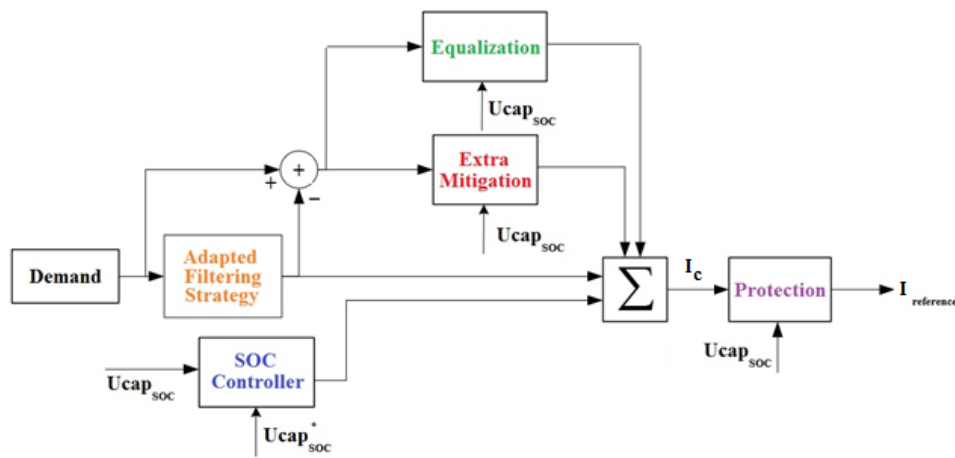


Figure 3.15. Smart Cell Control and Supervisory Unit

3.5. The Current Regulator

3.5.1. Proportional Integral Controller

A PI controller is implemented that is providing the duty cycle to control the converter. Thus, the output of the controller is bounded between zero and one. The regulator is parameterized according to the equation below, where y_{ref} denotes the reference signal.

$$e(t) = y_{ref}(t) - y(t) \Rightarrow y(t) = K_p e(t) + K_i \int_0^t e(\tau) d\tau \quad (3.24)$$

A simplified model of the converter is illustrated in Figure 3.16 .

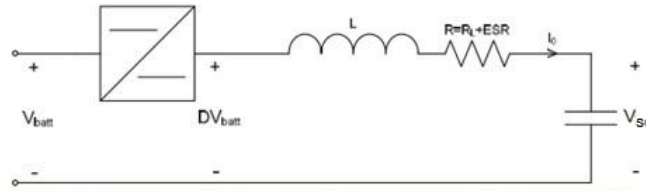


Figure 3.16. A simplified model of the converter

The current is related to the voltage across the inductor. For the current dynamics, the voltage across the supercapacitor V_{sc} is considered as a load disturbance to achieve a first order system. Since the time constant of the supercapacitor voltage is higher than that of the inductor current, this assumption seems to be reasonable. The simplified transfer function will be obtained as follows:

$$G(s) = \frac{I_{sc}(s)}{DV_{batt}(s) - V_{sc}} = \frac{1}{sL + R} \quad (3.25)$$

A block representation is shown in Figure 3.17. As the duty cycle D is a dimensionless parameter, the output of the controller will be divided by nonzero V_{batt} .

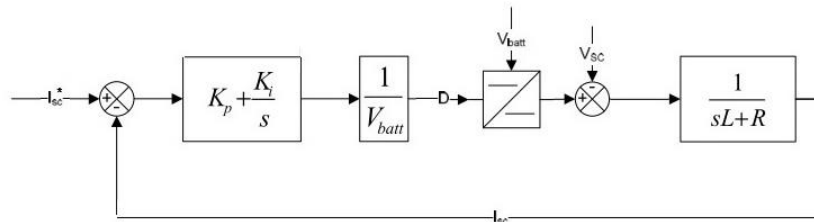


Figure 3.17. Control loop of the current regulator

A design method called “loop shaping” suggests that the desired first order closed loop system is specified as below where α is the bandwidth of the closed loop system [104].

$$T(s) = \frac{F(s)G(s)}{1 + F(s)G(s)} = \frac{\alpha}{s + \alpha} \quad (3.26)$$

To satisfy the equation above, we will have:

$$F(s)G(s) = \frac{\alpha}{s} \Rightarrow F(s) = \frac{\alpha}{s} G(s)^{-1} = \frac{\alpha}{s} (sL + R) = \alpha L + \frac{\alpha R}{s} \quad (3.27)$$

$$F(s) = K_p + \frac{K_i}{s} \quad (3.28)$$

$F(s)$ and $G(s)$ are the controller and the plant respectively in a unit feedback system. The equations above directly gives the regulator parameters that will set the bandwidth of the closed loop system. Practically, the values will be fine-tuned to achieve the best results.

$$K_p = \alpha L, K_i = \alpha R \quad (3.29)$$

3.5.2. Disturbance Rejection

The method called “active damping” introduced in [104] compensates for the first order transfer function approximation. This is illustrated in Figure 3.18

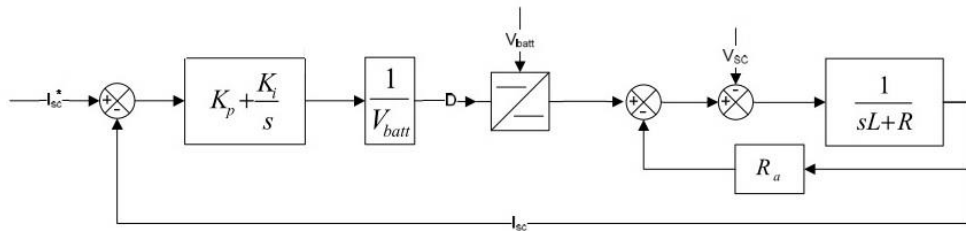


Figure 3.18. Implementation of active damping for disturbance rejection

The new transfer function will be as follows.

$$\hat{G}(s) = \frac{G(s)}{1 + R_a G(s)} = \frac{1}{sL + R + R_a} \quad (3.30)$$

Then we will have:

$$F(s)\hat{G}(s) = \frac{\alpha}{s} \Rightarrow F(s) = \frac{\alpha}{s} \hat{G}(s)^{-1} = \frac{\alpha}{s} (sL + R + R_a) = \alpha L + \frac{\alpha(R + R_a)}{s} \quad (3.31)$$

R_a is chosen to be $\alpha L - R$ which also gives new controller parameters as below:

$$K_p = \alpha L, K_i = \alpha^2 L \quad (3.32)$$

3.5.3. Anti-Windup

The output of the controller is the duty cycle that ranges between 0 and 1. In cases that the regulator output is limited, the integrating part keeps building up. The result will be a large value for the integrator when the reference value is met finally at the end. To prevent this, anti-windup strategy is added. The entire control system is shown in Figure 3.19.

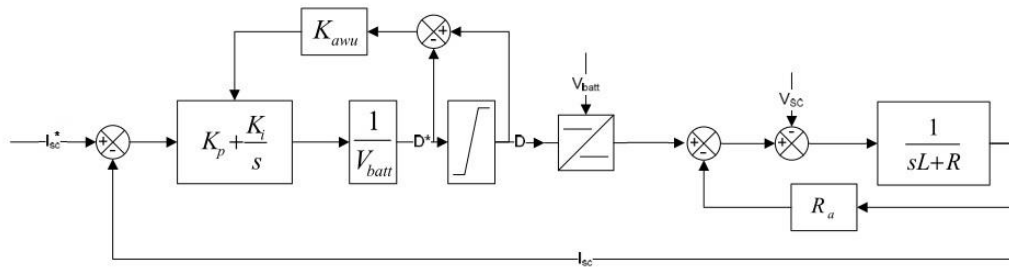


Figure 3.19. Complete control loop of the smart cell

3.5.4. Digital Implementation in the Microcontroller

A microcontroller will be used to implement the whole control strategies and current regulation process. Therefore, the regulator must be discretized. The bandwidth of the closed loop system should be much narrower than that of the sampling to ensure that the numerical approximations are accurate. This bandwidth can be controlled by adjusting the

regulator parameters via α described before. “Backward Euler” algorithm is used to approximate the integrator with T_s as the sampling period.

$$\int_{t_0}^t e(\tau) d\tau = T_s [e(t) + e(t - T_s) + \dots + e(t - nT_s)] \quad (3.33)$$

$$K_i \int_{t_0}^t e(\tau) d\tau = T_s K_i [e(t) + e(t - T_s) + \dots + e(t - nT_s)] = T_s K_i \sum_{k=0}^n e_k \quad (3.34)$$

This leads to the following relationship:

$$A_n = T_s K_i \sum_{k=0}^n e_k = T_s K_i e_n + A_{n-1} \quad (3.35)$$

The expression for the discrete PI regulator with active damping then becomes:

$$D_n^* = K_p e_n + T_s K_i \sum_{k=0}^n e_k - R_a i_n = K_p e_n + A_n - R_a i_n \quad (3.36)$$

To limit the duty cycle value between 0 and 1, the following constraint will be applied to the resultant value of D at each iteration.

$$D_n = \begin{cases} 1 & D_n^* > 1 \\ D_n^* & 0 < D_n^* < 1 \\ 0 & D_n^* < 0 \end{cases} \quad (3.37)$$

To add the anti-windup strategy to the discrete controller, the error input to the integrator is adapted as follows:

$$B_n = T_s K_i \sum_{k=0}^n e'_k = T_s K_i [e_n + K_{awu} (D_n - D_n^*)] + B_{n-1} \quad (3.38)$$

The duty cycle that includes anti-windup will be obtained as follows:

$$D_n = K_p e_n + B_n - R_a i_n \quad (3.39)$$

The current value will be sensed at each iteration and will be compared to the reference current value. The three iterative equations of (3.37), (3.38), and (3.39) are implemented numerically in the microcontroller to calculate the duty cycle based on the error at each time step to realize reference signal tracking. As a result, the ultracapacitor's current will track the reference signal generated by the main power control unit.

4. The Prototype and Results

4.1. Test Load profile

In order to investigate the effectiveness of hybridization, both the smart cell and the battery cell will be tested under the same load profiles and then the battery's condition will be compared. The load profiles are obtained by simulating a fictional electric car under certain drive cycles in Autonomie. More detailed is addressed in Appendix 1. HWFET, US06, UDDS, and LA92 cycles are selected to cover a complete range of conditions from normal urban to aggressive highway driving conditions.

Table 3 summarizes selected cycles and their characteristics. The corresponding load for all four drive cycles are shown in Figure 4.1 to Figure 4.4. To have a better understanding of acceleration and braking, the vehicle speed is also included in the diagrams. Negative current is assumed to be coming into the storage unit.

Table 3. Selected drive cycles for the test pupose in this study

Drive Cycle Name	Highway	Urban	Normal	Harsh
HWFET	•		•	
US06	•			•
UDDS		•	•	
LA92		•		•

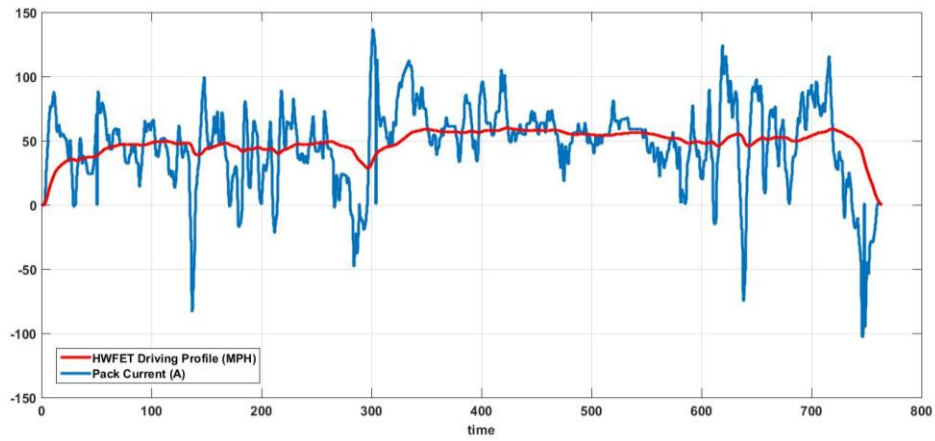


Figure 4.1. Pack current demanded under normal highway drive cycle, WHEFT

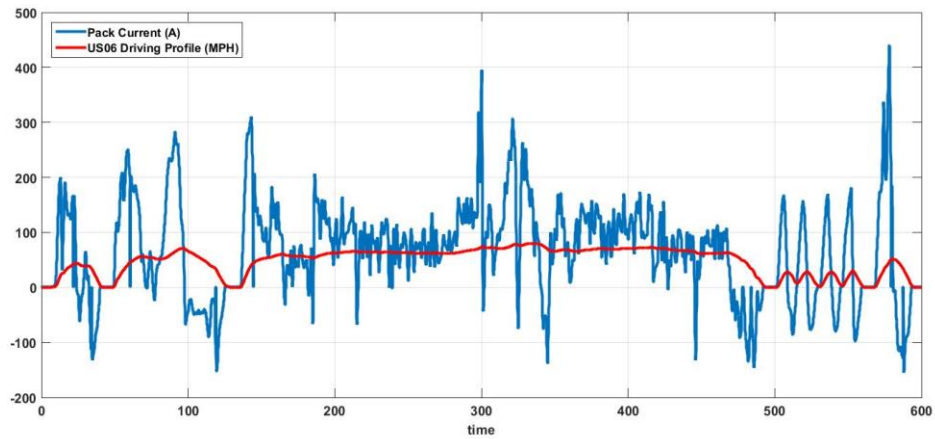


Figure 4.2. Pack current demanded under harsh highway drive cycles, US06

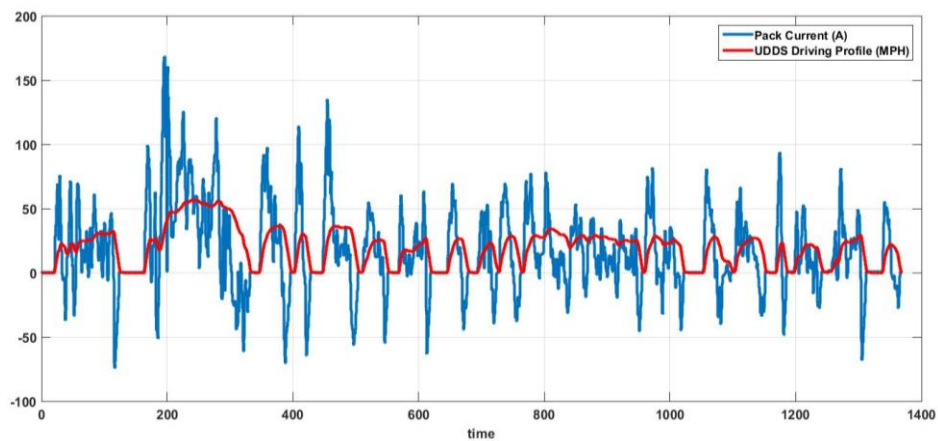


Figure 4.3. Pack current demanded under normal urban drive cycle, UDDS

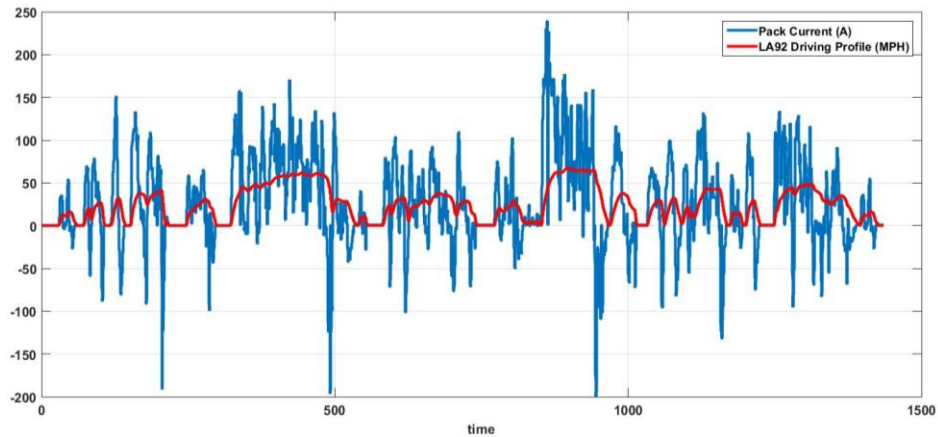


Figure 4.4. Pack current demanded under harsh urban drive cycles, LA92

The load profiles are scaled down by a factor of 20 to fit the safe operation range of the battery cell used experimentally. Figure 4.5 to Figure 4.8 show the current profiles that will be used for comparison both in simulation and experimentally. Note that the profiles after downscaling does not necessary represent a relationship with the mentioned drive cycles. Consequently, they will be referred to as load profiles 1 to 4.

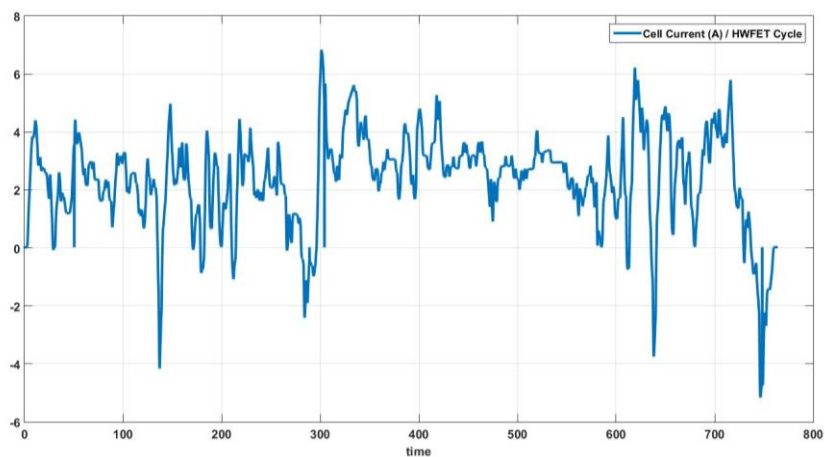


Figure 4.5. Cell level current demanded under normal highway drive cycle (Load 1)

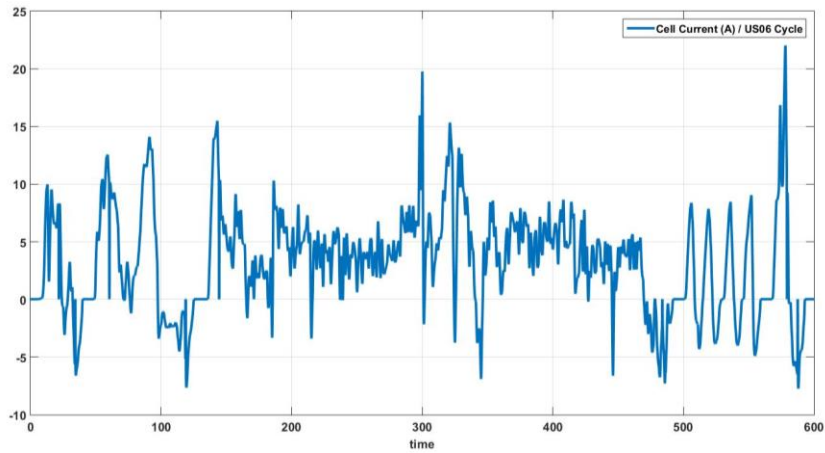


Figure 4.6. Cell level current demanded under harsh highway drive cycles (Load 2)

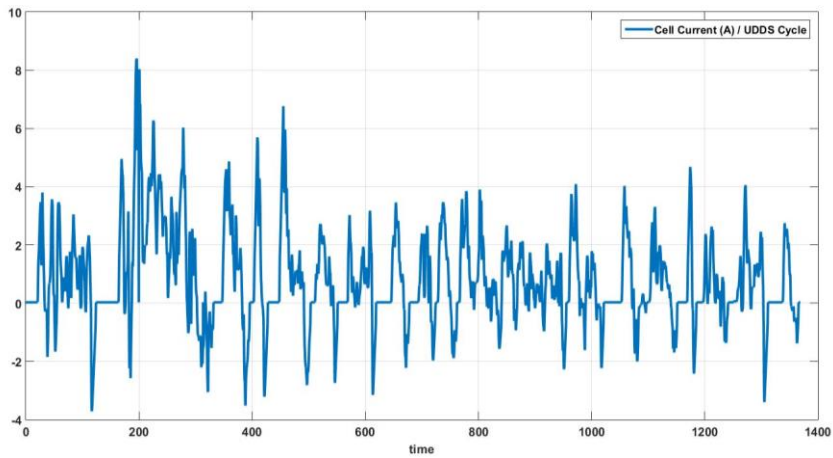


Figure 4.7. Cell level current demanded under normal urban drive cycle (Load 3)

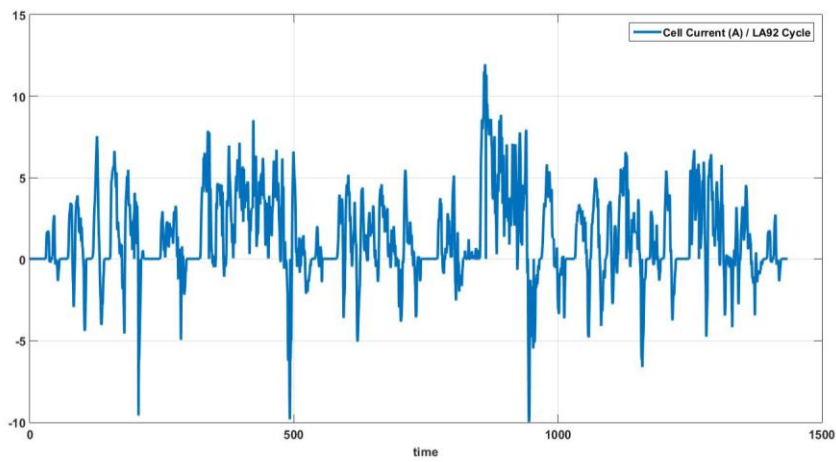


Figure 4.8. Cell level current demanded under harsh urban drive cycles (Load 4)



4.2. The Smart Cell Prototype: Design and Simulations

The prototype consists of a Batterist Li-Ion polymer battery cell (PF9744128VScLP), a Maxwell ultracapacitor (BCAPP0650P270K04), and a DC/DC converter that interfaces them. Technical details of the battery cell and the ultracapacitor are elaborated below in Table 4 and Table 5 respectively.

Table 4. Li-Ion battery cell characteristic

Nominal capacity (0.5 C)		5.4 Ah	
Nominal Voltage		3.7 V	
Impedance at 1 kHz		Max 3.5 mΩ	
Charging (continuous)	Voltage		4.2 V
	Current	Nominal	2.7 A
		Standard	5.4 A
		Maximum	16.2 A
Discharging (continuous)	Voltage		2.8 V
	Current	Nominal	2.7 A
		Standard	5.4 A
		Maximum	97.2 A
Cycle life (DoD 80% 0.5C/0.5C)		500 cycles	
Shelf life (23 °C)			
Operating temperature (charge)		0 to 45 °C	
Operating temperature (discharge)		-20to 60°C	
Storage temperature		-20to 45°C	
Weight		115 g	

Table 5. Maxwell ultracapacitors

	Cap. (F)	Vmax (V)	ESR (mΩ)	I burst (A)	I max (A)	Weight (g)	Energy (Wh)	Dimensions (mm)
	350	2.7	3.2	220	21-34	60	0.35	61.5x33.3
	650	2.7	0.8	600	54-88	160	0.66	51.5x60.4

The power converter is designed to be able to handle up to 300W as Table 6 shows. The battery on the DC bus determines the bus voltage. It is expected to have a voltage and current ripple of 0.1 at a switching frequency of 20 KHz.

Table 6. DC/DC converter characteristics

Max DC bus power	300 W
Max DC bus voltage	4.2 V
Current ripple	0.1
Switching frequency	20 kHz

Considering both buck and boost mode operations, the converter's inductance must be at least 6.6 mH based on equations (3.8) and (3.16). A 2.5 mF capacitor is used as the output capacitor of the power converter for the boost mode. The operation of the converter in buck and boost mode are simulated in PLECS as shown in Figure 4.9 to Figure 4.12. Note that the current for bi-directional convertors is always continuous.

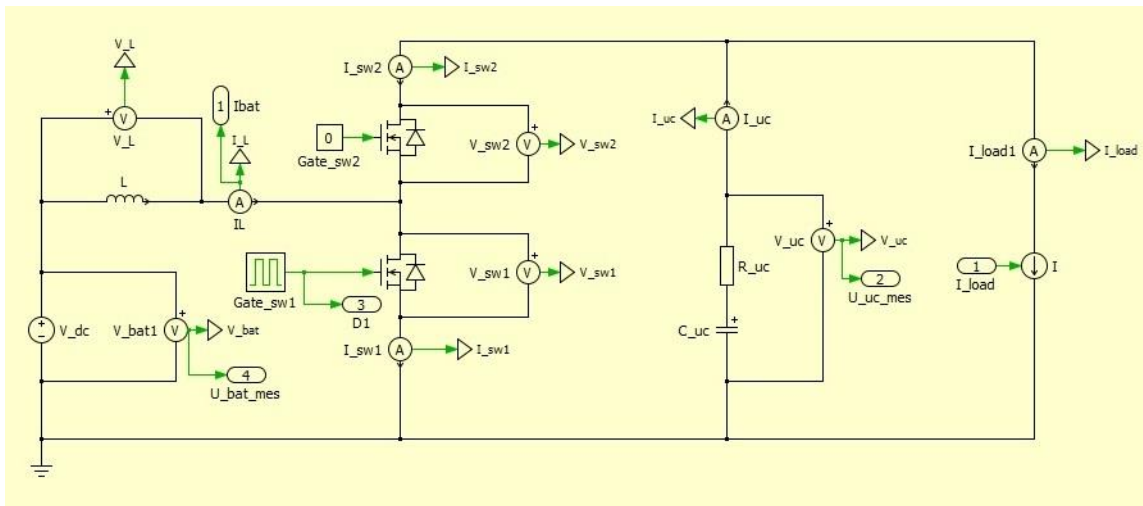


Figure 4.9. Simulation of the converter in PLECS in the boost mode

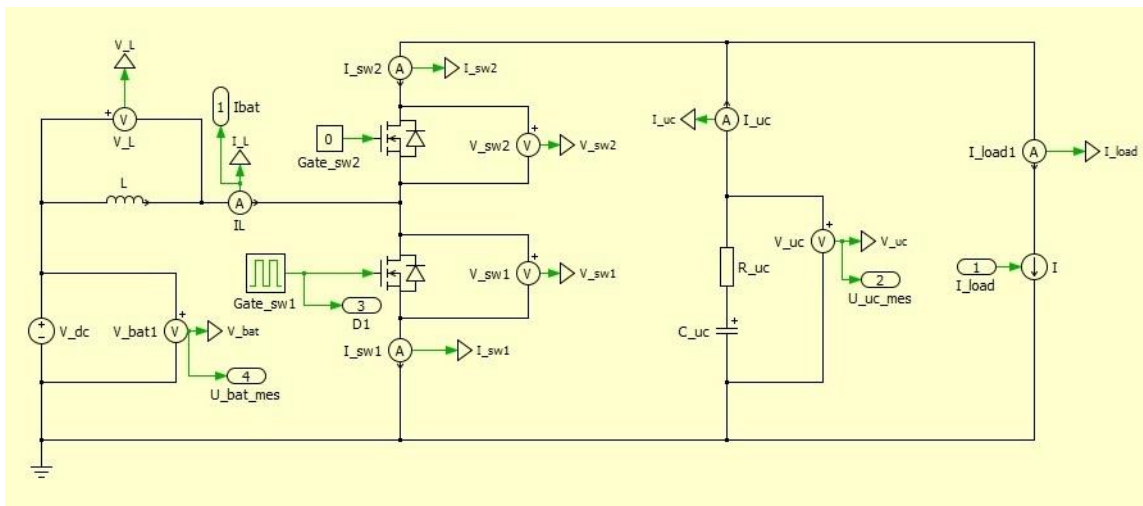


Figure 4.10. Simulation of the converter in PLECS in the buck mode

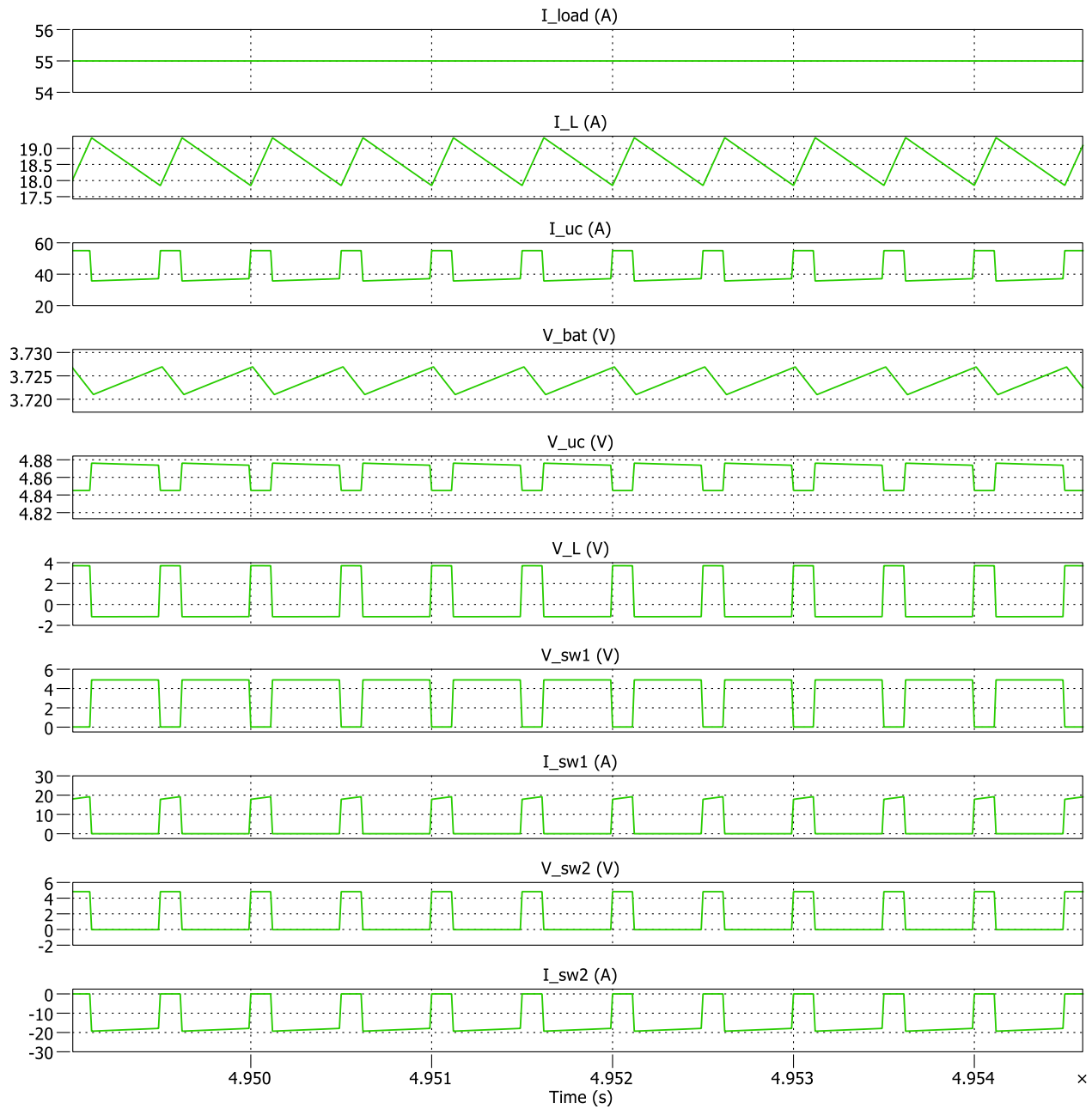


Figure 4.11. The power converter's operation in boost mode (Simulated in PLECS)

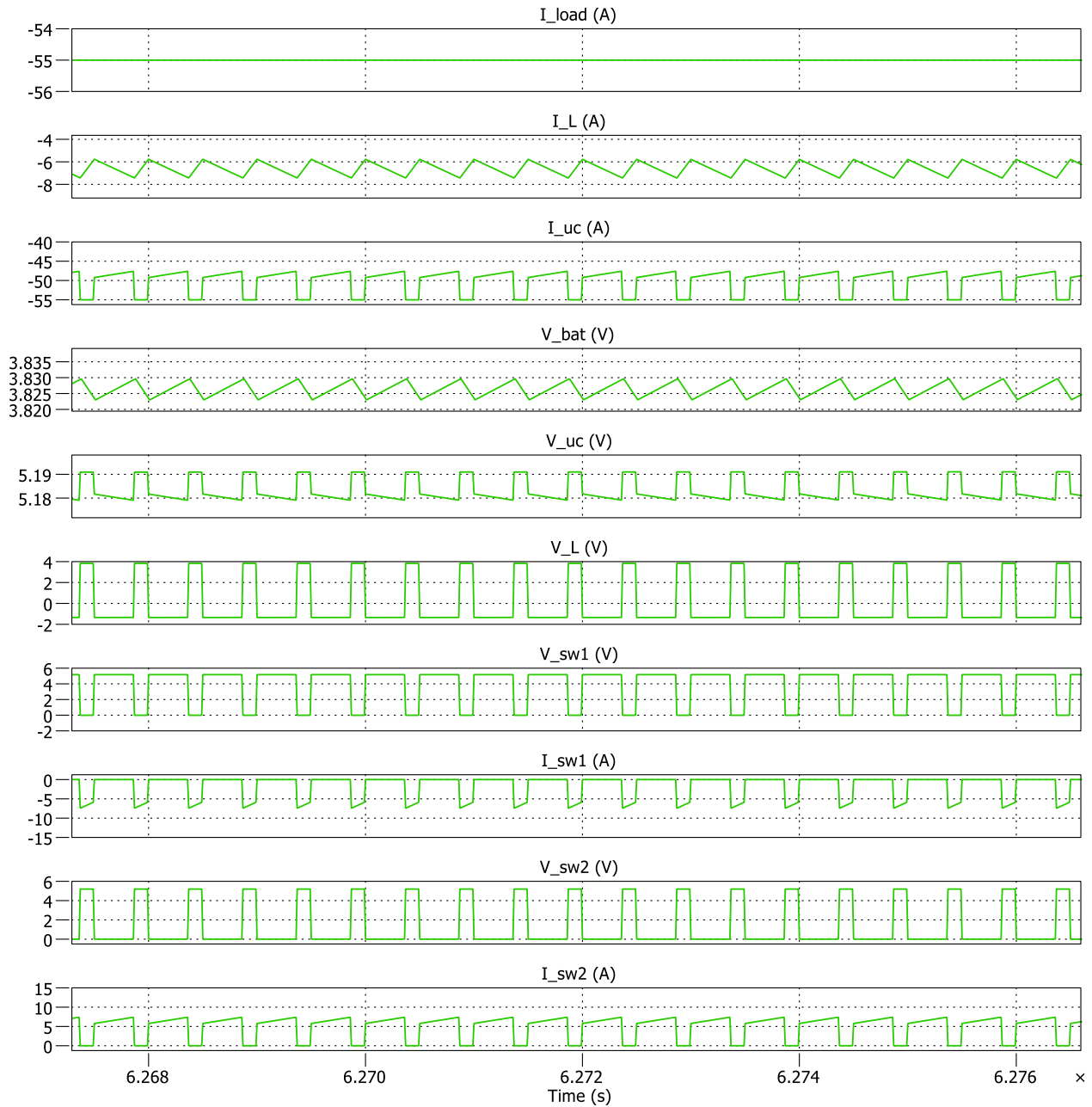


Figure 4.12. The power converter's operation in buck mode (Simulated in PLECS)

The smart cell is simulated in SIMULINK as shown in Figure 4.13. The “Electrical Power System” represents the battery, the ultracapacitor, and the converter that interfaces them. The output is fed back for the corresponding duty cycle. The “Power Management Unit” is discussed in 3.4. It generates a reference current signal that the ultracapacitor is supposed to follow. The “Current Regulator” is discussed in 3.5. It is a controller that provides the converter with appropriate duty cycle so that the ultracapacitor tracks the reference current. More detailed information is provided in Appendix 2.

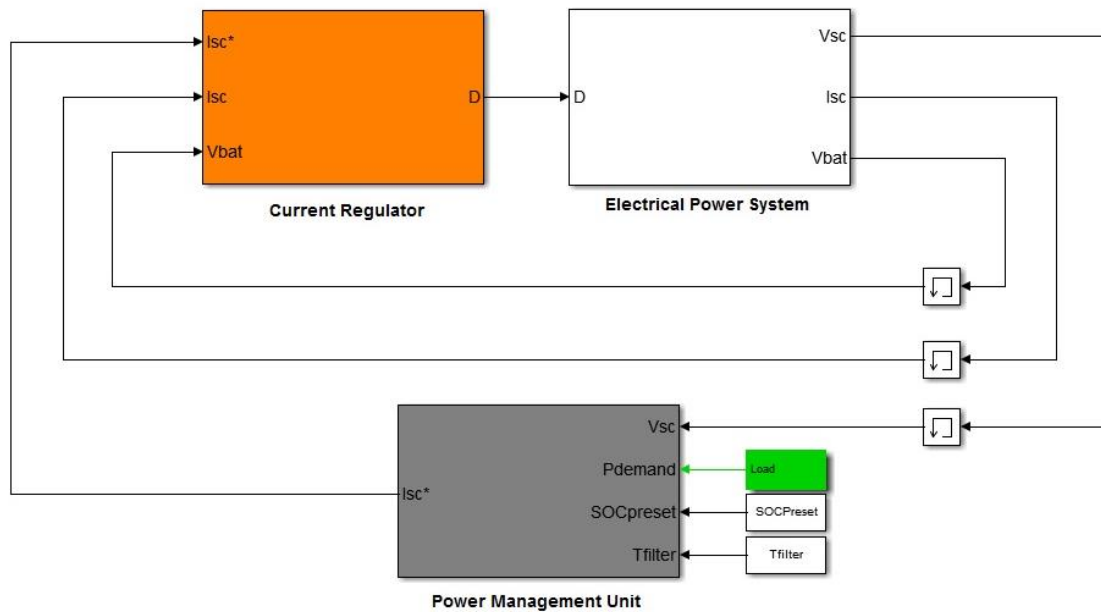


Figure 4.13. Simulation of the smart cell in SIMULINK

To investigate the effectiveness of the hybridization, the battery’s load share is compared for two cases. The first case is when the battery cell is exposed to the test load directly, while in the second case the smart cell provides for exactly the same test load. The simulation results are illustrated in Figure 4.14.

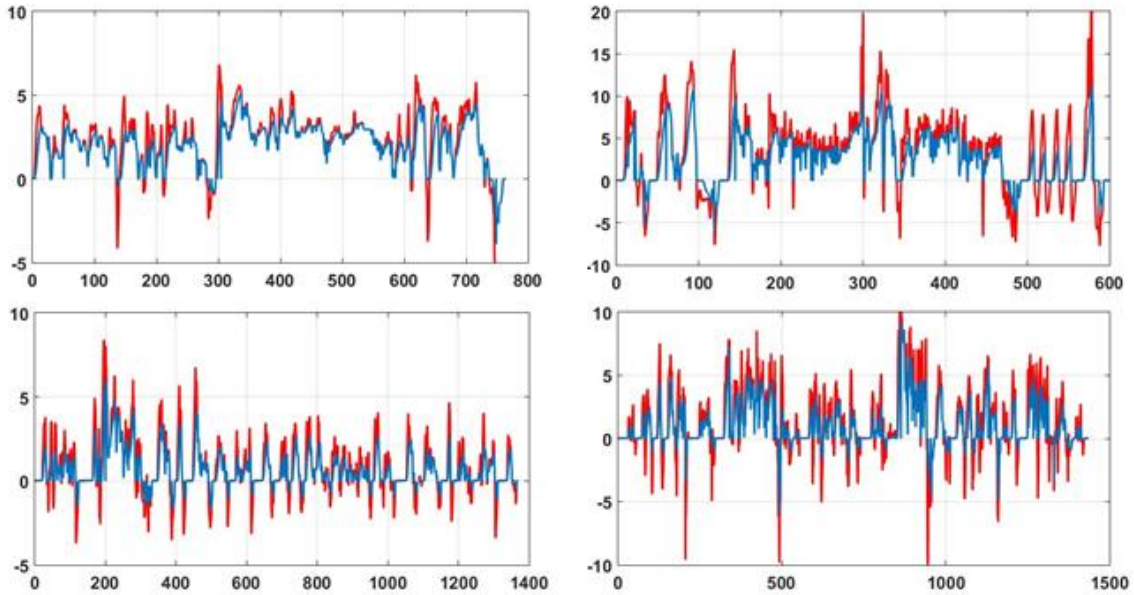


Figure 4.14. The battery's current simulated under 4 load profiles

The red lines represent the test load and the blue lines is the load share that the battery cell is exposed to in the smart cell. To quantify the difference between the two cases for each drive cycle, root mean square of the current is incorporated. The root mean square of the battery current defined in (4.1) is a measure of the heat created in the battery cell as well.

$$I_{rms} = \sqrt{\frac{1}{T} \int_0^T I_{batt}^2} \quad (4.1)$$

$$E = \frac{1}{2} \cdot R \cdot I_{rms}^2 \cdot t \quad (4.2)$$

In Figure 4.15 and Figure 4.16, the RMS of the battery cell is compared for three cases. The filtering reduces the RMS current while the adapted filtering shows further effectiveness. This is reasonable as the adaptation is designed to limit battery involvement.

The results can even be investigated intuitively by comparing the amplitude of the battery current in the smart cell with the test load in Figure 4.14.

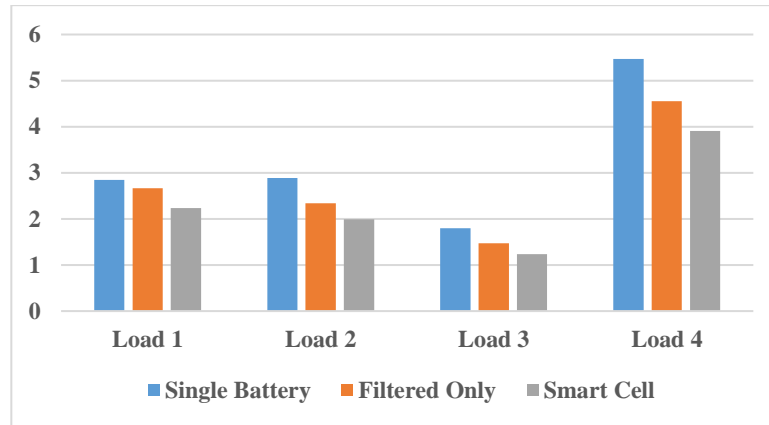


Figure 4.15. RMS of the battery current is decreasing as a result of hybridization (Simulation)

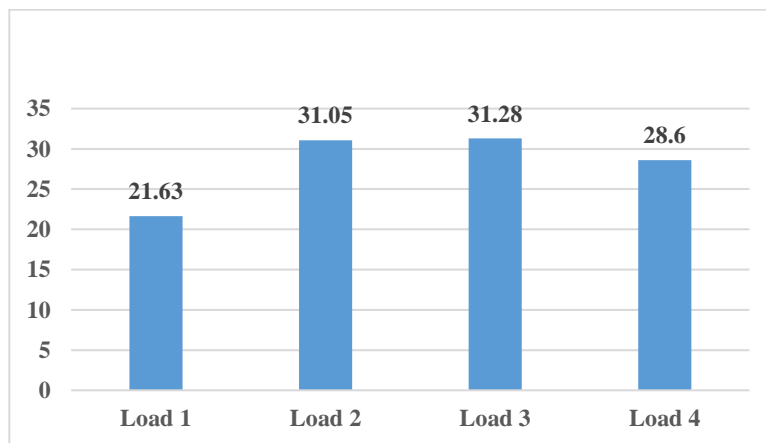


Figure 4.16. Percentage of the battery RMS current decrease for the smart cell (Simulation)

To further investigate the effectiveness of the power management strategies, the cycling of the battery cell is considered. State of charge stress factor is a measure defines in equation (4.3). By acquiring the power spectrum of the battery's SOC, we can determine how frequent and how deep the battery cell has been charged and discharged.

$$SOC_{stress} = \sum (|SOC(\omega)|^2 \cdot \omega) \quad (4.3)$$

To do so, the Fourier transform is applied to the state of charge of the battery to obtain the frequency components of the changes. The higher the frequency of charge and discharge, the more the battery cell is cycled. The square of the amplitude of the frequency components resembles the strength of the change in SOC at each frequency showing how deep the cycling has been.

Similar to the root mean square of the battery current, the stress factor is calculated and the improvement is illustrated in Figure 4.17 and Figure 4.18. It is noteworthy that the filtering strategy alone is pretty inefficient as the stress factor has remained unchanged or even got worst in some cases. After implementing the adaptation algorithm in the smart cell which eliminates mutual battery and ultracapacitor charge and discharge as a result of filtering, a significant improvement is achieved.

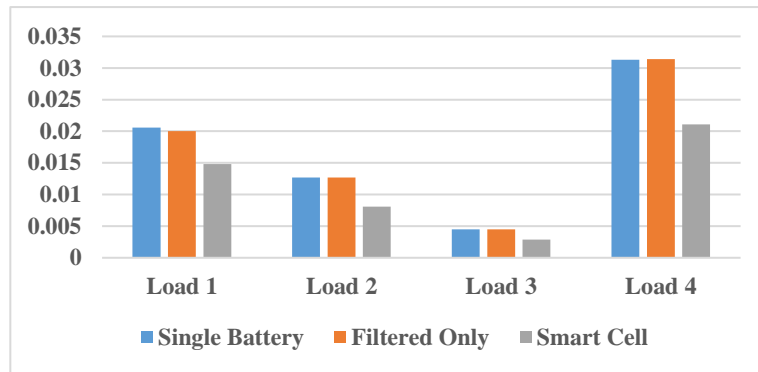


Figure 4.17. The SOC stress factor is decreasing as a result of hybridization (Simulation)

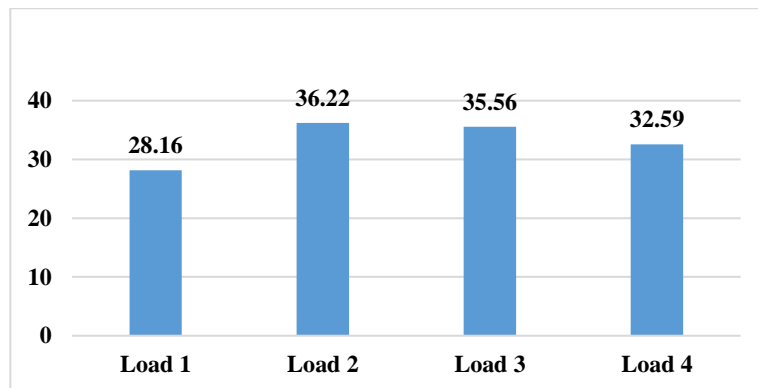


Figure 4.18. Percentage of the SOC stress factor decrease in the smart cell (Simulation)

4.3. Experimental Set Up and Test Results

The smart cell and the battery cell alone are exposed to the test loads generated by LabVIEW. The acquisition system is used to register signals for further analysis. The tests are performed in the lab setup shown in Figure 4.19. The control panel includes an oscilloscope to provide online state monitoring besides the acquisition system which is shown in more details in Figure 4.20 and Figure 4.21. The prototype is also illustrated in more details in Figure 4.22.

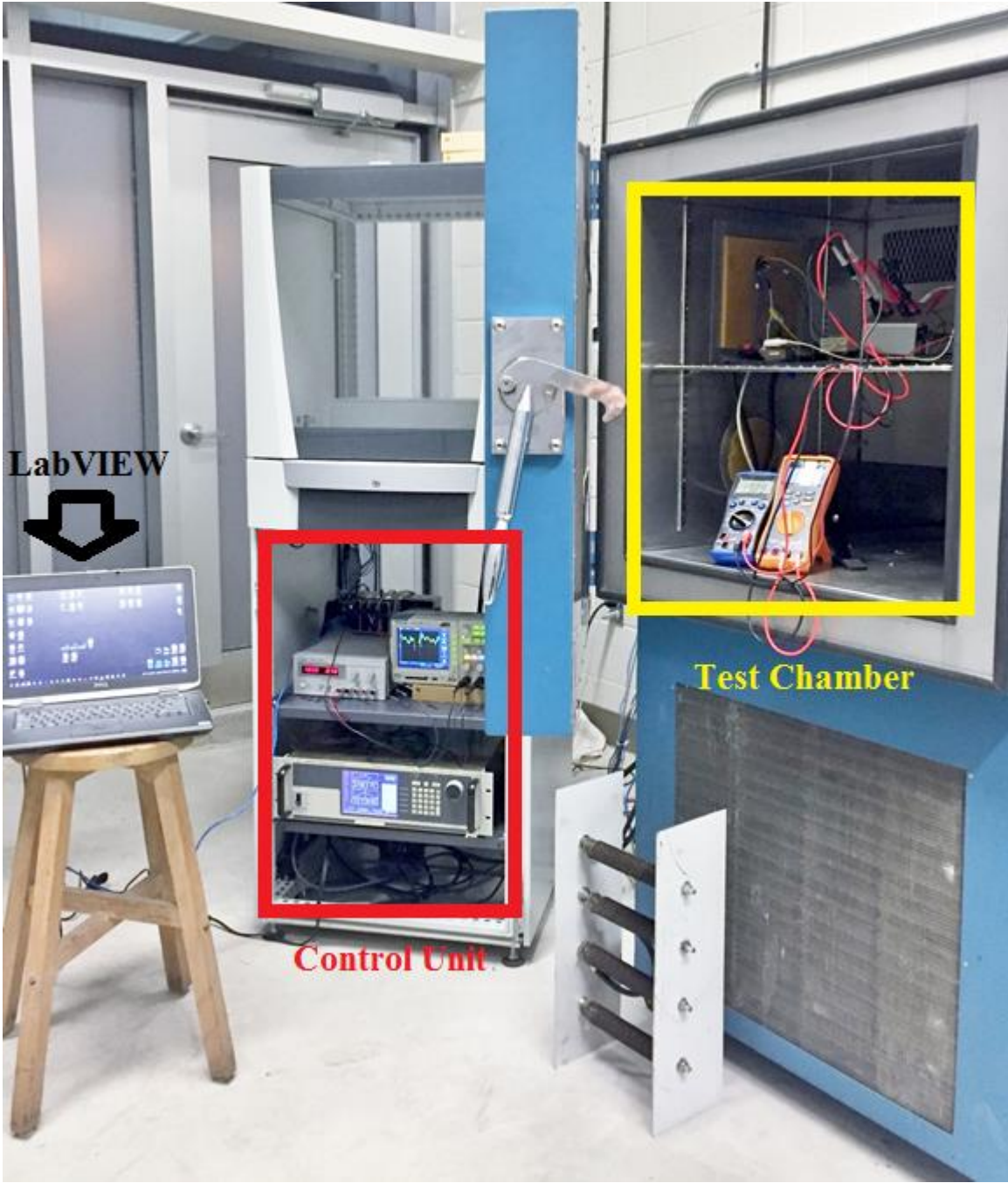


Figure 4.19. Experimental set up to evaluate smart cell's performance

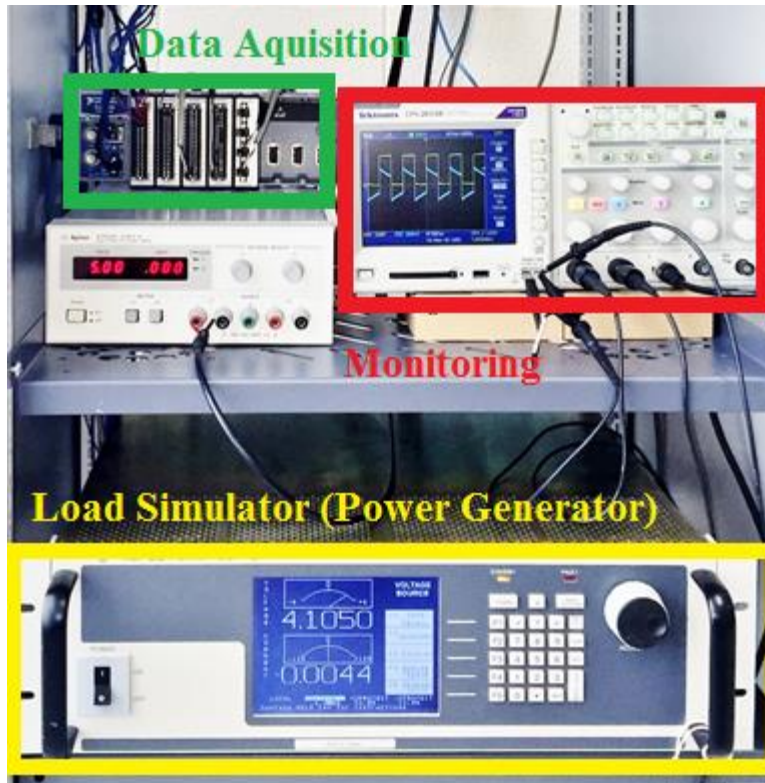


Figure 4.20. The control panel including generation, acquisition, and monitoring apparatus



Figure 4.21. The data acquisition module that captures and logs the signals for further analysis

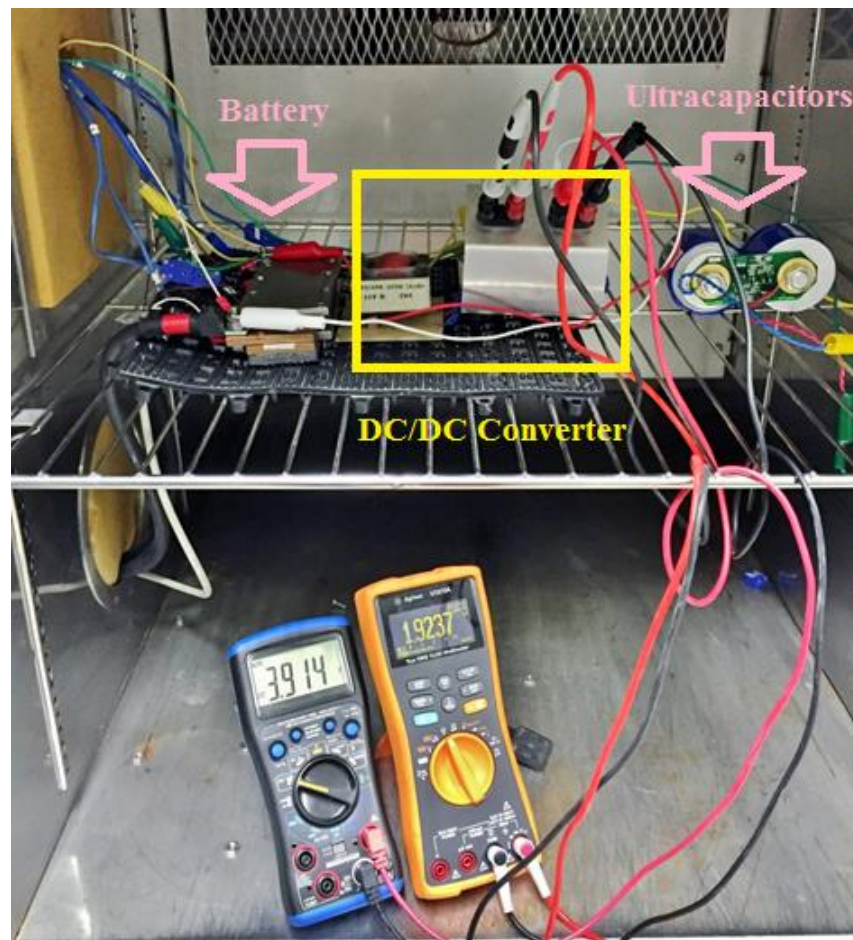
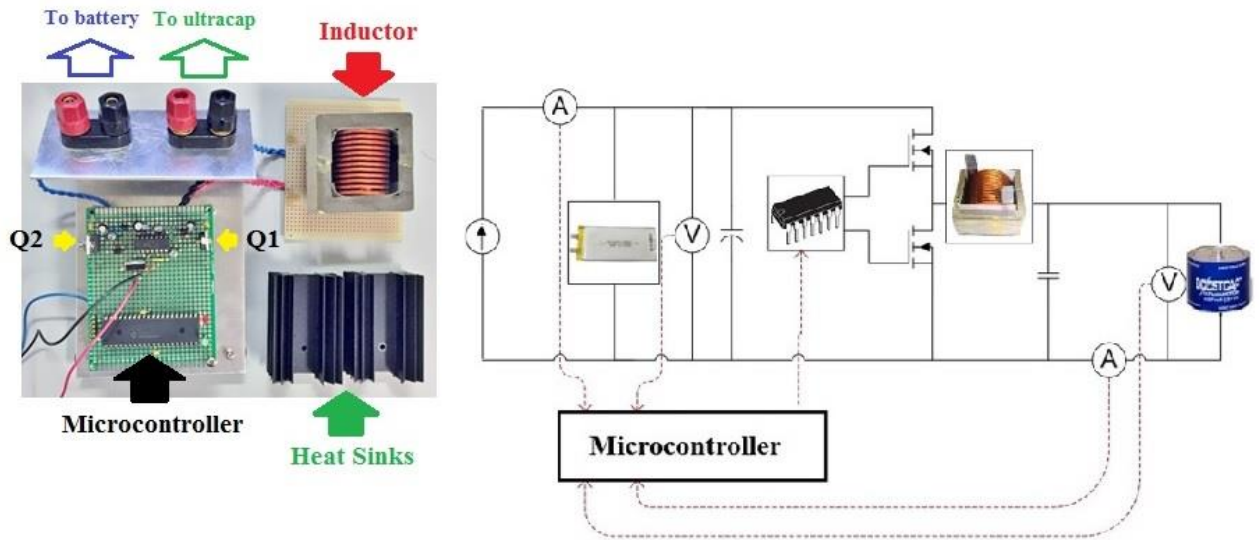


Figure 4.22. The prototype circuit

Figure 4.23 and Figure 4.24 compare a screenshot of the real time signals in the oscilloscope with the simulation results at the same time frame inside the red box. The amber signals in both charts are the load current requested from the smart cell. The blue signal is the current that the battery has provided. As expected, the battery is experiencing a smoother current where the pick is provided by the ultracapacitor. Also, the majority of the regenerative current is absorbed by the ultracapacitor to mitigate stresses.

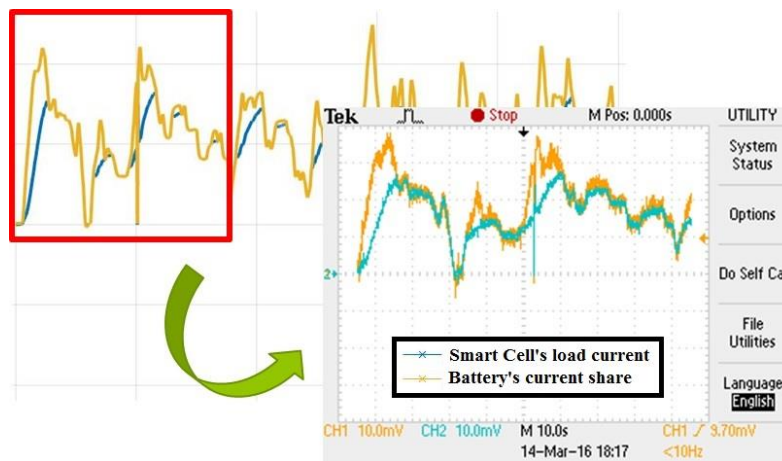


Figure 4.23. Load sharing in a snapshot of the oscilloscope compared to the simulation

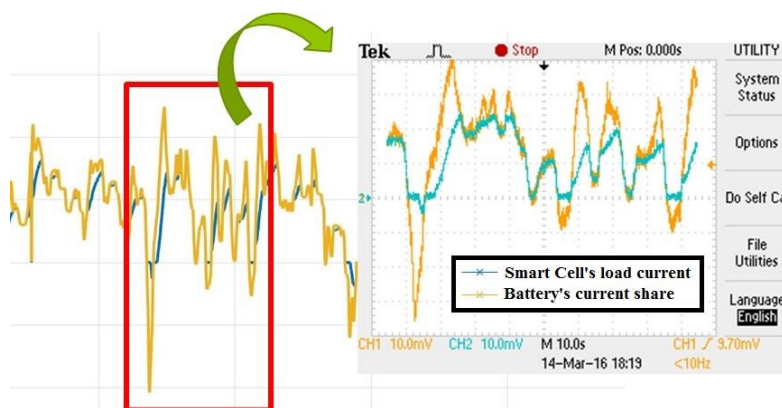


Figure 4.24. Load sharing in a snapshot of the oscilloscope compared to the simulation

Experimental load current sharing is shown for selected cycles in Figure 4.25 to Figure 4.28. The current provided by the ultracapacitor is illustrated separately while the battery's share is compared to the case that all the load is being supplied by the battery alone.

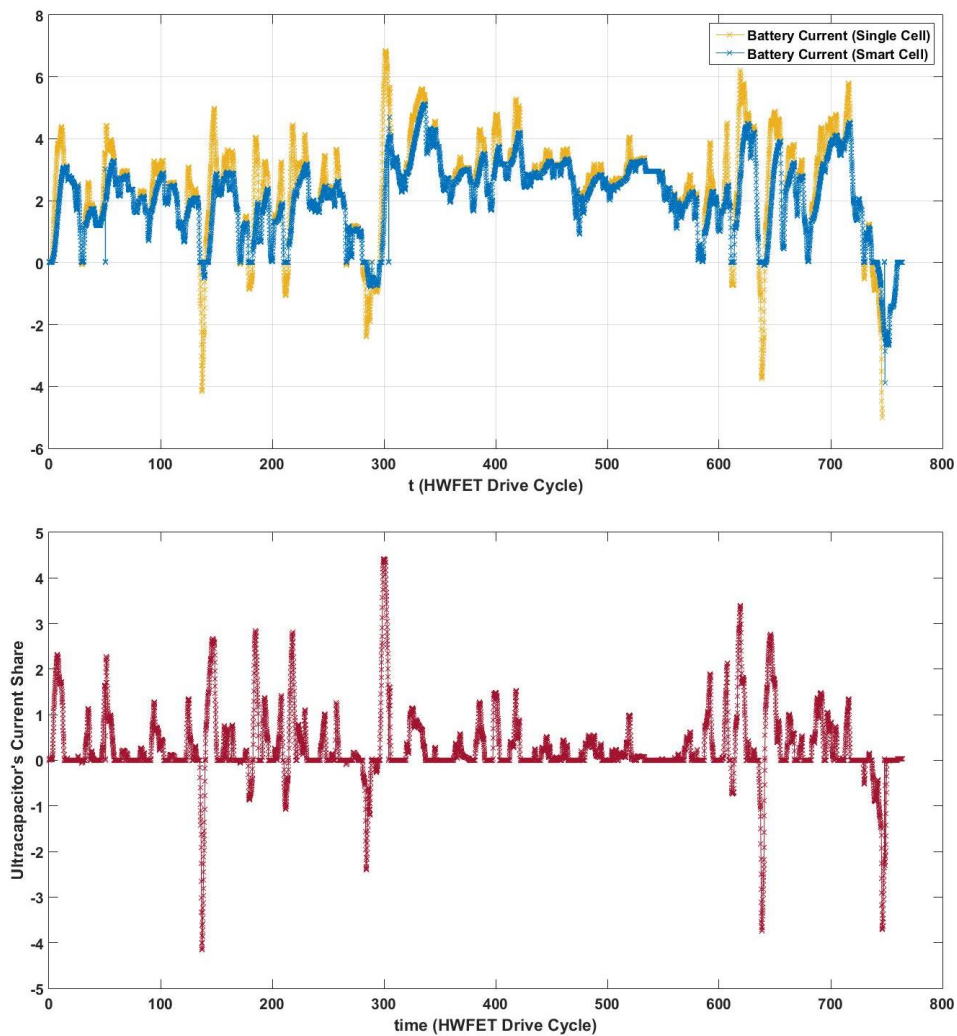


Figure 4.25. Experimental results under Load 1 / Demand, battery and ultracapacitor currents

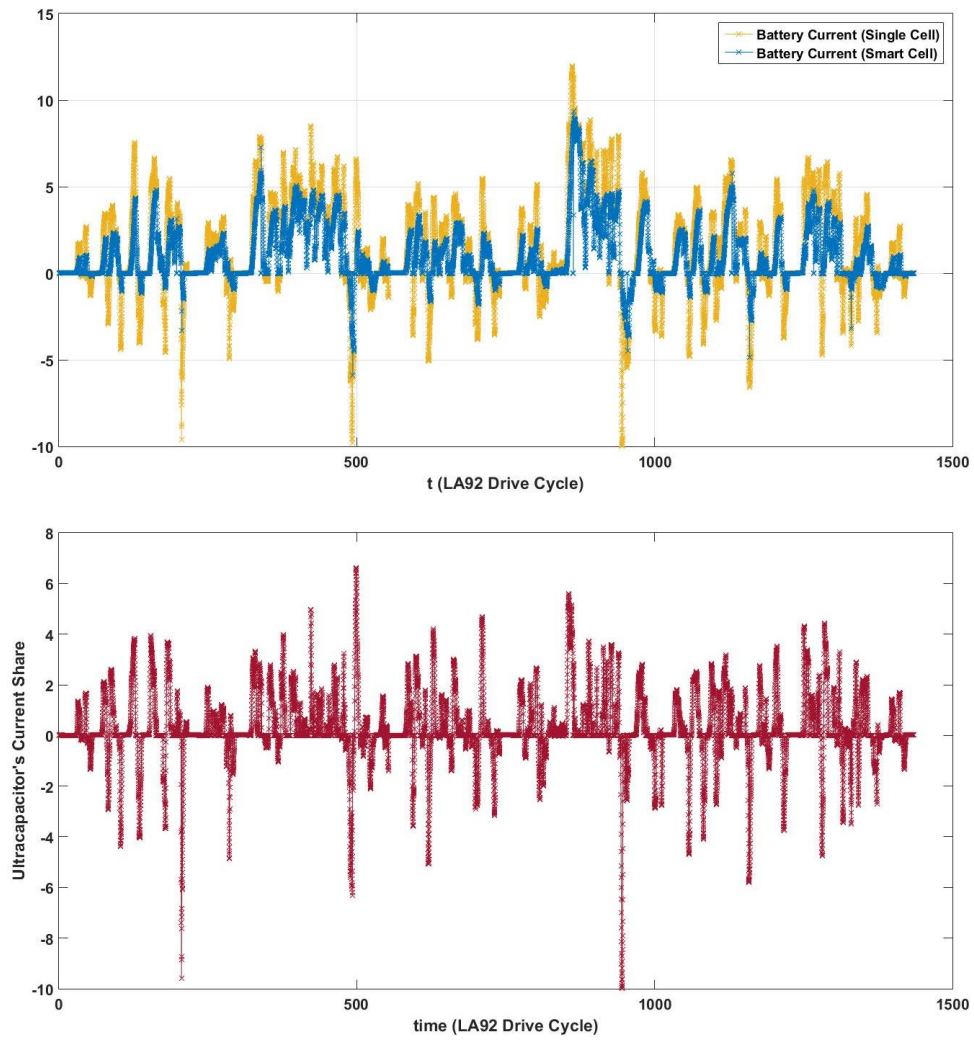


Figure 4.26. Experimental results under Load 2 / Demand, battery and ultracapacitor currents

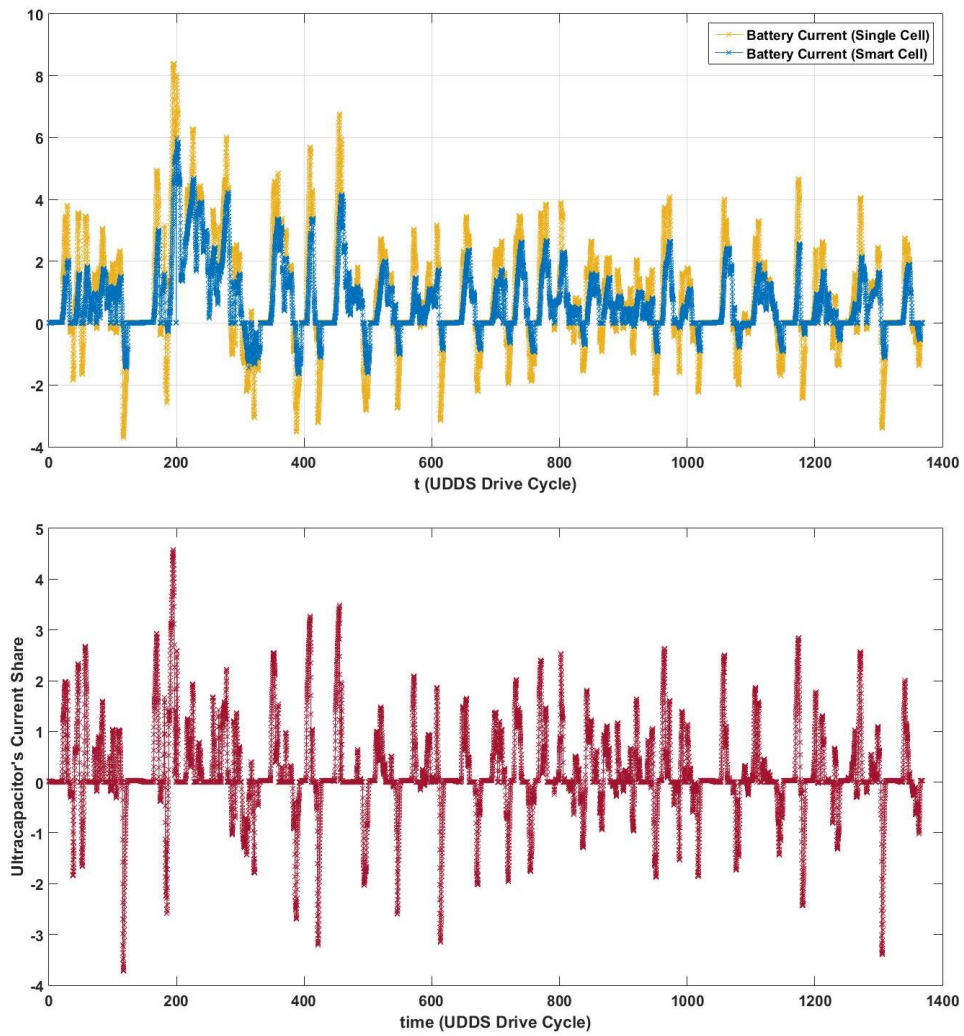


Figure 4.27. Experimental results under Load 3 / Demand, battery and ultracapacitor currents

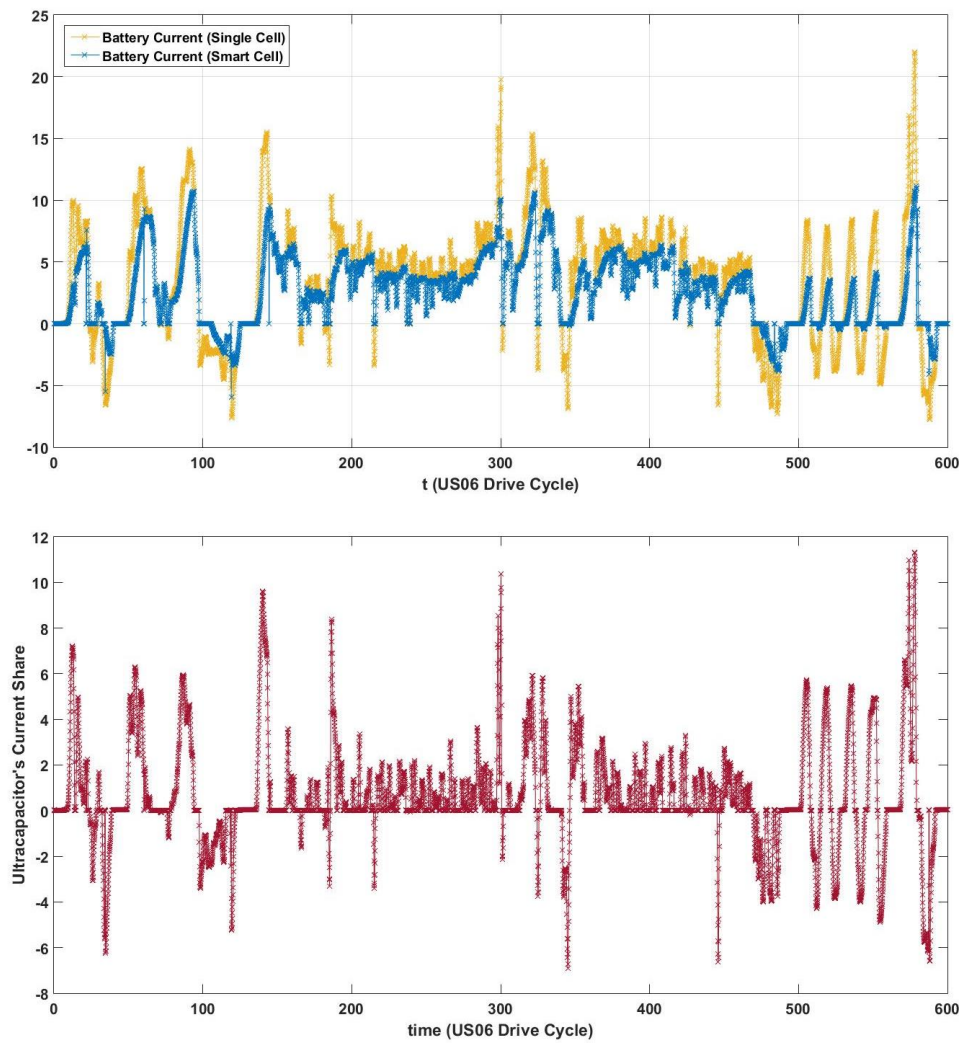


Figure 4.28. Experimental results under Load 4 / Demand, battery and ultracapacitor currents

To make the battery the only energy source of the hybrid cell, the initial state of charge of the ultracapacitor is selected to be the final value that the controller discussed in 3.4.2 tries to maintain. As a result, the net energy extracted and stored in the ultracapacitor during the course of the drive cycles will be zero for the sake of a fair comparison. Ultracapacitor's state of charge is shown for all selected drive cycles in Figure 4.29.

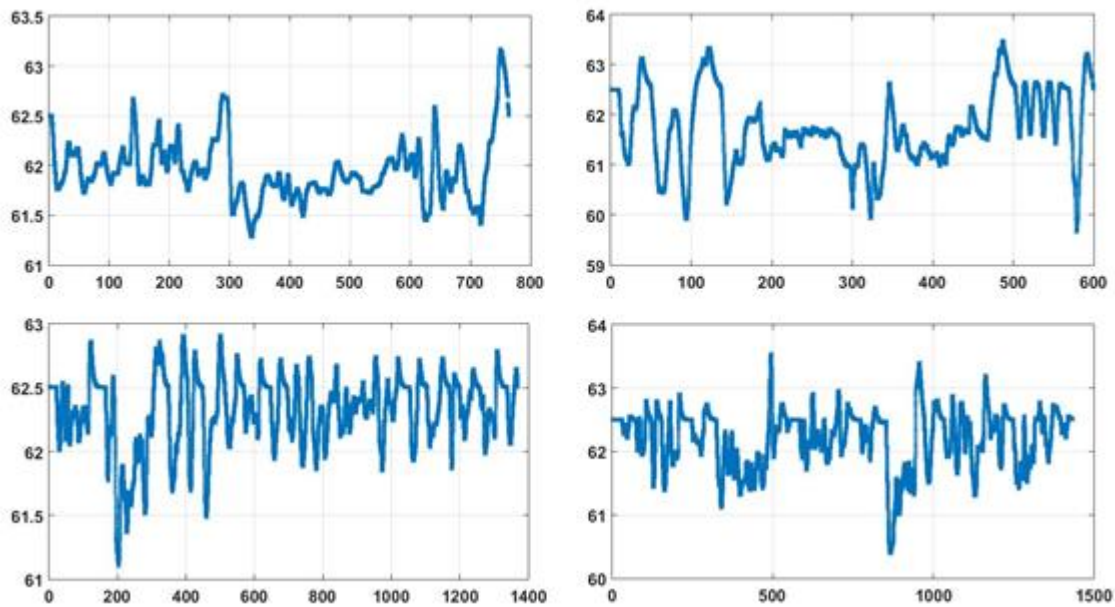


Figure 4.29. Ultracapacitor's SOC throughout the experimental tests

The battery's experimental cell voltage and its state of charge during the selected loads are illustrated in Figure 4.30 to Figure 4.33. As discussed earlier, the state of charge will be used to calculate the SOC stress factor which quantifies the cycling that the cell is experienced during the test.

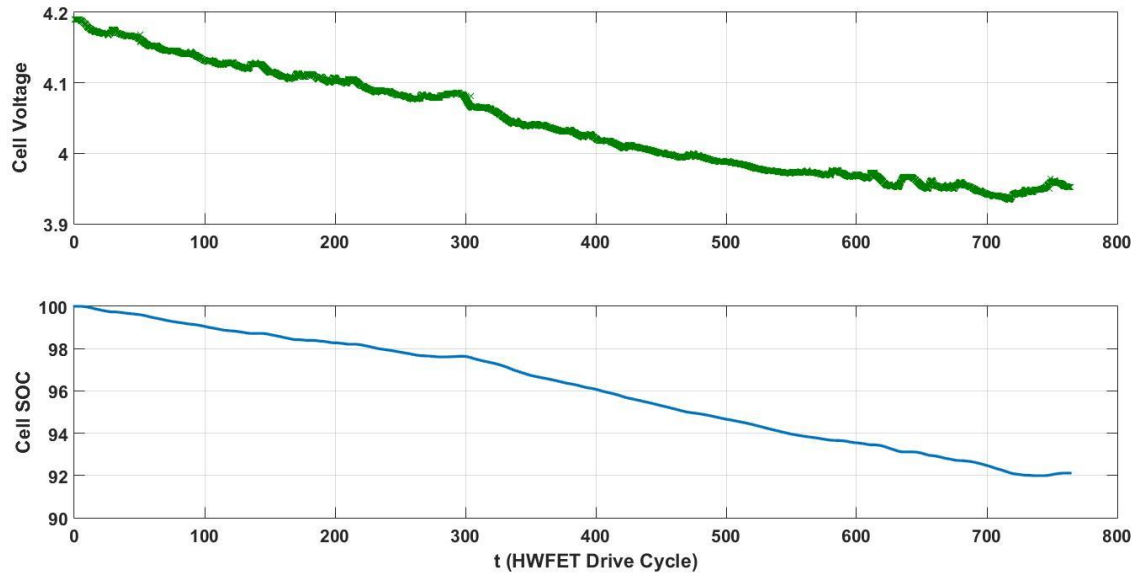


Figure 4.30. Experimental battery cell voltage and SOC / Load 1

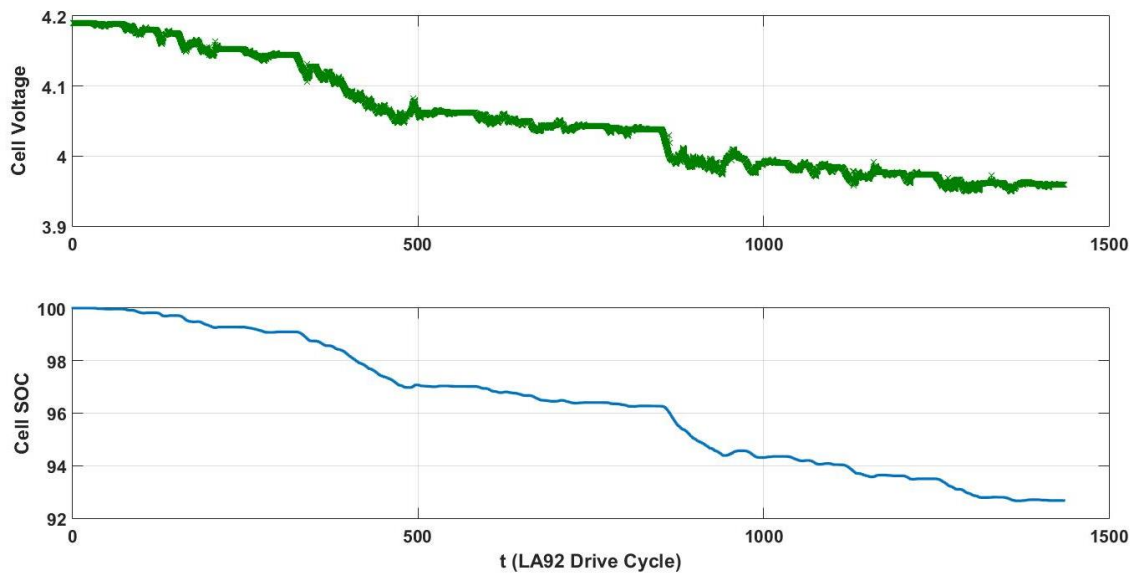


Figure 4.31. Experimental battery cell voltage and SOC / Load 2

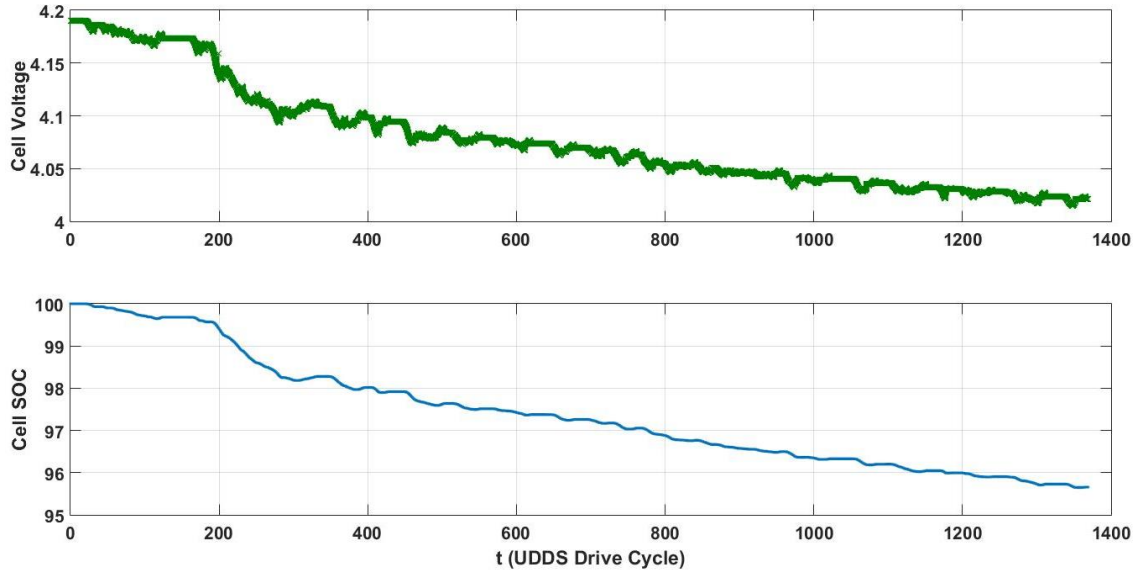


Figure 4.32. Experimental battery cell voltage and SOC / Load 3

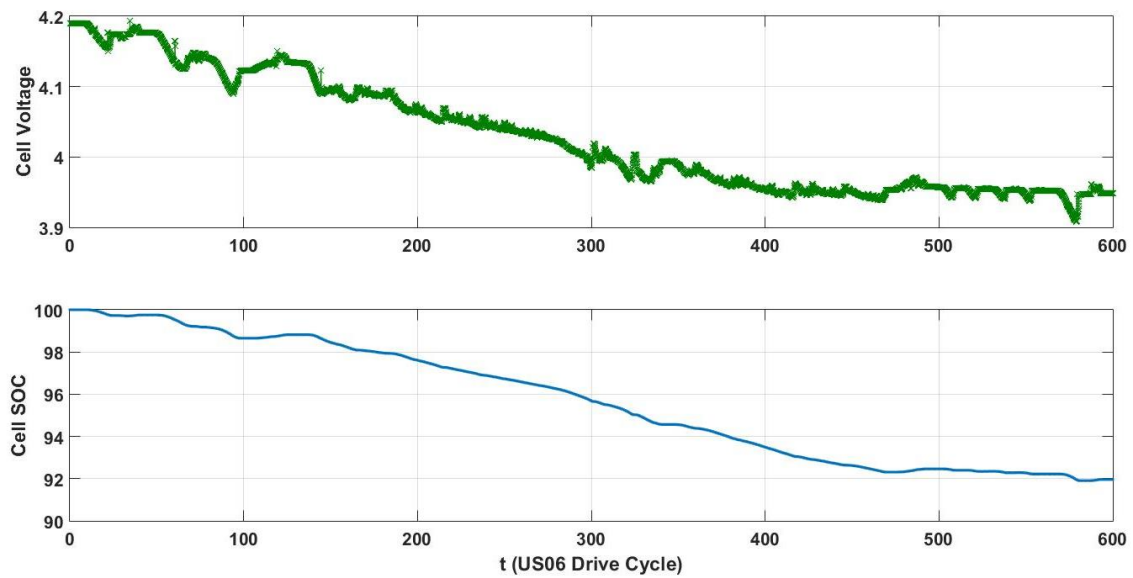


Figure 4.33. Experimental battery cell voltage and SOC / Load 4

Similar to simulations, the battery’s RMS current and the stress factor are used to quantify the effectiveness of the hybridization strategy. The RMS current is compared for the single battery cell and the same cell inside the smart cell in Figure 4.34. Figure 4.35 illustrates the percentage that the RMS current is decreased.

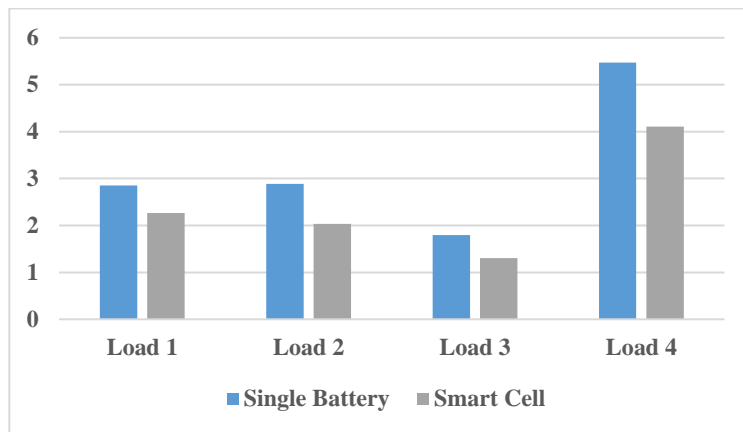


Figure 4.34. RMS of the battery’s current is decreasing as a result of hybridization (Experimental)

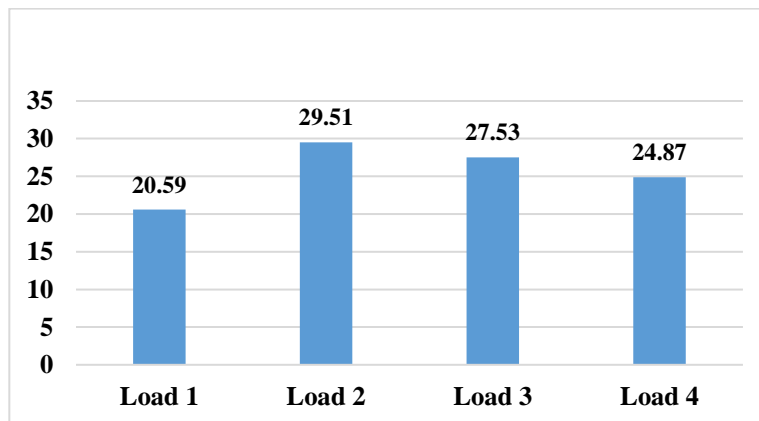


Figure 4.35. Percentage of the battery’s RMS current decrease for the smart cell (Experimental)

Similarly, the SOC stress factor is compared for the same cases as the RMS current in Figure 4.36. The percentage of improvement is also shown in Figure 4.37.

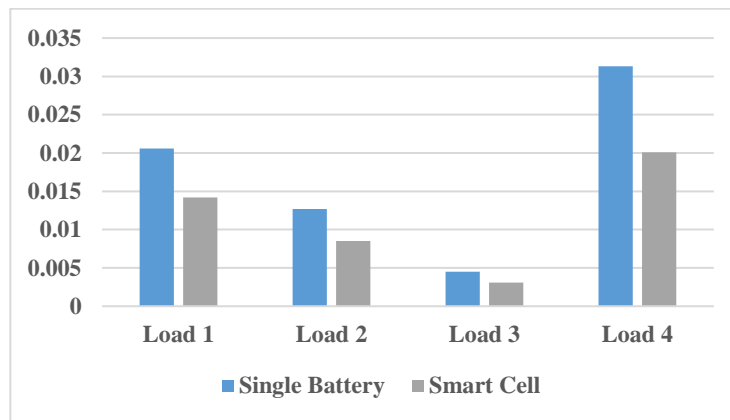


Figure 4.36. The SOC stress factor is decreasing as a result of hybridization (Experimental)

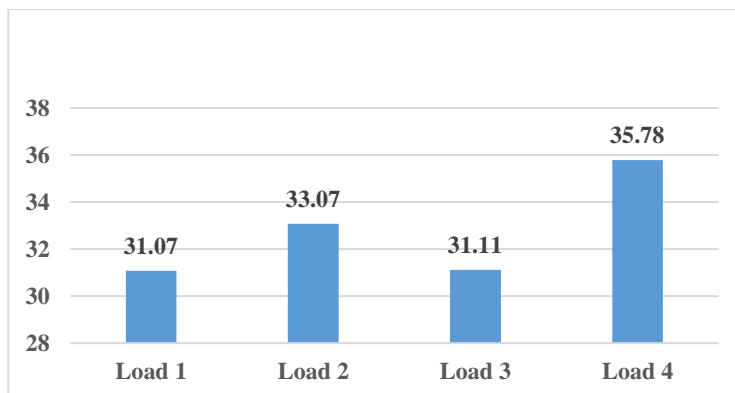


Figure 4.37. Percentage of the SOC stress factor decrease in the smart cell (Experimental)

The experimental results agree with the results obtained from the simulations. In both cases, the filtering strategy has eliminated the high frequency portion of the load and consequently, the battery is exposed to more smooth cycling. This agrees with smaller stress factor that refers to less charge and discharges and shallower cycling. Also, the filtering and load sharing strategy has reduced the load over the battery which is quantified in RMS of the current.

5. Conclusion

The electric energy storage is one major challenge in modern vehicular applications. Although Li-Ion batteries have demonstrated promising characteristics, their limited life cycle is a serious problem especially in inherently demanding and harsh applications. In an electric vehicle, the electric energy storage unit must be able to provide momentary current surges for sudden accelerations. Rather than limited power density, sudden demands are detrimental to battery health resulting in shorter battery life. This gets even more complicated considering the fact that the battery pack is supposed to recapture the regenerated energy during the course of braking.

In this research, a Li-Ion battery cell is hybridized actively with an ultracapacitor. The ultracapacitor is a high power electric storage element with a long life cycle that can handle both peak power provision and storage. Consequently, the stresses over the battery are mitigated with the expectation of longer battery life. An appropriate configuration is selected for this particular application after reviewing several hybridization schemes and available power converter structures.

A comprehensive power management unit is designed and implemented that is able to execute several strategies to mitigate battery stresses while improving power capabilities. The prevalent strategy is the filtering strategy that eliminates highly dynamic portion of load that is detrimental to battery health. Other strategies such as extra mitigation and equalization are intended to add an adaptive nature to the hybrid cell to relieve battery even more in case it is possible as a result of load conditions.

A current regulator is also designed and implemented to realize the proposed strategies by providing the power converter with proper duty cycle. The power management strategy creates a reference load profile for the ultracapacitor. The control loop forces the ultracapacitor to track this reference. This is done by generation of appropriate duty cycle that determines the output current of the converter.

Rather than simulation under a wide range of test loads, a prototype hybrid cell is built and tested in an experimental setup. Two performance factors are considered to quantify the effectiveness of the hybridization policy. The root mean square of the current passing through the battery gives a sense of how the battery is exposed. It also resembles the heat created as the result of battery's internal resistance. A factor called state of charge stress factor quantifies how the battery cell is cycled and how deep the cycling has been. Exposure to heat and high load, consecutive charges and discharges, and deep discharges are detrimental factors whose elimination contributes to battery life extension.

The experimental results agree with the simulations. As a result of load sharing with an auxiliary storage unit (the ultracapacitor), the overall load over the battery is decreased about 25% in both simulation and experimental. Also filtering the load over the battery has resulted in a smoother operating condition reflected by about 33% improvement in SOC stress factor. The more the filter's time constant, the more the battery load is getting smoother. In other words, the battery load changes slower by adopting a more aggressive filtering regime which results in longer battery life. In this case, the ultracapacitor must be large enough to be able to handle the load at the terminal.

The main target of this research has been to focus on increasing the battery life. Though, the optimization of the design is considered beyond the scope of this study. To optimize the design, we face contradicting target functions. For instance, the filtering strategy shifts the energy provision and recapturing towards the ultracapacitor. To cope with this, a larger ultracapacitor must be used. In other words, smoother battery operation comes with the expense of bigger and heavier ultracapacitor. A multiobjective optimization is necessary to find the optimal hybridization scheme.

The efficiency has not been studied either. In this research, the hybridization is achieved using a power converter which adds to the power losses. The losses come from the switching elements, inductor, ultracapacitor, and the electronics used for drive and control. Although soft switching technics are available to improve the efficiency of the power converter, the general judgment on the effectiveness of this hybridization strategy needs a thorough efficiency study. Study of multi-input converters in this regard looks necessary.

Finally, designing the whole pack using smart cells instead of the battery cells seems impossible without solving the multiobjective optimization that will determine the number of series and parallel smart cells inside the pack. This study has been the very first step to proving the concept experimentally and to build a prototype that would pave the way for further research. The design looks also very promising to be implemented on other applications especially with high capacity and large battery cells.

Bibliography

- [1] S. Lukic, J. Cao, R. C. Bansal, F. Rodriguez, and A. Emadi, "Energy storage systems for automotive applications," *IEEE Transactions on Industrial Electronics*, vol. 55, no. 6, pp. 2258–2267, 2008.
- [2] T. Trigg, P. Telleen, R. Boyd, and F. Cuenot, "Global EV Outlook: Understanding the Electric Vehicle Landscape to 2020," no. April, pp. 1–41, 2013.
- [3] Natural Resources Canada, "Canadian Vehicle Survey," 2009.
- [4] Environment Canada, "National Inventory Report, Greenhouse Gas Sources and Sinks in Canada," 2012.
- [5] Statistics Canada, "Report on Energy Supply and Demand in Canada," 2012.
- [6] S. Shafiee and E. Topal, "When will fossil fuel reserves be diminished?," *Energy Policy*, vol. 37, no. 1, pp. 181–189, 2009.
- [7] M. Z. Daud, A. Mohamed, and M. A. Hannan, "A review of the integration of Energy Storage Systems (ESS) for utility grid support," *Prz. Elektrotechniczny*, vol. 88, no. 10A, pp. 185–191, 2012.
- [8] R. M. Dell and D. a J. Rand, "Energy storage - A key technology for global energy sustainability," *J. Power Sources*, vol. 100, no. 1–2, pp. 2–17, 2001.
- [9] B. Bose, "Global Warming: Energy, Environmental Pollution, and the Impact of Power Electronics," *Ind. Electron. Mag. IEEE*, vol. 4, no. 1, pp. 6–17, 2010.
- [10] M. Asif and T. Muneer, "Energy supply, its demand and security issues for developed and emerging economies," *Renew. Sustain. Energy Rev.*, vol. 11, no. 7, pp. 1388–1413, 2007.
- [11] C. C. Chan and Y. S. Wong, "Electric vehicles charge forward," *IEEE Power Energy Mag.*, vol. 2, no. 6, pp. 24–33, 2004.
- [12] A. Affanni, A. Bellini, G. Franceschini, P. Guglielmi, and C. Tassoni, "Battery Choice and Management for New-Generation Electric Vehicles," *IEEE Trans. Ind. Electron.*, vol. 52, no. 5, pp. 1343–1349, Oct. 2005.
- [13] S. M. Lukic and A. Emadi, "Effects of drivetrain hybridization on fuel economy and

- dynamic performance of parallel hybrid electric vehicles,” *IEEE Trans. Veh. Technol.*, vol. 53, no. 2, pp. 385–389, 2004.
- [14] J. F. Donoghue and J. H. Burghart, “Constant Power Acceleration Profiles for Electric Vehicles,” *IEEE Trans. Ind. Electron.*, vol. IE-34, no. 2, pp. 188–191, 1987.
- [15] M. Farag, “Lithium-Ion Batteries: Modelling and State of Charge Estimation,” McMaster University, 2013.
- [16] G. L. Plett, “METHOD AND SYSTEM FOR BATTERY PARAMETER ESTIMATION,” US 7,315,789 B2, 2008.
- [17] G. L. Plett, “Kalman-Filter SOC Estimation for LiPB HEV Cells,” *System*, 2002.
- [18] G. L. Plett, “Extended Kalman filtering for battery management systems of LiPB-based HEV battery packs Part1,” *J. Power Sources*, vol. 134, no. 2, pp. 277–292, Aug. 2004.
- [19] R. Ahmed, M. El Sayed, I. Arasaratnam, J. Tjong, and S. Habibi, “Reduced-Order Electrochemical Model Parameters Identification and SOC Estimation for Healthy and Aged Li-Ion Batteries. Part II: Aged Battery Model and State of Charge Estimation,” *IEEE J. Emerg. Sel. Top. Power Electron.*, vol. 2, no. c, pp. 1–1, 2014.
- [20] J. Lo, “Effect of Temperature on Lithium-Iron Phosphate Battery Performance and Plug-in Hybrid Electric Vehicle Range by,” 2013.
- [21] D. Doerffel, “Testing and Characterisation of Large High-Energy Lithium-Ion Batteries for Electric and Hybrid Electric Vehicles.,” University of Southampton, 2007.
- [22] K. Young, C. Wang, L. Y. Wang, and K. Strunz, “Electric Vehicle Battery Technologies,” R. Garcia-Valle and J. A. Peças Lopes, Eds. New York, NY: Springer New York, 2013.
- [23] A. Khaligh and Z. Li, “Battery, Ultracapacitor, Fuel Cell, and Hybrid Energy Storage Systems for Electric, Hybrid Electric, Fuel Cell, and Plug-In Hybrid Electric Vehicles: State of the Art,” *IEEE Trans. Veh. Technol.*, vol. 59, no. 6, pp. 2806–2814, 2010.
- [24] H. Martin and M. Julander, “Battery-Supercapacitor Energy Storage,” 2008.
- [25] D. Sandeep and S. Dhameja, *Electric Vehicle Battery Systems*, 1st ed. Boston: Newnes, 2001.

- [26] J. Chatzakis, K. Kalaitzakis, N. C. Voulgaris, and S. N. Manias, "Designing a new generalized battery management system," *IEEE Trans. Ind. Electron.*, vol. 50, no. 5, pp. 990–999, 2003.
- [27] K. Kutluay, Y. Çadirci, Y. S. Özkazanç, and I. Çadirci, "A new online state-of-charge estimation and monitoring system for sealed lead-acid batteries in telecommunication power supplies," *IEEE Trans. Ind. Electron.*, vol. 52, no. 5, pp. 1315–1327, 2005.
- [28] L. Gauchia, "Nonlinear dynamic per-unit models for electrochemical energy systems . Application to a hardware-in-the-loop hybrid simulation," 2009.
- [29] A. Burke, "Ultracapacitors: Why, how, and where is the technology," *J. Power Sources*, vol. 91, no. 1, pp. 37–50, 2000.
- [30] J. Votano, M. Parham, and L. Hall, "Super Charged," *Chem. ...*, no. January 2005, 2004.
- [31] C. Ashtiani, R. Wright, and G. Hunt, "Ultracapacitors for automotive applications," *J. Power Sources*, vol. 154, no. 2, pp. 561–566, 2006.
- [32] D. Linzen, S. Buller, E. Karden, and R. W. De Doncker, "Analysis and evaluation of charge-balancing circuits on performance, reliability, and lifetime of supercapacitor systems," *IEEE Trans. Ind. Appl.*, vol. 41, no. 5, pp. 1135–1141, 2005.
- [33] J. Schiffer, D. Linzen, and D. U. Sauer, "Heat generation in double layer capacitors," *J. Power Sources*, vol. 160, no. 1, pp. 765–772, 2006.
- [34] P. Thounthong, B. Davat, and S. Raël, "Driver Friendly: Fuel Cell/Supercapacitor Hybrid Power Sources for Future Automotive Power Generation," *IEEE Power Energy Mag.*, no. february, pp. 69–76, 2008.
- [35] P. Thounthong, V. Chunkag, P. Sethakul, B. Davat, and M. Hinaje, "Comparative Study of Fuel-Cell Vehicle Hybridization with Battery or Supercapacitor Storage Device," *IEEE Trans. Veh. Technol.*, vol. 58, no. 8, pp. 3892–3904, Oct. 2009.
- [36] W. Schmittinger and A. Vahidi, "A review of the main parameters influencing long-term performance and durability of PEM fuel cells," *J. Power Sources*, vol. 180, no. 1, pp. 1–14, 2008.
- [37] B. Wahdame, S. Member, D. Candusso, X. Franc, F. Harel, D. Hissel, S. Member, and J. M. Kauffmann, "Analysis of a Fuel Cell Durability Test Based on Design of Experiment Approach," *IEEE Trans. Energy Convers.*, vol. 23, no. 4, pp. 1093–

1104, 2008.

- [38] C. C. Chan, "The state of the art of electric, hybrid, and fuel cell vehicles," *Proc. IEEE*, vol. 95, no. 4, pp. 704–718, 2007.
- [39] S. Rodrigues, N. Munichandraiah, and a. K. Shukla, "Review of state-of-charge indication of batteries by means of a.c. impedance measurements," *J. Power Sources*, vol. 87, no. 1, pp. 12–20, 2000.
- [40] A. Emadi, K. Rajashekara, S. S. Williamson, and S. Lukic, "Topological overview of hybrid electric and fuel cell vehicular power system architectures and configurations," *IEEE Transactions on Vehicular Technology*, vol. 54, no. 3, pp. 763–770, 2005.
- [41] C. C. Chan, "An overview of electric vehicle technology," *Proc. IEEE*, vol. 81, no. 9, pp. 1202–1213, 1993.
- [42] C. C. Chan, A. Bouscayrol, and K. Chen, "Electric, Hybrid, and Fuel-Cell Vehicles: Architectures and Modeling," *IEEE Trans. Veh. Technol.*, vol. 59, no. 2, pp. 589–598, Feb. 2010.
- [43] M. Ceraolo, a. Di Donato, and G. Franceschi, "A General Approach to Energy Optimization of Hybrid Electric Vehicles," *IEEE Trans. Veh. Technol.*, vol. 57, no. 3, pp. 1433–1441, 2008.
- [44] M. Shams-Zahraei and A. Z. Kouzani, "A study on plug-in hybrid electric vehicles," *IEEE Reg. 10 Annu. Int. Conf. Proceedings/TENCON*, pp. 1–5, 2009.
- [45] J. L. J. Liu, H. P. H. Peng, and Z. Filipi, "Modeling and Control Analysis of Toyota Hybrid System," *Proceedings, 2005 IEEE/ASME Int. Conf. Adv. Intell. Mechatronics.*, pp. 24–28, 2005.
- [46] S. Golbuff, "Optimization of a plug-in hybrid electric vehicle," *Mech. Eng.*, no. August, 2006.
- [47] D. Sotingco, "A Simulation-Based Assessment of Plug-in Hybrid Electric Vehicle Architectures," MIT, 2012.
- [48] C. Sae, "SAE Ground Vehicle Standards," 2010.
- [49] D. Hissel, D. Candusso, and F. Harel, "Fuzzy-clustering durability diagnosis of polymer electrolyte fuel cells dedicated to transportation applications," *IEEE Trans. Veh. Technol.*, vol. 56, no. 5 I, pp. 2414–2420, 2007.

- [50] A. F. Burke, "Batteries and Ultracapacitors for Electric, Hybrid, and Fuel Cell Vehicles," *Proc. IEEE*, vol. 95, no. 4, pp. 806–820, Apr. 2007.
- [51] J. Bauman and M. Kazerani, "A comparative study of fuel-cell-battery, fuel-cell-ultracapacitor, and fuel-cell-battery-ultracapacitor vehicles," *IEEE Trans. Veh. Technol.*, vol. 57, no. 2, pp. 760–769, 2008.
- [52] S.-Y. (Ben) Choe, J.-W. Ahn, J.-G. Lee, and S.-H. Baek, "Dynamic Simulator for a PEM Fuel Cell System With a PWM DC/DC Converter," *IEEE Trans. Energy Convers.*, vol. 23, no. 2, pp. 669–680, 2008.
- [53] S. Jain and V. Agarwal, "An integrated hybrid power supply for distributed generation applications fed by nonconventional energy sources," *IEEE Trans. Energy Convers.*, vol. 23, no. 2, pp. 622–631, 2008.
- [54] P. Thounthong, S. Raël, and B. Davat, "Test of a PEM fuel cell with low voltage static converter," *J. Power Sources*, vol. 153, no. 1, pp. 145–150, 2006.
- [55] J. Schiffer, O. Bohlen, R. W. de Doncker, and D. U. Sauer, "Optimized Energy Management for FuelCell-SuperCap Hybrid Electric Vehicles VPP Track 4: Energy Storage Components/Systems," *2005 IEEE Veh. Power Propuls. Conf.*, pp. 716–723, 2005.
- [56] E. Schaltz, A. Khaligh, and P. Rasmussen, "Investigation of battery/ultracapacitor energy storage rating for a Fuel Cell Hybrid Electric Vehicle," *2008 IEEE Veh. Power Propuls. Conf.*, pp. 1–6, 2008.
- [57] E. Schaltz and P. Rasmussen, "Design and Comparison of Power Systems for a Fuel Cell Hybrid Electric Vehicle," *2008 IEEE Ind. Appl. Soc. Annu. Meet.*, pp. 1–8, 2008.
- [58] G. Ren, G. Ma, and N. Cong, "Review of electrical energy storage system for vehicular applications," *Renew. Sustain. Energy Rev.*, vol. 41, pp. 225–236, 2015.
- [59] M. Zandi, A. Payman, J. Martin, S. Pierfederici, B. Davat, and F. Meibody-Tabar, "Energy Management of a Fuel Cell / Supercapacitor / Battery Power Source for Electric Vehicular Applications," *IEEE Trans. Veh. Technol.*, vol. 60, no. 2, pp. 433–443, 2011.
- [60] J. J. Awerbuch and C. R. Sullivan, "Control of ultracapacitor-battery hybrid power source for vehicular applications," *2008 IEEE Energy 2030 Conf. ENERGY 2008*, no. November, 2008.
- [61] A. C. Baisden and A. Emadi, "ADVISOR-based model of a battery and an ultra-

- capacitor energy source for hybrid electric vehicles,” *IEEE Trans. Veh. Technol.*, vol. 53, no. 1, pp. 199–205, 2004.
- [62] M. B. Camara, H. Gualous, F. Gustin, and A. Berthon, “Design and New Control of DC/DC Converters to Share Energy Between Supercapacitors and Batteries in Hybrid Vehicles,” *IEEE Trans. Veh. Technol.*, vol. 57, no. 5, pp. 2721–2735, Sep. 2008.
- [63] D. L. Cheng and M. G. Wismer, “Active control of power sharing in a battery/ultracapacitor hybrid source,” *ICIEA 2007 2007 Second IEEE Conf. Ind. Electron. Appl.*, pp. 2913–2918, 2007.
- [64] M. E. Choi, S. W. Kim, and S. W. Seo, “Energy management optimization in a battery/supercapacitor hybrid energy storage system,” *IEEE Trans. Smart Grid*, vol. 3, no. 1, pp. 463–472, 2012.
- [65] J. W. Dixon, I. a N. Nakashima, F. Arcos, and M. Ortúzar, “Test Results in an Electric Vehicle Using a Combination of Ultracapacitors and Zebra Battery,” *Fuel Cell*, vol. 18650, no. 3, pp. 565–572, 2006.
- [66] A. Du Pasquier, I. Plitz, S. Menocal, and G. Amatucci, “A comparative study of Li-ion battery, supercapacitor and nonaqueous asymmetric hybrid devices for automotive applications,” *J. Power Sources*, vol. 115, pp. 171–178, 2003.
- [67] a. Emadi, “A New Battery/UltraCapacitor Hybrid Energy Storage System for Electric, Hybrid, and Plug-In Hybrid Electric Vehicles,” *IEEE Trans. Power Electron.*, vol. 27, no. 1, pp. 122–132, 2012.
- [68] L. Gao, R. a. Dougal, and S. Liu, “Active power sharing in hybrid battery/capacitor power sources,” *Eighteenth Annu. IEEE Appl. Power Electron. Conf. Expo. 2003. APEC '03.*, vol. 1, pp. 497–503, 2003.
- [69] L. Gao, R. a Dougal, S. Member, and S. Liu, “Power Enhancement of an Actively Controlled Battery / Ultracapacitor Hybrid,” vol. 20, no. 1, pp. 236–243, 2005.
- [70] M. Gopikrishnan, “Battery/ultra capacitor hybrid energy storage system for electric, hybrid and plug-in hybrid electric vehicles,” *Middle - East J. Sci. Res.*, vol. 20, no. 9, pp. 1122–1126, 2014.
- [71] G. Guidi, T. M. Undeland, and Y. Hori, “Effectiveness of Supercapacitors as Power-Assist in Pure EV Using a Sodium-Nickel Chloride Battery as Main Energy Storage,” *Evs24*, pp. 1–9, 2009.
- [72] S. D. G. Jayasinghe, D. M. Vilathgamuwa, and U. K. Madawala, “A direct

- integration scheme for battery-supercapacitor hybrid energy storage systems with the use of grid side inverter,” in *2011 Twenty-Sixth Annual IEEE Applied Power Electronics Conference and Exposition (APEC)*, 2011, vol. 1, pp. 1388–1393.
- [73] S. D. G. Jayasinghe, D. M. Vilathgamuwa, and U. K. Madawala, “A new method of interfacing battery/supercapacitor energy storage systems for distributed energy sources,” *2010 Conf. Proc. IPEC*, pp. 1211–1216, 2010.
- [74] Wei Li, G. Joos, and J. Belanger, “Real-Time Simulation of a Wind Turbine Generator Coupled With a Battery Supercapacitor Energy Storage System,” *IEEE Trans. Ind. Electron.*, vol. 57, no. 4, pp. 1137–1145, Apr. 2010.
- [75] D. J. Miller and M. Technologies, “Power Electronic Interface for an Ultracapacitor as the Power Buffer in a Hybrid Electric Energy Storage System,” 2012.
- [76] J. M. Miller, “Trends in Vehicle Energy Storage Systems: Batteries and Ultracapacitors to Unite,” *2008 IEEE Veh. Power Propuls. Conf.*, 2008.
- [77] J. M. Miller and R. Smith, “Ultra-capacitor assisted electric drives for transportation,” *IEEE Int. Electr. Mach. Drives Conf. 2003. IEMDC’03.*, vol. 2, pp. 670–676, 2003.
- [78] J. M. Miller, “Energy storage technology markets and application’s: Ultracapacitors in combination with lithium-ion,” *7th International Conf. Power Electron. ICPE’07*, pp. 16–22, 2008.
- [79] J. M. Miller, M. Ehsani, and G. Yimin, “Understanding power flows in HEV eCVT’s with ultracapacitor boosting,” *2005 IEEE Veh. Power Propuls. Conf. VPPC*, vol. 2005, pp. 742–746, 2005.
- [80] R. M. Schupbach and J. C. Balda, “Comparing DC-DC converters for power management in hybrid electric vehicles,” *IEEE Int. Electr. Mach. Drives Conf. 2003. IEMDC’03.*, vol. 3, no. C, pp. 1369–1374, 2003.
- [81] G. Sikha and B. N. Popov, “Performance optimization of a battery-capacitor hybrid system,” *J. Power Sources*, vol. 134, no. 1, pp. 130–138, 2004.
- [82] P. Thounthong, E. Phatiphatthoungseminpl-nancyfr, I. National, P. De Lorraine, A. De, and F. De Haye, “A Control Strategy of Fuel Cell / Battery Hybrid Power Source for Electric Vehicle Applications,” *Fuel Cell*.
- [83] A. Tobias and J. Groot, “Alternative Energy Storage System for Hybrid Electric Vehicles,” Chalmers, 2003.

- [84] C. Xiang, Y. Wang, S. Hu, and W. Wang, "A New Topology and Control Strategy for a Hybrid Battery-Ultracapacitor Energy Storage System," pp. 2874–2896, 2014.
- [85] M. E. Choi and S. W. Seo, "Robust energy management of a battery/supercapacitor hybrid energy storage system in an electric vehicle," *2012 IEEE Int. Electr. Veh. Conf. IEVC 2012*, 2012.
- [86] a D. I. Napoli, F. Crescimbin, M. Ieee, F. G. Cappon, and L. Solero, "Control Strategy for Multiple Input DC-DC Power Converters Devoted to Hybrid Vehicle Propulsion Systems," pp. 1036–1041, 2002.
- [87] O. C. Onar and a. Khaligh, "A novel integrated magnetic structure based DC/DC converter for hybrid battery/ultracapacitor energy storage systems," *IEEE Trans. Smart Grid*, vol. 3, no. 1, pp. 296–307, 2012.
- [88] J. Cao and A. Emadi, "A new battery/ultra-capacitor hybrid energy storage system for electric, hybrid and plug-in hybrid electric vehicles," *2009 IEEE Veh. Power Propuls. Conf.*, pp. 941–946, 2009.
- [89] S. Castano, L. Gauchia, and J. Sanz-Feito, "Effect of Packaging on Supercapacitors Strings Modeling: Proposal of Functional Unit Defined Around Balancing Circuit," *IEEE Trans. Components, Packag. Manuf. Technol.*, vol. 3, no. 8, pp. 1390–1398, Aug. 2013.
- [90] F. van Mulders, J. M. Timmermans, Z. McCaffrey, J. van Mierlo, and P. van den Bossche, "Supercapacitor enhanced battery traction systems - concept evaluation," *World Electr. Veh. J.*, vol. 2, no. 2, pp. 32–45, 2008.
- [91] M. Ortúzar, J. Moreno, and J. Dixon, "Ultracapacitor-based auxiliary energy system for an electric vehicle: Implementation and evaluation," *IEEE Trans. Ind. Electron.*, vol. 54, no. 4, pp. 2147–2156, 2007.
- [92] P. Bhatnagar and R. . Nema, "Control techniques analysis of DC-DC converter for photovoltaic application using SIMSCAPE," *2012 IEEE 5th India Int. Conf. Power Electron.*, vol. 2, pp. 1–6, 2012.
- [93] J. Cai, Q. Zhong, and D. Stone, "A Compact Power Converter for Hybrid Energy Systems."
- [94] M. B. Camara, H. Gualous, F. Gustin, A. Berthon, and B. Dakyo, "DC/DC Converter Design for Supercapacitor and Battery Power Management in Hybrid Vehicle Applications—Polynomial Control Strategy," *IEEE Trans. Ind. Electron.*, vol. 57, no. 2, pp. 587–597, Feb. 2010.

- [95] S. Chakraborty, A. K. Jain, and N. Mohan, "Novel converter topology and algorithm for simultaneous charging and individual cell balancing of multiple Li-ion batteries," *INTELEC 2004. 26th Annu. Int. Telecommun. Energy Conf.*, 2004.
- [96] H.-W. Chang, W.-H. Chang, and C.-H. Tsai, "Integrated single-inductor buck-boost or boost-boost DC-DC converter with power-distributive control," *2009 Int. Conf. Power Electron. Drive Syst.*, vol. 1, no. c, pp. 1184–1187, Nov. 2009.
- [97] B. Eckardt, A. Hofmann, S. Zeltner, and M. Maerz, "Automotive Powertrain DC/DC Converter with 25kW/dm³ by using SiC Diodes," *PCIM Eur.*, 2006.
- [98] A. Di Napoli, F. Crescimbin, L. Solero, F. Caricchi, and F. G. Capponi, "Multiple-input DC-DC power converter for power-flow management in hybrid vehicles," *Conf. Rec. 2002 IEEE Ind. Appl. Conf. 37th IAS Annu. Meet. (Cat. No.02CH37344)*, vol. 3, pp. 1578–1585, 2002.
- [99] F. Nejabatkhah, S. Danyali, S. H. Hosseini, M. Sabahi, and S. M. Niapour, "Modeling and Control of a New Three-Input DC–DC Boost Converter for Hybrid PV/FC/Battery Power System," *IEEE Trans. Power Electron.*, vol. 27, no. 5, pp. 2309–2324, May 2012.
- [100] I. C. Paktron, "Density and High Temperature Power Systems Used in EV , HEV and PHEV DC Link & Filter Capacitors," pp. 1–30, 2012.
- [101] A. M. Rahimi and A. Emadi, "Active damping in DC/DC power electronic converters: A novel method to overcome the problems of constant power loads," *IEEE Trans. Ind. Electron.*, vol. 56, no. 5, pp. 1428–1439, 2009.
- [102] L. Solero, A. Lidozzi, and J. A. Pomilio, "Design of multiple-input power converter for hybrid vehicles," *IEEE Trans. Power Electron.*, vol. 20, no. 5, pp. 1007–1016, 2005.
- [103] B. Lin, S. Member, C. Yang, and D. Wang, "Asymmetrical Converter," pp. 1209–1214, 2005.
- [104] H. N. Lennart Harnfors, "Control of Variable Speed Drives." Course compendium, Malardalen University, Sweden, 2002.
- [105] National Instrument, "NI cDAQ-9188 Datasheet," no. 866, pp. 1–12, 2014.
- [106] National Instrument, "NI 9264 Datasheet," pp. 1–12, 2016.
- [107] KEPCO, "BOP-MG 1KW Datasheet," no. 1–194, 2014.

- [108] National Instrument, “NI 9239 Datasheet,” pp. 1–14, 2016.
- [109] National Instrument, “NI 9205 Datasheet,” pp. 1–14, 2015.
- [110] Infineon, “OptiMOS T2 Datasheet,” pp. 1–9, 2007.
- [111] International Rectifier, “IR2110 High/Low side driver datasheet,” vol. 2110, pp. 1–18.
- [112] Microchip, “PIC16F45K20 Datasheet,” pp. 1–456, 2010.

Appendix 1: Autonomie Simulations

The default electric vehicle profile in Autonomie 1210 released on 08/12/2010 is used with a 280 KW electric motor and total mass of 2217.676 Kg. The remaining parameters are all set to the default values in the commercial software. The simulation scheme is shown in Figure A.1. Effects of environment, grading, and the driver are considered in the simulation as well.

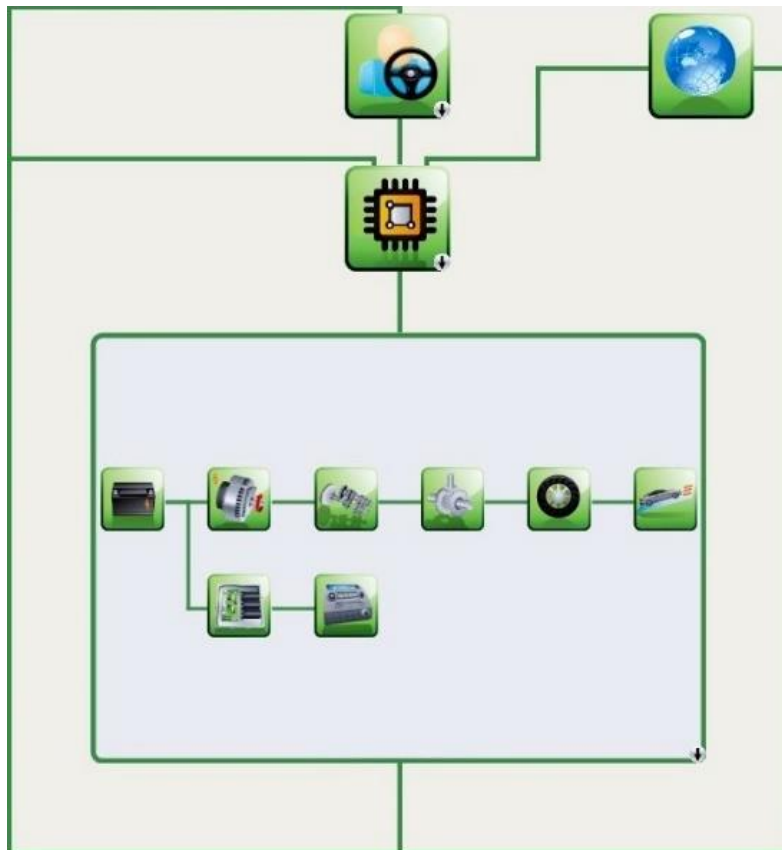


Figure A.1. The simulation set up in Autonomie

Figure A.2 shows the power transmission scheme. The main path starts with the electric storage unit followed by the electric motor. Then the gearbox transmits the power through the final drive to the wheels. The second path at the bottom represents the power consumption of electronics in the vehicle.



Figure A.2. Power transmission scheme in Autonomie, the simulation software.

Appendix 2: SIMULINK Simulations

The smart cell is simulated in SIMULINK. The main simulation scheme shown in Figure 4.13 is composed of three main blocks.

1. *Electrical Power System*: The block is shown in Figure A. 3. The battery and the ultracapacitor are interfaced with the power convertor that is controlled with the duty cycle. The duty cycle is the input signal that comes from the current regulator block.

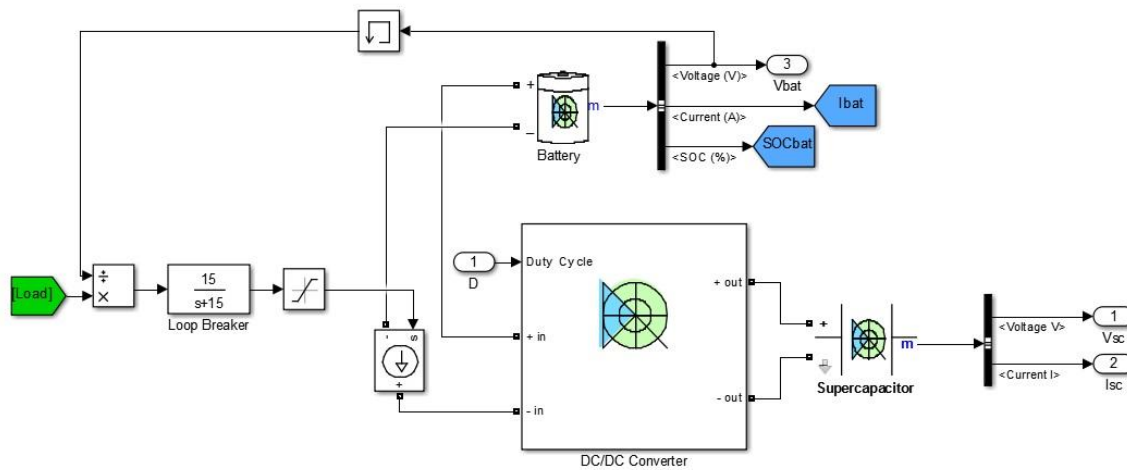


Figure A. 3. Simulation of the smart cell in SIMULINK / Electric Power System

2. *Current Regulator*: The current regulator shown in Figure A. 4 is a digital PI controller that is designed and implemented as discussed in 3.5. The block receives ultracapacitor's reference current as an input from the control and management unit and produces an appropriate duty cycle that will be fed to the electric power system.

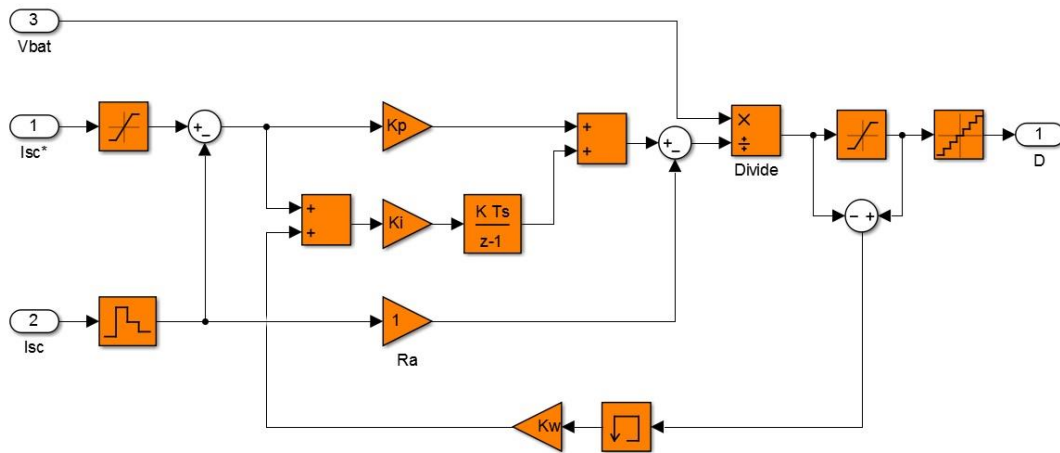


Figure A. 4. Simulation of the smart cell in SIMULINK / Current Regulator

3. *Power Management Unit*: This block determines the reference signal that the ultracapacitor's current will track as shown in Figure 3.15. All of the control strategies discussed in section 3.4 are implemented in this block that is illustrated in Figure 5.5.

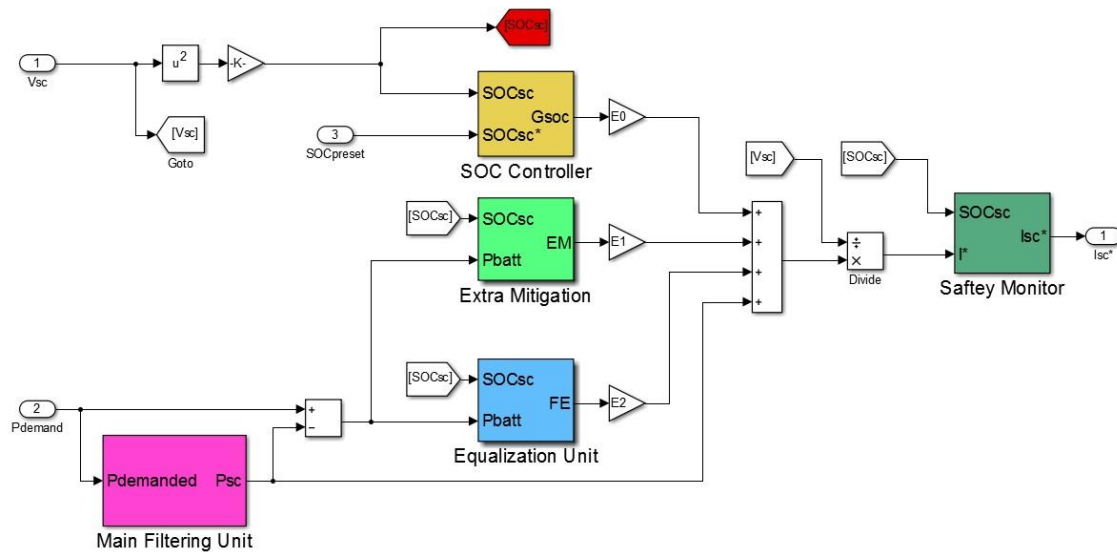


Figure 5.5. Simulation of the smart cell in SIMULINK / Power Management Unit

The “Power Management Unit” is composed of four major blocks. The “Extra Mitigation” and the “Equalization” units that are discussed in details in sections 3.4.4 and 3.4.3 are shown in Figure A.6.

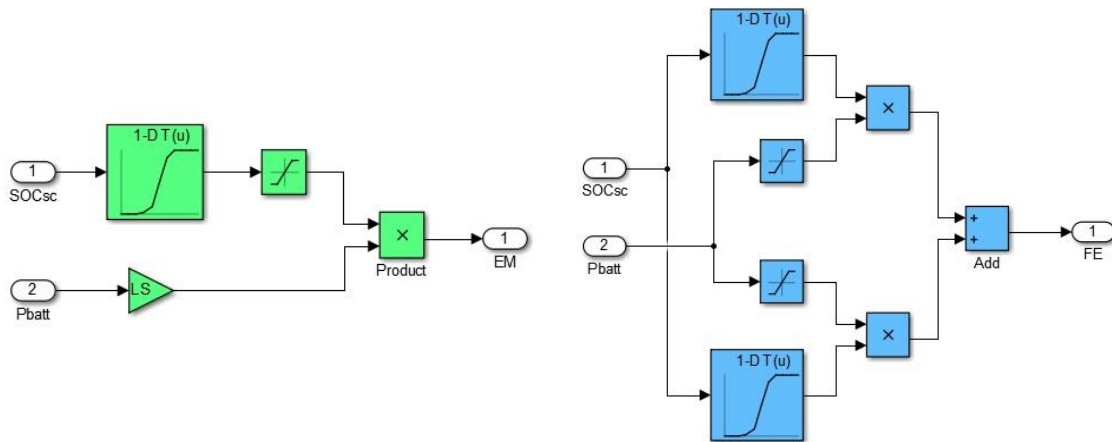


Figure A.6. Simulation of the smart cell in SIMULINK / Extra mitigation (left), Equalizer (right)

Also, A PI controller is designed to control the state of charge of the ultracapacitor as discussed in 3.4.2. Figure A.7 shows the corresponding block used in the simulations. The controller tries to maintain a certain level of SOC given as an input to the block.

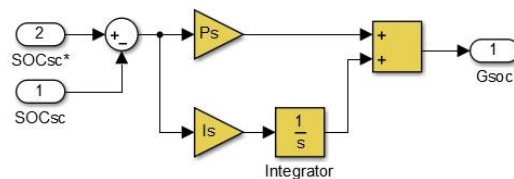


Figure A.7. Simulation of the smart cell in SIMULINK / Ultracapacitor's SOC controller

The adaptation algorithm and its necessity is discussed in details in 3.4.1. Figure 5.8 shows SIMULINK realization of the adaptation algorithm.

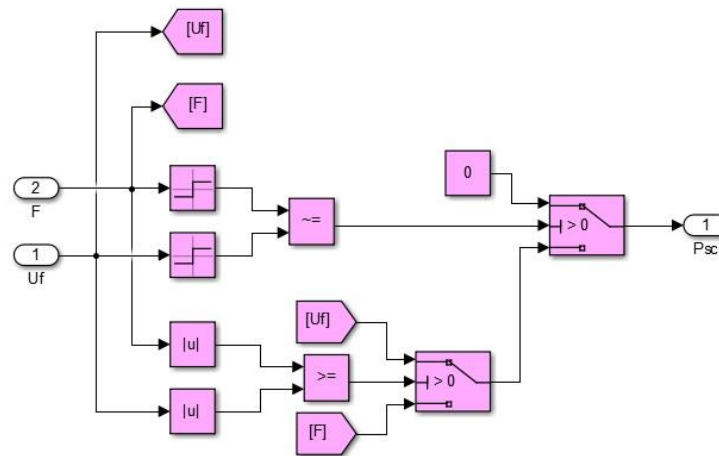


Figure 5.8. Simulation of the smart cell in SIMULINK / The Adaptation Algorithm

The piece of code to calculate SOC stress factor defined in (4.3) is shown in Figure A.9.

```
function [stress] = freqspec(x,y)

% x=stime y=SOcbatt

Fs = 1/(x(end)-x(end-1));           %sampling freq
NFFT = length(y);
Y = abs(fft(y,NFFT)/NFFT);          %make fft
freq = Fs*(0:NFFT-1)/NFFT;          %creat freq vector
Y = Y(1:ceil(NFFT/2));
freq = freq(1:ceil(NFFT/2));

%%SOC Stress
f0 = 2;                               %Lower value of ferq vector
f1 = find(freq>1,1)-1;
stress = sum(freq(f0:f1).*(Y(f0:f1)).^2);
```

Figure A.9. Calculation of SOC stress factor in MATLAB

Appendix 3: Lab Equipment

The comparison and testing procedure is performed under simulated load cycles. LabVIEW is used to both create the waveforms and also capture the data for further analysis. Different modules are mounted over the data acquisition chassis for each specific application. The chassis NI cDAQ-9188 is shown in Figure A.10. More technical information is provided in [105].



Figure A.10. The data acquisition chassis NI cDAQ-9188 [105].

NI 9264 shown in Figure A.11 is a 16 channel $\pm 10V$ analog Output module. This module creates an analogue voltage signal that represents the load cycle. The power supply KEPCO BOP-MG 1KW has the ability to generate up to $\pm 150A$ proportional to the analogue voltage fed to its analogue input which is connected to module NI9264. The load signal will be created by the LabVIEW and then fed to the power supply. More technical details about the analogue output module and the power supply are provided in [106] and [107] respectively.



Figure A.11. NI 9264 analogue output module [106].

NI 9239 and NI 9205 shown in Figure 5.12 are analogue input modules that can capture an analogue signal with 24 bit and 16 bit resolution respectively. They are used to capture signals for further analysis and calculations. Technical details are available at [108] and [109] respectively.



Figure 5.12. Analogue input modules used to capture signals for further analysis

Appendix 4: The Prototype Circuit

The circuit is built on a fast prototyping PC Board with each element soldered on it. The board was strengthened with a solid line of lead to reinforce it for higher currents. OptiMOS-T2 switches were selected for this application that are ultra-low $R_{ds(on)}$ and automotive electronics council qualified. The technical details are available in [110]. To drive the switches and deal with the technical difficulties of a half bridge circuit, the high-low side driver IR2110 is used that is able to provide up to 2A and 20V. Technical details are available in [111]. The switching circuit with its driver is shown in Figure A.13.

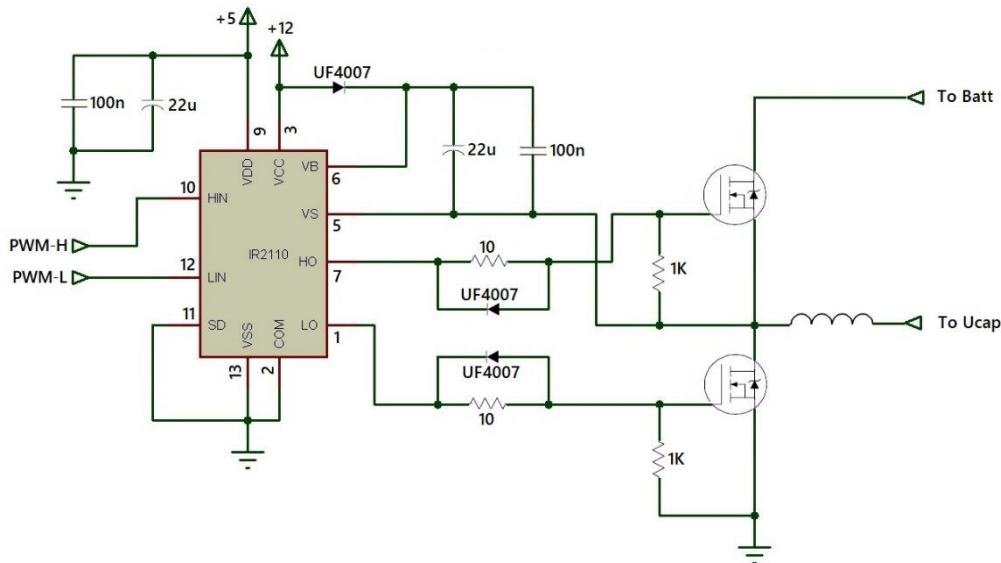


Figure A.13. Half bridge drive circuit

The microcontroller used is PIC18F45K20 with up to 64MHz crystal modes, 13 external channels of 10 bit ADC, up to 35 high current sink/source I/O, enhanced CCP with programmable dead time to drive power electronic bridges. The pinout is shown in Figure A.14. The chip can be programmed directly on the prototype circuit built. The oscillator circuit for the microcontroller is also shown in Figure A.15.

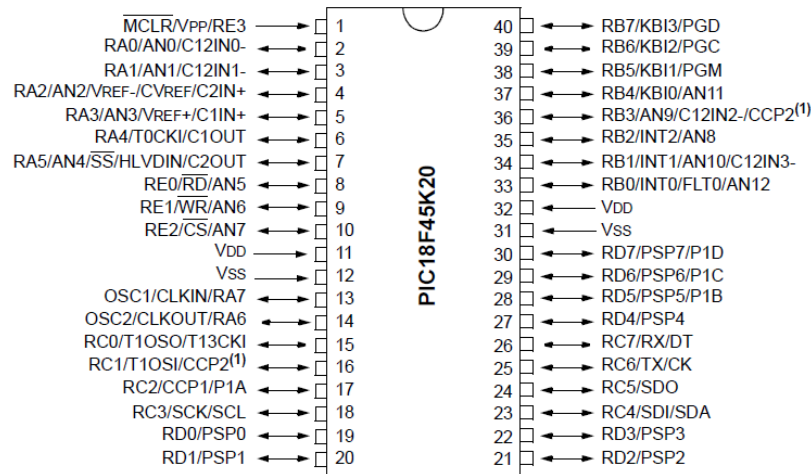


Figure A.14. Pinout for PIC18F45K20

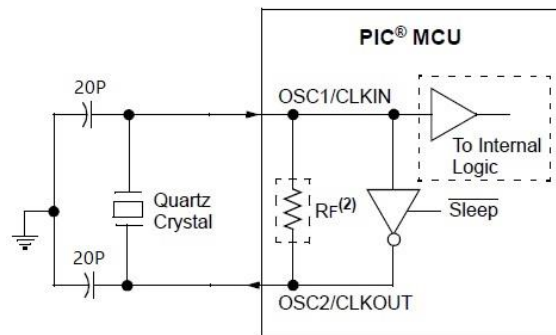


Figure A.15. Oscillator connection of the microcontroller

P1A, and P1B pins are used as the outputs of the enhanced PWM mode. They are connected to PWM-H and PWM-L pins in Figure A.13 to drive the switching circuit. The analogue input mode in AN5 to AN8 is selected as the input for the ADC to get feedback from the power circuit. More details about the microcontroller is provided in [112]. The overall connection of the parts is discussed in Figure 4.22 earlier.

Appendix 5: The Microcontroller Coding

The initiation of the chip determines the operation mode, frequency, port associations and settings required for safe operation. The main routine is shown in Figure A.16 (a). The Interrupt Service Routine or ISR is the routine that goes on as long as there is an error between the set point and the measured signal. This routine is illustrated in Figure A.16 (b) and coloured with the same dark blue as the flowchart is illustrated. The blocks in the flowcharts are highlighted inside the code in the form of comments.

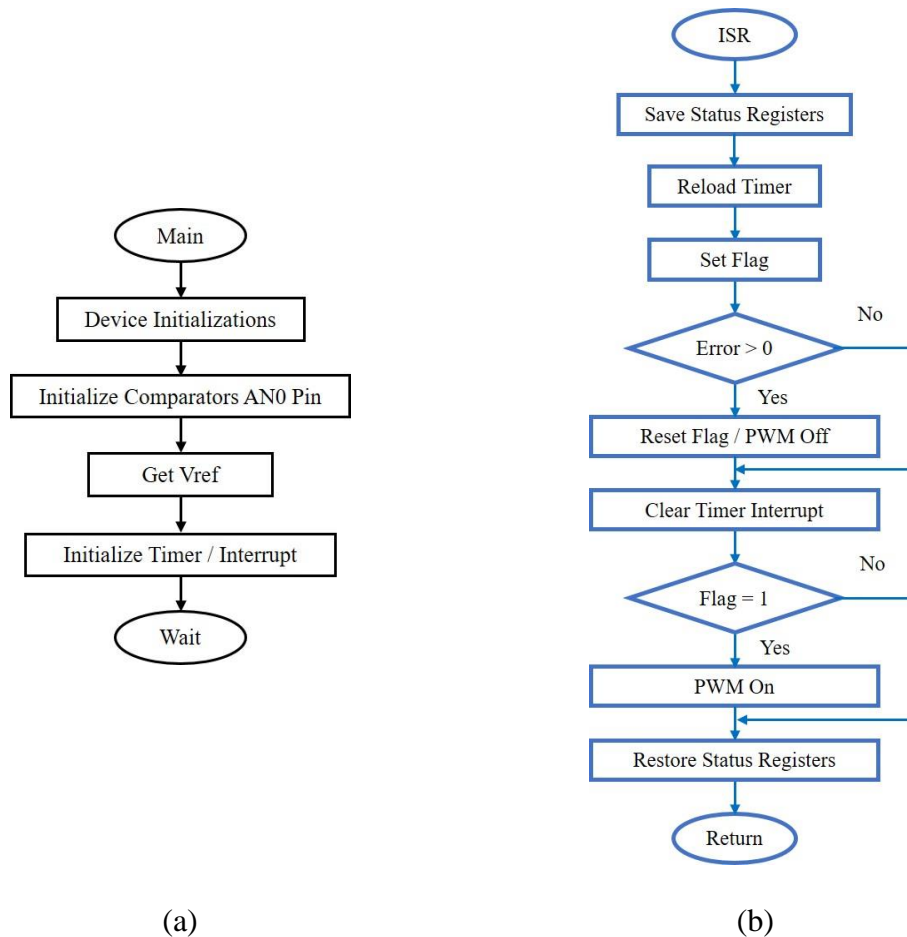


Figure A.16. Flowcharts of (a) the chip initialization (b) the interrupt routine